Étude de la perfusion cérébrale par Arterial Spin Labeling en IRM à 1.5T chez le nouveau-né et l'enfant

Maïa Proisy

UNIVERSITE BIOLOGIE BRETAGNE SANTE LOIRE

UNIVERSITÉ DE RENNES 1

THESE DE DOCTORAT DE

L'UNIVERSITE DE RENNES 1
COMUE UNIVERSITE BRETAGNE LOIRE

ECOLE DOCTORALE N° 605
Biologie Santé
Spécialité : « *Analyse et traitement de l'information et des images médicales*»

Par
Maïa PROISY

Étude de la perfusion cérébrale par Arterial Spin Labeling en IRM à 1.5T chez le nouveau-né et l'enfant

Thèse présentée et soutenue à Rennes/Montréal, le 12 décembre 2018
Unité de recherche : Unité/Projet VisAGeS U1228 INRIA/INSERM IRISA, UMR CNRS 6074

Rapporteurs avant soutenance :

Mathieu DEHAES	Professeur associé, Université de Montréal
Guillaume GORINCOUR	Professeur d'université – Praticien Hospitalier, Université Aix-Marseille

Composition du Jury :

Président :	Nathalie BODDAERT	Professeur d'université – Praticien Hospitalier, Université Paris V
Examinateurs :	Christian BARILLOT	Directeur de recherche, CNRS Rennes
	Nathalie BODDAERT	Professeur d'université – Praticien Hospitalier, Université Paris V
	Mathieu DEHAES	Professeur associé, Université de Montréal
	Guillaume GORINCOUR	Professeur d'université – Praticien Hospitalier, Université Aix-Marseille
	Laurent RIFFAUD	Professeur d'université – Praticien Hospitalier, Université Rennes 1
Dir. de thèse :	Jean-Christophe FERRÉ	Professeur d'université – Praticien Hospitalier, Université Rennes 1

Remerciements

Je remercie sincèrement et chaleureusement :

Monsieur le Professeur Jean-Christophe Ferré

Monsieur le Professeur Guillaume Gorincour

Monsieur le Professeur Mathieu Dehaes

Monsieur le Professeur Laurent Riffaud

Madame le Professeur Nathalie Boddaert

Monsieur Christian Barillot

Monsieur François Rousseau

Madame Isabelle Corouge

Madame Elise Bannier

Monsieur Antoine Legouhy

Toute l'équipe de Radiopédiatrie du CHU de Rennes, en particulier Monsieur le Docteur Bertrand Bruneau, Madame le Docteur Catherine Tréguier, les manipulateurs d'IRM de l'Hôpital Sud et toute l'équipe de Radiologie du CHU de Rennes

Tous nos collègues des services cliniques médico-chirurgicaux de pédiatrie en particulier les médecins des services d'urgence pédiatrique, de neurochirurgie pédiatrique et de réanimation néonatale

Madame le Docteur Aline Carsin-Vu et Madame le Docteur Domitille Cadiot

Madame Christiane Bourdeau

Madame Amélie Nicolas

Toute l'équipe Visages et la plateforme Neurinfo

Toute l'équipe du CHU Sainte-Justine à Montréal

La Société Française de Radiologie (SFR), le CHU de Rennes, l'Ecole des Docteurs de l'UBL et le Conseil Régional de Bretagne, l'Agence Nationale de la Recherche (ANR Projet MAIA)

Ma famille

à Julien et Eulalie

Table des matières

Abréviations

ASL	= Arterial Spin Labeling
AAL	= Automated Anatomical Labeling
ATT	= Arterial Transit Time
BET	= Brain Extraction Tool
pCASL	= Pseudo-Continuous Arterial Spin Labeling
CA-CP	= Commissure Antérieure – Commissure Postérieure
CASL	= Continuous Arterial Spin Labeling
CBF/DSC	= Cerebral Blood Flow; Debit Sanguin Cérébral
HIE	= Hypoxo-Ischemic Encephalopathy
J3, J10	= 3^{ieme} jour de vie, 10^{ieme} jour de vie
NGC	= Noyaux Gris Centraux
MNI	= Montreal Neurological Institute
PASL	= Pulsed Arterial Spin Labeling
PLD	= Post Labeling Delay
SPM	= Statistical Parametric Mapping
SIBM	= Signaux et Images en Biologie et Médecine
$T1_{blood}$	= Temps de relaxation du sang
TI	= Temps d'Inversion
TOF-MRA	= Time of Flight – Magnetic Resonance Angiography

Résumé

L'imagerie IRM de perfusion par Arterial Spin Labeling (ASL) ou marquage des spin artériels a pour principal avantage d'être une méthode d'imagerie non invasive (non irradiante et sans injection de produit de contraste exogène), particulièrement adaptée à l'imagerie cérébrale pédiatrique. Sa facilité de mise en œuvre explique l'engouement pour cette séquence et de nombreuses applications cliniques émergentes. Cette technique initialement développée chez l'adulte nécessite une adaptation à la population pédiatrique, aussi bien des paramètres d'acquisition et de quantification que des algorithmes de traitement d'images.

La perfusion cérébrale globale et régionale évolue physiologiquement, parallèlement à l'âge et au développement neurocognitif. Il existe plusieurs méthodes d'étude de la perfusion cérébrale pédiatrique. Dans ce contexte, deux revues de littérature ont été réalisées et publiées : l'une portant sur les différentes techniques d'imagerie de la perfusion cérébrale chez les nouveau-nés, l'autre se focalisant sur la technique d'ASL en pédiatrie et ses applications cliniques.

Puis la chaine de traitement des images morphologiques et de perfusion ASL, développée chez l'adulte au sein de notre unité, a été adaptée aux enfants puis aux nouveau-nés. Ces deux populations ont effectivement des problématiques différentes, en particulier le rapport signal sur bruit de l'ASL est très bon chez les enfants, mais nettement moins bon chez les nouveau-nés, et les images morphologiques ont un contraste différent en raison d'une myélinisation incomplète à la naissance.

Grace à l'adaptation de la chaine de traitement, des travaux de recherche clinique ont pu être finalisés (2 publiés, 1 soumis) illustrant l'intérêt de l'étude de la perfusion cérébrale dans 3 situations : l'étude de l'évolution de la perfusion cérébrale normale chez l'enfant entre 6 mois et 15ans ; l'étude de la perfusion cérébrale chez les enfants souffrant d'une première crise de migraine avec aura ; et enfin l'étude de l'évolution de la perfusion cérébrale entre le 3^{ieme} et le 10^{ieme} jour de vie chez les enfants souffrant d'asphyxie périnatale et traités par hypothermie.

Plusieurs projets restent en cours sur le sujet, avec d'autres challenges de traitement et d'analyse d'image (enfants de neurochirurgie avec modifications morphologiques du cerveau, ou enfants prématurés par exemple), dans la continuité ce qui a été fait au cours de cette thèse.

Préambule

Cette thèse a été réalisée au sein de l'unité de recherche Visages U1228, en collaboration étroite avec le CHU de Rennes.

L'Unité/Equipe-projet VisAGeS - U1228 (responsable M. Christian Barillot) est une équipe de recherche labellisée conjointement par l'Inserm (Institut National de la Santé et de la Recherche Médicale) et l'Inria (Institut de Recherche en Informatique et Automatique) et appartenant à l'IRISA (UMR CNRS 6074, Université de Rennes I). Elle se consacre au développement de nouveaux algorithmes de traitement d'images médicales comme la fusion d'images (recalage et visualisation), la segmentation et analyse d'images, ou encore la gestion d'informations relative à l'image en santé.

Les données IRM ont été acquises au CHU de Rennes, dans le service d'imagerie médicale (Pr. Jean-Yves Gauvrit) sur le site de l'Hôpital Sud dans le département d'imagerie pédiatrique (Dr Bertrand Bruneau). L'inclusion des enfants et la réalisation des IRM a été possible grâce à une excellente collaboration avec les services cliniques de pédiatrie, de néonatologie, des urgences pédiatriques et de neurochirurgie.

Le sujet de cette thèse est en continuité avec mon sujet de master 2 intitulé « mise au point d'une séquence d'ASL à 3T pour l'étude de la perfusion cérébrale chez le nouveau-né (Master SIBM : Signaux et Images en Biologie et Médecine – Université Rennes 1), dont le stage de 6 mois a été réalisé à l'University College of London (Pr N.J. Robertson et Pr X. Golay).

Introduction générale

L'imagerie de perfusion par Arterial Spin Labeling (ASL) ou marquage des spin artériels est une technique IRM qui utilise comme traceur endogène les protons du sang artériel, marqués magnétiquement. Elle a été développée chez l'adulte depuis les années 1990 (Detre et al., 1992; Williams et al., 1992). De nombreux progrès technologiques ont permis le développement de cette technique, avec l'apparition d'applications cliniques (Deibler et al., 2008a, 2008b), principalement pour étude de la perfusion cérébrale, mais aussi en IRM fonctionnelle d'activation cérébrale (Raoult et al., 2012) et pour étude de la perfusion d'autres organes. Les travaux sont plus rares chez l'enfant, mais en pleine expansion, et cette

technique est très prometteuse en imagerie pédiatrique car non invasive, n'utilisant pas de rayonnement ionisant ou d'injection de produit de contraste exogène.

Le principe général de la technique ASL est la réalisation d'une image contrôle et d'une image marquée. La soustraction de ces deux images permet d'obtenir une image pondérée en perfusion. En raison d'une différence de signal très faible entre les deux images, le couple image marquée-image contrôle est répété plusieurs dizaines de fois. Elle a l'avantage de pouvoir être répétée au cours d'un même examen, et de permettre une quantification absolue du débit sanguin cérébral (ou Cerebral Blood Flow = CBF). De manière générale, son principal inconvénient est un faible rapport signal sur bruit, avec une résolution spatiale limitée. Cet inconvénient est contrebalancé chez l'enfant du fait d'un CBF basal plus élevé que chez l'adulte, augmentant ainsi le signal (Biagi et al., 2007). A l'inverse, chez le nouveau-né l'utilisation de la séquence est un challenge technique en raison d'un cerveau de petite taille et d'un CBF physiologiquement très bas comparativement aux enfants et à l'adulte.

Les cartographies de perfusion cérébrales générées automatiquement par le logiciel constructeur limitent les analyses à des analyses visuelles (en routine clinique) ou à des analyses quantitatives par positionnement manuel de régions d'intérêt. La maitrise des paramètres de quantification, de correction de mouvement ou encore une analyse statistique plus poussée et automatisée nécessitent un traitement des images morphologiques (3D-T1) et des images natives d'ASL à l'aide de logiciels de traitement d'image. Une chaine de traitement automatisée nommée autoASL, basée sur l'utilisation du logiciel SPM8 (Wellcome Trust Centre for Neuroimaging, University College of London, UK) et Matlab® (The MathWorks, Inc.), a été développée antérieurement au sein de l'équipe Visages, sur des populations adultes à 3T. Elle a été largement éprouvée sur des populations adultes. Aucun essai n'avait été effectué jusqu'à lors sur des images pédiatriques, provenant d'un autre site, et d'une machine IRM 1.5T.

L'objectif de cette thèse était donc d'adapter les paramètres d'acquisition de la séquence ASL à des populations pédiatriques au CHU de Rennes, et d'adapter la chaine de traitement automatisée des images morphologiques et des images de perfusion cérébrale pour obtenir des valeurs de perfusion cérébrale dans différentes régions d'intérêt dans différentes situations cliniques.

Chapitre 1 – Imagerie de la perfusion cérébrale en pédiatrie

Les premières études de la perfusion cérébrale en imagerie utilisaient les techniques de médecine nucléaire. Elles ont mis en évidence une évolution globale et régionale de la perfusion cérébrale en rapport avec l'âge. Dans une étude SPECT utilisant le 133Xe chez 42 enfants considérés comme normaux, âgés de 2 jours à 19 ans (Chiron et al., 1992) le CBF global était très bas à la naissance (plus bas que chez l'adulte) puis maximal à l'âge de 5-6 ans (50-85% plus élevé que chez adultes). Puis il existait une décroissance pour atteindre des valeurs adultes entre 15 et 19 ans. L'évolution selon les régions corticales cérébrales montrait des valeurs relatives de CBF (valeurs de CBF régionales exprimées en % du CBF global) plus élevées et une augmentation plus rapide dans le cortex primaire (cortex visuel primaire, cortex auditif et cortex sensorimoteur) que dans le cortex associatif (cortex associatif unimodal parieto-temporal et occipital, cortex associatif polymodal pariéto-temporal, associatif pré-frontal et aire de Broca), en accord avec le développement de l'enfant.

Il existe parallèlement une évolution du métabolisme du glucose mesuré en PET 18-FDG (Chugani et al., 1987). Dans cette étude menée chez 29 enfants considérés comme normaux, le métabolisme glucidique était maximal dans le cortex sensori-moteur, les thalamus, le tronc cérébral et le vermis, chez les nouveau-nés de moins de 5 semaines. A l'âge de 3 mois il existait une augmentation dans le cortex pariétal, temporal et primaire visuel, les noyaux gris centraux et le cortex cérébelleux. Le pic dans le cortex frontal et occipital dorsolatéral était atteint environ à l'âge de 6-8 mois. De manière globale les valeurs de captation du glucose dans la substance grise étaient basses à la naissance et augmentaient rapidement jusqu'à l'âge de 2 ans, puis le pic était atteint vers 3-4 ans pour rester en plateau jusqu'à 9 ans. Ensuite il existait une décroissance pour atteindre les valeurs adultes vers 16-18 ans.

Des données similaires ont été retrouvées en scanner de perfusion cérébrale (Wintermark et al., 2004) dans une étude rétrospective menée chez 77 enfants âgés de 7 jours à 18 ans. Il s'agit de la seule étude dans la littérature avec cette modalité d'imagerie. Le pic perfusionnel était atteint entre 2 et 4 ans (x 2.5 valeurs adultes) puis les valeurs adultes vers l'âge de 7 ans. L'évolution régionale retrouvait un pic perfusionnel du cortex primaire sensori-moteur dans les premiers mois de vie, puis un pic du CBF relatif dans le cortex temporal et pariétal, les basal ganglia, entre 1 et 4 ans. L'augmentation dans cortex frontal se faisait en dernier.

Une limite importante de ces études est que les enfants ont été considérés comme normaux a posteriori, car le scanner ne retrouvait pas de lésion, mais avec les données récentes de la littérature on sait qu'il peut exister des modifications perfusionnelles sans anomalie morphologique (Boulouis et al., 2017).

Il est maintenant plus facile d'obtenir des données chez des sujets sains, du fait de l'absence d'irradiation en IRM. Ainsi une étude a été menée en IRM de perfusion par ASL chez 202 enfants sains âgés entre 5-18 ans (Taki et al., 2011). L'évolution du CBF dans la substance grise selon l'âge montrait une forme en U inversée dans la plupart des régions cérébrales. L'âge du pic de CBF était variable selon les régions et les lobes, avec une augmentation allant du lobe occipital (moins de 5 ans) au lobe frontal (vers 11 ans), en passant par le temporal et pariétal (vers 9 ans). Peu de changements étaient retrouvés dans la substance grise profonde (noyaux gris centraux) et les hippocampes dans cette étude s'intéressant à des enfants de plus de 5 ans.

Pour résumer, ces données de la littérature avec différentes techniques d'imagerie de la perfusion cérébrale démontrent que la perfusion cérébrale évolue parallèlement à la maturation cérébrale, qui commence par les fonctions basiques (fonctions motrices et sensitives) puis se poursuit par les fonctions cognitives et exécutives. Il n'existe pas dans la littérature de différence de perfusion cérébrale selon le sexe ou les hémisphères chez l'enfant (Carsin-Vu et al., 2018; Hales et al., 2014; Wintermark et al., 2004).

Au début de cette thèse, les données de la littérature concernant l'ASL chez les nouveau-nés était assez limitées. Ainsi, afin de savoir ce qui était connu de la perfusion cérébrale dans cette population (valeurs normales et techniques existantes), une revue de la littérature a permis de faire un état de l'art sur le sujet, dans la continuité de mon master 2 SIBM (Proisy et al., 2016b). Dans ce contexte, une étude prospective pour étude de la perfusion ASL chez les nouveau-nés souffrant d'asphyxie périnatale a été menée dans le cadre de cette thèse (Chapitre 4).

Parallèlement, une revue de littérature se focalisant sur la technique d'ASL en pédiatrie, a permis dans un premier temps de connaitre les valeurs normales de perfusion cérébrale chez l'enfant avec cette technique, puis de faire une synthèse des applications cliniques publiées dans la littérature (Proisy et al., 2016a). De nouvelles études concernant les applications cliniques de l'ASL en pédiatrie ont été publiées depuis la rédaction de notre revue de

littérature (Boulouis et al., 2017; Li et al., 2017; Wong et al., 2017). Effectivement, les applications cliniques sont en plein développement, avec des indications émergentes du fait de la facilité de mise en œuvre. Une étude sur les migraines avec aura, a été menée et publiée dans le cadre d'une thèse de médecine (Domitille Cadiot) (Chapitre 3). Enfin, ces travaux nous ont permis de constater qu'il existait un manque de données sur perfusion cérébrale normale entre 6 mois et 4 ans, vraisemblablement en rapport avec la nécessité de réaliser une sédation à cet âge pour la réalisation de l'IRM. De là est né le sujet de master 2 et de thèse de médecine, confié à Aline Carsin-Vu, sur une étude rétrospective menée à Rennes (Chapitre 3).

“Brain Perfusion Imaging in Neonates: An Overview. AJNR 2016”

Published April 14, 2016 as 10.3174/ajnr.A4778

Brain Perfusion Imaging in Neonates: An Overview

M. Proisy, S. Mitra, C. Uria-Avellana, M. Sokolska, N.J. Robertson, F. Le Jeune, and J.-C. Ferré

ABSTRACT

SUMMARY: The development of cognitive function in children has been related to a regional metabolic increase and an increase in regional brain perfusion. Moreover, brain perfusion plays an important role in the pathogenesis of brain damage in high-risk neonates, both preterm and full-term asphyxiated infants. In this article, we will review and discuss several existing imaging techniques for assessing neonatal brain perfusion.

ABBREVIATIONS: ASL = arterial spin-labeling; HIE = hypoxic-ischemic encephalopathy; NIRS = near-infrared spectroscopy

Brain perfusion can be assessed by a number of imaging techniques that have been developed in recent decades. These include PET, SPECT, perfusion CT, diffuse optical spectroscopy, DSC–MR imaging, arterial spin-labeling (ASL), and sonography. The physiology of perfusion can be characterized by many parameters such as CBF (whole-brain or regional CBF to ≥1 anatomic region), CBV, and MTT. Some of these parameters may be obtained depending on the perfusion technique and type of tracer used.[1] The results of brain perfusion imaging techniques are usually expressed as CBF. Most of these techniques rely on the use of endogenous or exogenous tracers and involve different technical requirements and mathematic models.[2-4] Wintermark et al[5] published a literature review of brain perfusion imaging techniques in adults and addressed the feasibility of applying the techniques to children. However, in view of the features of neonatal physiology and pathology, the advantages and disadvantages may differ between adults and children. For example, bedside techniques are an advantage for high-risk neonates. Noninvasive and nonradiating methods that have been recently developed owing to advances in medical imaging techniques are highly suitable for neonates.[6,7] However, given the smaller head size and lower physiologic brain perfusion compared with older children and adults, noninvasive MR perfusion imaging is still challenging.

Neonatal encephalopathy secondary to hypoxic-ischemic injury around birth is an important problem worldwide. Diagnosis is based on clinical, electroencephalographic, and MR imaging findings. Hypoxic-ischemic encephalopathy (HIE) is a major cause of perinatal mortality and morbidity.[8] For a few years, induced hypothermia has been used as neuroprotective treatment for neonatal HIE, reducing the extent of neurologic damage and improving outcome.[9,10] However, a considerable number of infants still have an abnormal outcome. Several preclinical research studies are also being conducted on drugs that may act synergistically or additively with hypothermia.[11,12] Transfontanellar ultrasound and MR imaging provide invaluable information about neonates with HIE for determining positive findings and differential diagnoses, predicting neuromotor outcome, and helping to counsel parents about long-term outcome.[13] Moreover, MRI is an effective biomarker for treatment response.[14] In addition to conventional MR imaging scoring,[15] some quantitative biomarkers could provide more objective information, such as DWI with regional ADC measurements,[16] ^{1}H-MR spectroscopy, and ^{31}P-MR spectroscopy.[17]

Brain perfusion plays an important role in the pathogenesis of brain damage in high-risk neonates, both preterm and full-term asphyxiated neonates.[18,19] Hypoxic-ischemic injury leads to reduced blood flow to the brain followed by restoration of blood flow and the initiation of a cascade of pathways. The neurotoxic biochemical cascade of lesions after reperfusion, known as "reperfusion injury," is the primary target for neuroprotective inter-

From the Department of Radiology (M.P., J.-C.F.), Rennes University Hospital, France; Department of Neonatology (M.P., S.M., C.U.-A., N.J.R.), University College London Hospital, Institute for Women's Health, University College of London, London, UK; Inserm VisAGeS Unit U746 (M.P., J.-C.F.), Inria, Rennes 1 University, Rennes, France; Institute of Neurology (M.S.), University College of London, London, UK; and Department of Nuclear Medicine (F.L.J.), Centre Eugène Marquis, Rennes, France.

This work was performed with the support of the Société Française de Radiologie (2012 Research Grant).

Please address correspondence to Maïa Proisy, MD, Department of Radiology, Pediatric Imaging, Rennes University Hospital, 16 Boulevard de Bulgarie, BP 90347, 35203 Rennes Cedex 2, France; e-mail: maia.proisy@chu-rennes.fr

Indicates open access to non-subscribers at www.ajnr.org

Indicates article with supplemental on-line table.

http://dx.doi.org/10.3174/ajnr.A4778

ventions.[10,12] In preterm infants, white matter injury is a major cause of cerebral palsy, which is also assumed to be mainly due to a lack of blood flow and oxygen delivery.[20]

It is critical to understand the development of early changes in the injured neonatal brain. A better understanding of the pattern of perfusion and the relationship with other therapeutic and outcome biomarkers would serve as a decision aid to improve support for high-risk neonates.

In this article, we will review and discuss several existing imaging techniques for assessing neonatal brain perfusion (On-line Table).

Practical Aspects of Data Acquisition in Neonates

There is no consensus regarding the practical aspects of data acquisition, and each institution may have its own practice. Often, infants younger than 3 months of age are imaged without sedation unless they are receiving sedative medication for clinical indications. We use the "feed and bundle" method to perform nonsedated neonatal MR imaging. Ventilated infants in the intensive care unit are usually sedated with morphine. Moreover, depending on the clinical condition, additional drugs may be given, antiepileptic drugs or vasopressors. In infants older than 3–5 months of age, sedation may be required. Sedation status remains an important consideration in pediatric imaging. Indeed, sedation may have an impact on cerebral perfusion. There are few data in the literature about how sedation or general anesthesia may alter perfusion.[21,22]

Without sedation, a rigid head stabilization (head lightly fixed) is required to perform most imaging (MR imaging, PET, SPECT, CTP). The longer the examination, the longer the immobilization is required. Near-infrared spectroscopy (NIRS) does not require rigid head stabilization because the optical fibers are embedded in a "cap" attached to the infant's head.

Brain Perfusion Measurements by Using Nuclear Medicine Methods

Nuclear medicine methods were the first ones used to assess CBF in adults and neonates.[23,24] Correlation with structural information (CT or MR imaging) is highly desirable for accurate interpretation.

Positron-Emission Tomography. The PET technique measures radiopharmaceuticals labeled with positron emitters using a PET scanner. PET is used to assess regional CBF by using injected H_2O or inhaled CO_2 labeled with the isotope oxygen 15 (^{15}O). PET with ^{15}O water provides an accurate and reproducible quantitative measurement of CBF and is considered the criterion standard method. However, ^{15}O-PET uses ionizing radiation, and the technique is not widely available (there is a need for close proximity to a cyclotron) because the tracer has an extremely short half-life. Moreover, PET is not available at the bedside or for emergencies. Data processing to obtain maps is automatically generated by the workstation; then the results can be visually interpreted on a computer screen. The underlying mathematic model for data postprocessing is the Kety-Schmidt model.[5]

In 1983, Volpe et al[23] conducted the first study demonstrating the use of PET for determining regional CBF in neonates. Altman et al[25] measured mean CBF in 16 preterm infants (CBF = 4.9–23 mL/100 g/min) and 14 term infants (CBF = 9.0–73 mL/100 g/min). Volpe et al[18] studied regional CBF in 17 asphyxiated term infants during the acute stage of their illness and showed a symmetric decrease in CBF to the parasagittal regions, more marked posteriorly than anteriorly. Those findings explain the ischemic lesions related to impaired cerebral perfusion in the watershed regions.

PET by using ^{18}F-fluorodeoxyglucose evaluates the regional cerebral metabolic rate (Fig 1). In neonates, the highest cerebral metabolic rates for glucose are located in the primary sensorimotor cortex, thalamus, brain stem, and cerebellar vermis. The cingulate cortex, basal ganglia, and hippocampal regions may also have a relatively high glucose metabolism compared with most of the cerebral cortex.[26] A recent study conducted on 60 infants, including 24 infants with HIE,[27] showed that cerebral glucose metabolism increased with gestational age and that the standardized uptake values were lower in infants with HIE than in healthy term infants, especially in the subcortical white matter, thalamus, and basal ganglia areas, and correlated with the degree of severity of HIE, except for the basal ganglia. Batista et al[28] suggested that there is a transient increase in glucose metabolism in the basal ganglia after perinatal hypoxia and that it may be associated with excess glutamatergic activity in the basal ganglia, leading to severe damage.

Single-Photon Emission CT. SPECT provides tomographic images of radiopharmaceutical distribution. It involves the inhalation or intravenous injection of xenon 133 (^{133}Xe), with technetium Tc99m hexamethylpropyleneamine oxime (^{99m}Tc-HMPAO) or iodine 123 *N*-isopropyl-p-iodoamphetamine (^{123}I-IMP). Due to neonatal brain physiology and biodistribution, HMPAO is a more reliable tracer of CBF distribution in neonates compared with adults.[29]

SPECT is a suitable bedside method that is cheaper and more widely available than PET imaging. HMPAO and IMP only show distribution and do not provide quantitative results, unlike xenon. The greatest disadvantage in using the SPECT technique in children is the ionizing radiation. The technique also yields poor resolution and requires a long examination time (20–25 minutes). Data processing to obtain maps takes about 5 minutes. The underlying mathematic model for data postprocessing is the Kety-Schmidt model for the ^{133}Xe and ^{123}I-IMP or the microsphere principle for the Tc99m tracers. Because the uptake of ^{99m}Tc-HMPAO is not linearly related to CBF, the maps obtained are not quantitative in the current standardized settings and require special correction. The relative CBF maps can be statistically evaluated compared with the healthy control to depict the regions with abnormal perfusion.[5]

Xenon clearance, by using inhaled xenon gas, is another technique that is closely related to SPECT and has been extensively used in adults and neonates.[30] Patient motion is a serious limitation of the technique, which, moreover, does not cover the whole brain. The mean CBF with the xenon technique has been estimated at around 50 mL/100 g/min in 7 healthy neonates[31] and 9.5–11.7 mL/100 g/min in 22 preterm infants during the first 3 days of life.[32] Changes in ^{123}I-IMP uptake in neonates reflecting relative CBF during the first month of life have been shown to be related to myelination development.[33] In term neonates, up-

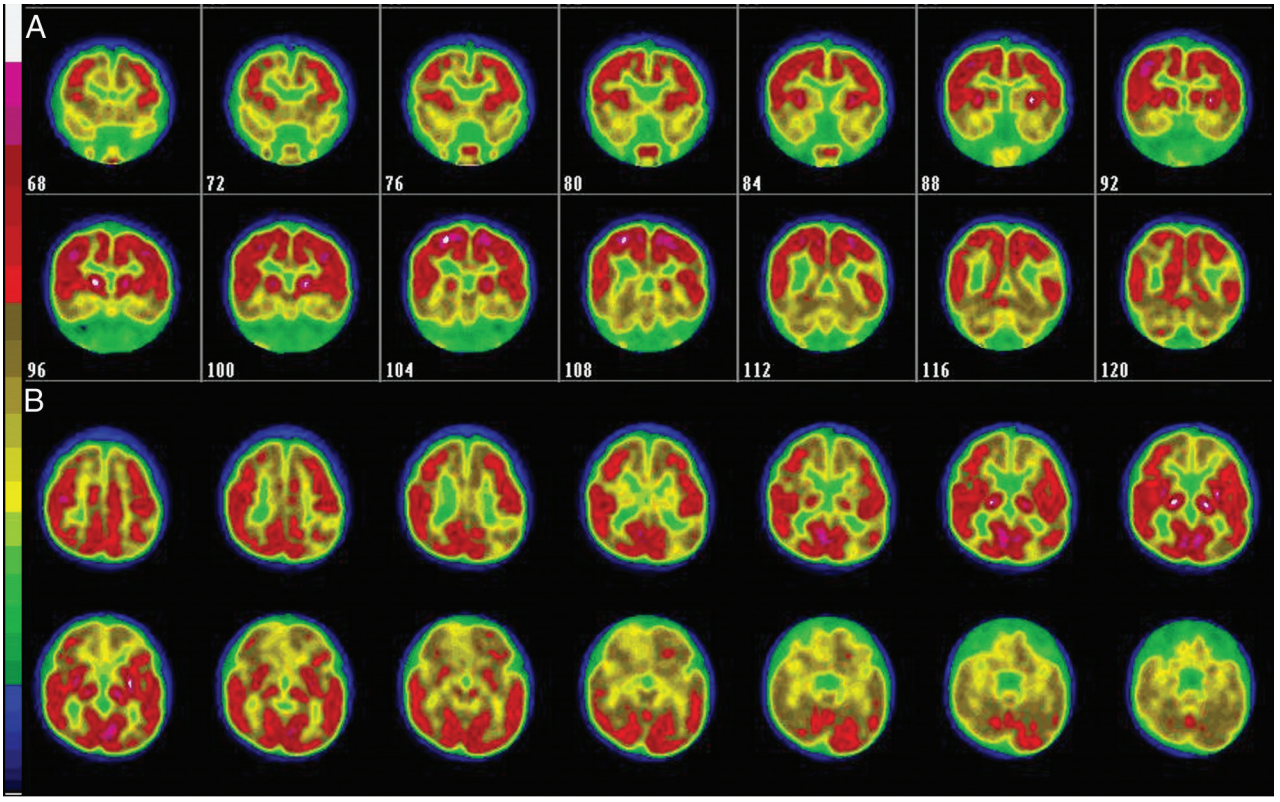

FIG 1. Coronal (*A*) and axial (*B*) cerebral ^{18}F-FDG PET images of a 9-month-old infant with tuberous sclerosis show multiple hypometabolic areas in the frontal and temporal cortex. Courtesy of Prof. Eric Guedj, CHU Timone, Marseille, France.

take was predominantly located in the thalami, brain stem, and central cerebellum, with relatively less cortical activity, except in the perirolandic cortex. Moreover, Pryds and Greisen[32] showed that an intraindividual variation in CBF was positively related to changes in partial pressure of carbon dioxide in arterial blood and inversely related to changes in hemoglobin concentration.

Brain Perfusion Measurements by Using Perfusion CT

Perfusion CT has been widely used in adults and can be performed easily and rapidly. This technique provides a reliable quantitative estimation of CBF, CBV, and MTT by using a first-pass tracer methodology after intravenous injection of a bolus of iodinated contrast material. It involves very rapid data acquisition that is feasible in emergency situations.[34,35] However, due to its invasive nature and radiation dose, very few studies have included neonates. Data processing requires perfusion CT software using either rate-of-upslope estimation of CBF or deconvolution analysis.[5] Images of CBF, CBV, and MTT maps are interpreted on a workstation with visual assessment and quantitative analysis with ROIs. Wintermark et al[36] assessed age-related variations in quantitative brain perfusion CT in children from 7 days to 18 years of age without brain abnormality, including 10 patients younger than 12 months of age. The rCBF findings were consistent with other techniques and showed age-specific variations with a peak at 2–4 years of age. The variation in CBF estimates was due to more pronounced age-related changes in MTT than in CBV.

Brain Perfusion Measurements by Using Near-Infrared Spectroscopy

Near-infrared spectroscopy, described first by Jöbsis in 1977,[37] can be used as a continuous noninvasive real-time monitoring tool for assessment of cerebral oxygenation and hemodynamics. The principles of NIRS are based on the relative transparency of biologic tissues to light in the near-infrared spectrum (700–1000 nm) and different absorption of light by different chromophores in this spectrum (eg, hemoglobin and cytochrome C oxidase). NIRS measures the concentration changes of oxy- and deoxyhemoglobin, which can be used to derive changes in total hemoglobin (an indicator of cerebral blood volume) and hemoglobin difference (indicates cerebral oxygenation).[38] Using spatially resolved spectroscopy, NIRS measures regional oxygenation saturation and reflects the balance of tissue oxygen supply and demand. In comparison with other techniques, application of NIRS is relatively easier. Improved NIRS probes are now available in different sizes to cover premature infants to term neonates. Although NIRS monitors have been used in adult neurointensive care units and theaters for some time now, the introduction of these monitors into neonatal intensive care has been slow. In recent years, several NICUs have started using this as part of the routine decision-making process, particularly for the preterm population.

Edwards et al[39] first described the measurement of cerebral blood flow, and Meek et al[40] showed that low CBF on the first day of life is a risk factor for severe intraventricular hemorrhage. Diffuse correlation spectroscopy is a newer NIRS tech-

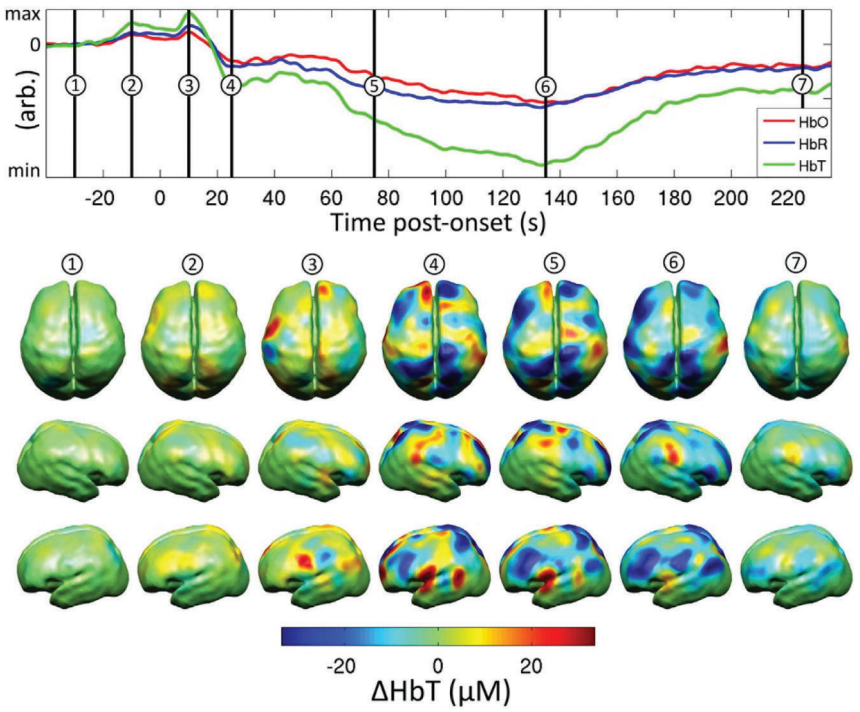

FIG 2. Reconstructed images showing the changes in cerebral blood volume (ΔHbT) in the dorsal and left and right lateral views during a seizure in a neonate with hypoxic-ischemic encephalopathy. The upper axes show the changes in hemoglobin concentration spatially averaged across the gray matter surface. Seven distinct time points are identified. All data are changes relative to a baseline, defined as the mean of the period between 60 and 30 seconds before the electrographic seizure onset. Reproduced from Singh et al.[48]

nique that offers a direct and continuous monitoring of microvascular cerebral blood flow.[41] Using hemoglobin difference as an indicator of CBF, Tsuji el al[42] described a high coherence between CBF and mean arterial blood pressure and a strong association of the loss of cerebral autoregulation with an increased incidence of severe germinal matrix–intraventricular hemorrhage or periventricular leukomalacia. The loss of autoregulation in the very preterm population was strongly related to mortality.[43]

Following perinatal hypoxia-ischemia in term infants, CBF and CBV were elevated and were associated with low oxygen extraction and the loss of reactivity to CO_2.[44] This loss of the autoregulatory mechanism with loss of cerebrovascular tone happens during the first 24 hours after the insult before secondary energy failure ensues. In a recent study, regional oxygenation saturation increased and fractional tissue oxygen extraction decreased after 24 hours in 18 neonates with poor outcome following HIE.[45] High tissue oxygenation values were noted on day 1 following perinatal hypoxia and were significantly higher in the group with abnormal 1-year outcome.[46] These findings were further supported by a combined NIRS-ASL study[47]: a strong correlation was noted between NIRS-measured regional cerebral oxygen saturation and CBF measured by ASL in infants with severe encephalopathy. Specific changes in cortical hemodynamics and oxygenation were described in previous NIRS studies during and after neonatal seizures (Fig 2).[48]

Brain Perfusion Measurements Using Sonography

Kehrer et al[49,50] have shown the feasibility of measuring CBF volume with Doppler sonography of the extracranial cerebral arteries in infants. Another way to assess overall CBF is to measure the total blood flow to the brain (sum of blood flow in the internal carotid arteries and basilar artery) and to divide it by the brain volume. Doppler sonography is noninvasive, lacking radiation exposure, innocuous, and suitable for bedside follow-up and has good interobserver reproducibility.[51] However, the disadvantages include the absence of regional CBF measurements, the use of an estimated brain weight, the need for the patient to be motionless for about 20 minutes, and strict compliance with a standardized study protocol/meticulous examination to achieve accurate and reliable measurements.[50] In healthy term neonates, the velocities in the ICAs and basilar artery are between 15 and 35 cm/s.[52] As shown with other techniques, the values of CBF volume increased with postmenstrual age from 33 mL/min at 34 weeks to 85 mL/min at 42 weeks.[49] Approximate CBF (mL/100 g/min) was calculated by using an estimated brain weight (the equation was based on head circumference measurements). CBF also increases from 21 to 23 mL/100 g/min after birth to 46–53 mL/100 g/min at 6 months of age and remains stable from 6 to 30 months of age, reflecting rising metabolic demand.[53]

Microbubble ultrasound is a new and reliable cerebral perfusion imaging technique that provides a qualitative estimation of cerebral perfusion and has been described in healthy adults and patients with stroke.[54] Yet, to our knowledge, no study has been conducted on neonates, mainly because microbubble ultrasound is not licensed for use in children.

Brain Perfusion Measurements by Using MR Imaging

Regarding practical aspects of MR imaging, one of the main advantages is that perfusion imaging is a part of the whole examination. The perfusion sequence could be added at the end of the morphologic MR imaging, which is usually clinically required.

Dynamic-Susceptibility Contrast MR Imaging. The dynamic-susceptibility contrast MR imaging technique measures the T2 or T2* decrease during the first pass of an exogenous endovascular susceptibility contrast agent. DSC–MR imaging is a nonradiating procedure, with high SNR and a higher spatial resolution than PET and SPECT, in addition to offering fast acquisition times. Regional hemodynamic changes can be assumed and different parameters such as CBV, TTP, and MTT can be estimated to calculate CBF. Parameters are calculated in a few minutes

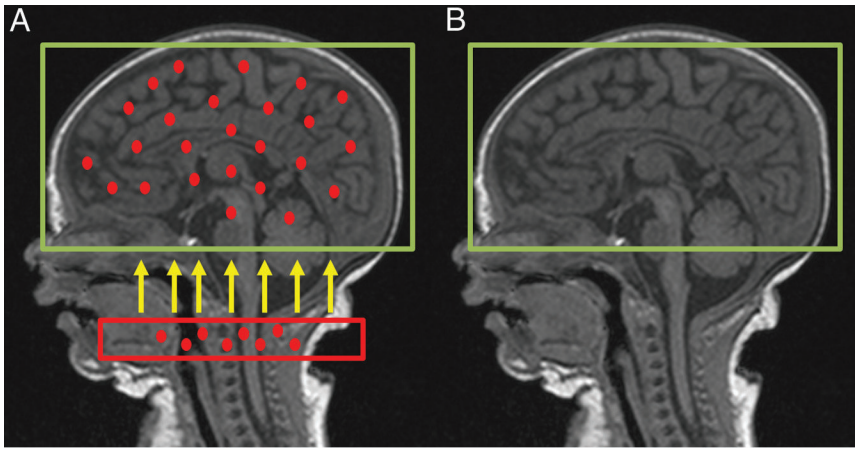

FIG 3. Schematic diagram of ASL shows the labeling plane (*red box*) in the neck and the imaging volume (*green box*). *A*, Acquisition of labeled image after a delay to allow the labeled blood to flow into the brain tissue. *B*, Acquisition of the control image.

by using commercially available software. However, the maps provide only relative measurements. Quantification of CBF by DSC is controversial, mainly due to the nonlinear relationship between signal intensity and gadolinium concentration.[55] Maps can be interpreted visually or semiquantitatively by calculating the ratio between the values in an ROI placed in the abnormal area and an ROI placed in the contralateral area considered a normal reference. Longitudinal studies involving repeated measurements during a single scanning session are not possible due to the lack of reliable absolute quantification. Despite the above-mentioned advantages, DSC–MR imaging can be difficult to perform in infants due to gadolinium administration. There have been fewer studies of DSC–MR imaging in children, and particularly neonates, than in adults.[56-59] Hand injections are preferred over power injections in infants, with less reproducibility. Wintermark et al[58] were the first to assess PWI in 5 term neonates with HIE on early (days 2–4) and late MR imaging (days 9–11). On the early MR imaging, a hyperperfusion pattern was detected in areas of hypoxic-ischemic brain damage, corresponding to the reperfusion phase. On the late scans, hyperperfusion persisted in the cortical gray matter.

Phase-Contrast MR Imaging. One other noninvasive, accurate, and reproducible MR imaging method has been reported in a small number of studies.[60,61] The blood flow in the internal carotid arteries and basilar artery at the base of the skull is measured by using phase-contrast MR imaging, and the brain volume is measured by using segmentation of anatomic MR images. Data processing consists of multiplying the mean velocity across an ROI (measured by the phase-contrast MR imaging sequence) by the vessel area. Flow to the brain is computed as the sum of flow in the 2 internal carotid arteries and the basilar artery. Brain volume is estimated by using segmentation software by using a dedicated neonatal brain segmentation algorithm. Mean CBF is computed by dividing the total flow to the brain by the brain volume.

In the study by Varela et al,[60] the results for 21 infants showed good agreement with literature data, with a rapid increase during the first year of life, from 25–60 mL/100 mL of tissue/min. The mean velocities (over the cardiac cycle, the area of each vessel and all 3 arteries) were <20 cm/s in term neonates and rose to 30 cm/s at 50 weeks. However, only mean overall CBF can be assessed with this method.

Arterial Spin-Labeling. Brain perfusion imaging by using arterial spin-labeling is a noninvasive technique that uses endogenous blood water as a freely diffusible tracer. Arterial blood protons are magnetically labeled with a radiofrequency inversion pulse applied below the imaging section in the neck vessels (Fig 1). Several labeling methods exist, including continuous ASL, pulsed ASL, and pseudocontinuous ASL.[62] In continuous ASL, a long flow-induced inversion pulse is applied. In pulsed ASL, a short inversion pulse is applied to a larger region of the neck. Pseudocontinuous ASL is a hybrid method that uses a train of short radiofrequency pulses to mimic the effects of continuous ASL (Fig 3). The best recommended ASL method is the pseudocontinuous ASL labeling method, mainly because of a higher SNR and less labeling artifacts.[63,64] However, there is a lack of data in the literature regarding the specific neonatal population, and more study is needed.

A labeled image is acquired after a sufficient time to allow the labeled spins to reach the imaging section, known as the postlabeling delay. A control image is acquired without labeling. Subtraction of the 2 images yields a perfusion-weighted image. Because the signal difference is only 0.5%–1.5% of the full signal, multiple repetitions are needed to improve the signal-to-noise ratio. Subsequently, to obtain a quantitative perfusion map, a quantitative model is required to calculate the relationship between the perfusion-weighted image and CBF.

Certain technical adjustments to the imaging parameters are required to account for the fundamental differences between the pediatric and adult populations.[65,66] It is challenging to perform ASL MR imaging in neonates due to the low baseline CBF compared with children and adults, coupled with the low SNR of the method. As an example, velocities are lower in neonates than in children, increasing with postmenstrual age,[67] and the optimum postlabeling delay for contrast-to-noise ratio has been correlated with the mean velocity in the carotid arteries.[68]

Moreover, in children and neonates, there is a physiologic improvement in the SNR compared with healthy adults due to a longer tissue T1, longer blood T1, and the higher blood-brain partition coefficient of water.[65] Blood T1 variations have a greater effect on perfusion than tissue T1 variations.[69] Varela et al[70] established a linear correlation between the inverse of blood T1 and hematocrit in 12 neonates. This may offer the possibility of blood T1 estimations from recent hematocrit measurements.

Measuring CBF in neonates by using ASL therefore requires several adaptations of acquisition and related parameters used for quantification. Another point is the lack of standardization of image-processing methods. In clinical practice, CBF maps are generally automatically generated by the manufac-

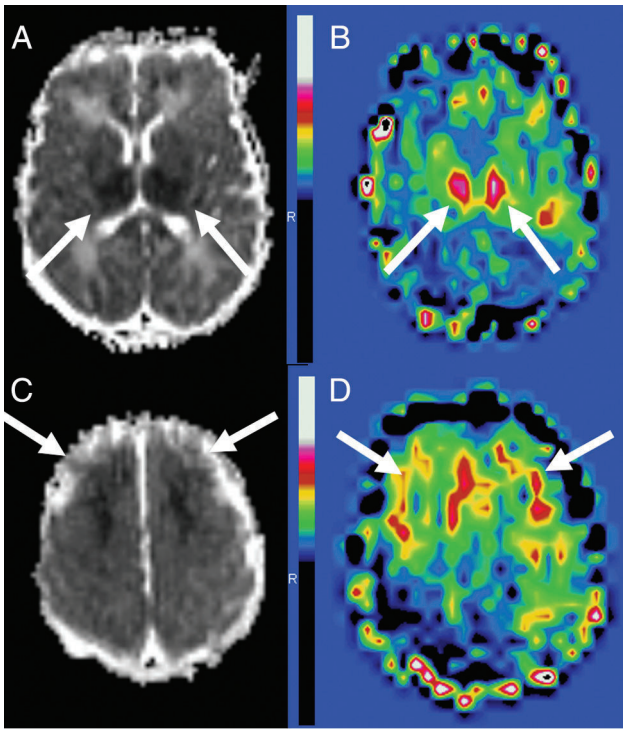

FIG 4. HIE ASL. Asphyxiated neonate treated with hypothermia showing ischemic injury on MR imaging obtained on day 3 of life. The ADC map shows restricted diffusion in the bilateral thalami and lentiform nuclei (*A*) and in the frontal watershed areas (*C*) (*arrows*). ASL perfusion map (*B* and *D*) reveals higher perfusion within the same areas (*arrows*).

turer workstation with assumed or measured quantification parameters.

A few studies have been conducted in neonates by using ASL. Miranda et al[71] were the first to show the feasibility of pulsed ASL at 1.5T in 29 unsedated healthy preterm infants at term-equivalent age and in term neonates. Other studies in healthy children show that ASL appears sensitive to regional and age-related differences in CBF in preterm, term neonates, and infants at 3 months[72] and from 3 to 5 months of age.[73] These results are consistent with previous studies demonstrating regional variation in brain maturation. Some studies have been conducted in asphyxiated neonates, showing early hyperperfusion in brain areas subsequently exhibiting injury,[74] and that regions with low ADC intensity are highly correlated with co-located regions of increased ASL CBF intensity (Fig 4).[75] Asphyxiated neonates treated with hypothermia developing brain injury usually displayed hypoperfusion on day of life 1 and hyperperfusion on day of life 2–3 in the study of Wintermark et al.[74] If performed during the second week of life, MR imaging reveals rather a hypoperfusion in the thalamus of infants with injury on MR imaging.[76] De Vis et al[77] showed a significant correlation between a higher perfusion in the basal ganglia and thalami, perfusion on day of life 2–7, and a worse neurodevelopmental outcome in neonates with HIE.

To summarize, ASL is a noninvasive method without venous cannulation or radiation that is repeatable within the same session and provides absolute quantification of CBF. Given the noninvasiveness of the technique, it is highly suitable for neonates.

CONCLUSIONS

Brain perfusion may play a role in neonatal brain injury and therefore serves as a complementary biomarker to help determine neuroprotective therapeutic strategies. With the development of noninvasive methods, assessment of neonatal brain perfusion has become easier. ASL is a very promising tool for assessing neonatal brain perfusion: It is a totally noninvasive method easily available and providing quantitative regional CBF values. However, the method warrants technical adjustments to make it more widely available.

ACKNOWLEDGMENTS

The authors thank Prof. Eric Guedj (CHU Timone, Marseille, France) for providing PET images and Ms Tracey Westcott for editorial assistance.

Disclosures: Maïa Proisy—*RELATED*: *Grant*: research grant 2012 Société Française de Radiologie (French Society of Radiology). Nicola J. Robertson—*UNRELATED*: *Grants/Grants Pending*: Chiesi Pharmaceutici S.p.A (research grant)*; *Royalties*: Chiesi, *Comments*: for licensing of intellectual property. *Money paid to the institution.

REFERENCES

1. Leiva-Salinas C, Provenzale JM, Kudo K, et al. **The alphabet soup of perfusion CT and MR imaging: terminology revisited and clarified in five questions.** *Neuroradiology* 2012;54:907–18 CrossRef Medline
2. Kety SS, Schmidt CF. **The nitrous oxide method for the quantitative determination of cerebral blood flow in man: theory, procedure and normal values.** *J Clin Invest* 1948;27:476–83 CrossRef Medline
3. Meier P, Zierler KL. **On the theory of the indicator-dilution method for measurement of blood flow and volume.** *J Appl Physiol* 1954;6:731–44 Medline
4. Ostergaard L, Weisskoff RM, Chesler DA, et al. **High resolution measurement of cerebral blood flow using intravascular tracer bolus passages, Part I: mathematical approach and statistical analysis.** *Magn Reson Med* 1996;36:715–25 CrossRef Medline
5. Wintermark M, Sesay M, Barbier E, et al. **Comparative overview of brain perfusion imaging techniques.** *Stroke* 2005;36:e83–99 CrossRef Medline
6. Goff DA, Buckley EM, Durduran T, et al. **Noninvasive cerebral perfusion imaging in high-risk neonates.** *Semin Perinatol* 2010;34:46–56 CrossRef Medline
7. Wintermark P. **Injury and repair in perinatal brain injury: insights from non-invasive MR perfusion imaging.** *Semin Perinatol* 2015;39:124–29 CrossRef Medline
8. Volpe JJ. **Neonatal encephalopathy: an inadequate term for hypoxic-ischemic encephalopathy.** *Ann Neurol* 2012;72:156–66 CrossRef Medline
9. Gluckman PD, Wyatt JS, Azzopardi D, et al. **Selective head cooling with mild systemic hypothermia after neonatal encephalopathy: multicentre randomised trial.** *Lancet* 2005;365:663–70 CrossRef Medline
10. Shankaran S, Laptook AR, Ehrenkranz RA, et al; National Institute of Child Health and Human Development Neonatal Research Network. **Whole-body hypothermia for neonates with hypoxic-ischemic encephalopathy.** *N Engl J Med* 2005;353:1574–84 CrossRef Medline
11. Faulkner S, Bainbridge A, Kato T, et al. **Xenon augmented hypothermia reduces early lactate/N-acetylaspartate and cell death in perinatal asphyxia.** *Ann Neurol* 2011;70:133–50 CrossRef Medline
12. Kelen D, Robertson NJ. **Experimental treatments for hypoxic ischaemic encephalopathy.** *Early Hum Dev* 2010;86:369–77 CrossRef Medline

13. Rutherford M, Malamateniou C, McGuinness A, et al. **Magnetic resonance imaging in hypoxic-ischaemic encephalopathy.** *Early Hum Dev* 2010;86:351–60 CrossRef Medline
14. Rutherford M, Ramenghi LA, Edwards AD, et al. **Assessment of brain tissue injury after moderate hypothermia in neonates with hypoxic-ischaemic encephalopathy: a nested substudy of a randomised controlled trial.** *Lancet Neurol* 2010;9:39–45 CrossRef Medline
15. Barkovich AJ, Hajnal BL, Vigneron D, et al. **Prediction of neuromotor outcome in perinatal asphyxia: evaluation of MR scoring systems.** *AJNR Am J Neuroradiol* 1998;19:143–49 Medline
16. Alderliesten T, de Vries LS, Benders MJ, et al. **MR imaging and outcome of term neonates with perinatal asphyxia: value of diffusion-weighted MR imaging and ^{1}H MR spectroscopy.** *Radiology* 2011;261:235–42 CrossRef Medline
17. Cheong JL, Cady EB, Penrice J, et al. **Proton MR spectroscopy in neonates with perinatal cerebral hypoxic-ischemic injury: metabolite peak-area ratios, relaxation times, and absolute concentrations.** *AJNR Am J Neuroradiol* 2006;27:1546–54 Medline
18. Volpe JJ, Herscovitch P, Perlman JM, et al. **Positron emission tomography in the asphyxiated term newborn: parasagittal impairment of cerebral blood flow.** *Ann Neurol* 1985;17:287–96 CrossRef Medline
19. Greisen G. **Autoregulation of cerebral blood flow in newborn babies.** *Early Hum Dev* 2005;81:423–28 CrossRef Medline
20. Back SA, Han BH, Luo NL, et al. **Selective vulnerability of late oligodendrocyte progenitors to hypoxia-ischemia.** *J Neurosci* 2002;22:455–63 Medline
21. Todd MM, Weeks J. **Comparative effects of propofol, pentobarbital, and isoflurane on cerebral blood flow and blood volume.** *J Neurosurg Anesthesiol* 1996;8:296–303 CrossRef Medline
22. Harreld JH, Helton KJ, Kaddoum RN, et al. **The effects of propofol on cerebral perfusion MRI in children.** *Neuroradiology* 2013;55:1049–56 CrossRef Medline
23. Volpe JJ, Herscovitch P, Perlman JM, et al. **Positron emission tomography in the newborn: extensive impairment of regional cerebral blood flow with intraventricular hemorrhage and hemorrhagic intracerebral involvement.** *Pediatrics* 1983;72:589–601 Medline
24. Fockele DS, Baumann RJ, Shih WJ, et al. **Tc-99m HMPAO SPECT of the brain in the neonate.** *Clin Nucl Med* 1990;15:175–77 CrossRef Medline
25. Altman DI, Powers WJ, Perlman JM, et al. **Cerebral blood flow requirement for brain viability in newborn infants is lower than in adults.** *Ann Neurol* 1988;24:218–26 CrossRef Medline
26. Chugani HT. **A critical period of brain development: studies of cerebral glucose utilization with PET.** *Prev Med* 1998;27:184–88 CrossRef Medline
27. Shi Y, Zhao JN, Liu L, et al. **Changes of positron emission tomography in newborn infants at different gestational ages, and neonatal hypoxic-ischemic encephalopathy.** *Pediatr Neurol* 2012;46:116–23 CrossRef Medline
28. Batista CE, Chugani HT, Juhász C, et al. **Transient hypermetabolism of the basal ganglia following perinatal hypoxia.** *Pediatr Neurol* 2007;36:330–33 CrossRef Medline
29. Børch K, Greisen G. **99mTc-HMPAO as a tracer of cerebral blood flow in newborn infants.** *J Cereb Blood Flow Metab* 1997;17:448–54 Medline
30. Greisen G. **Cerebral blood flow in preterm infants during the first week of life.** *Acta Paediatr Scand* 1986;75:43–51 CrossRef Medline
31. Chiron C, Raynaud C, Mazière B, et al. **Changes in regional cerebral blood flow during brain maturation in children and adolescents.** *J Nucl Med* 1992;33:696–703 Medline
32. Pryds O, Greisen G. **Effect of PaCO2 and haemoglobin concentration on day to day variation of CBF in preterm neonates.** *Acta Paediatr Scand Suppl* 1989;360:33–36 Medline
33. Tokumaru AM, Barkovich AJ, O'uchi T, et al. **The evolution of cerebral blood flow in the developing brain: evaluation with iodine-123 iodoamphetamine SPECT and correlation with MR imaging.** *AJNR Am J Neuroradiol* 1999;20:845–52 Medline
34. Eastwood JD, Lev MH, Provenzale JM. **Perfusion CT with iodinated contrast material.** *AJR Am J Roentgenol* 2003;180:3–12 CrossRef Medline
35. Wintermark M, Cotting J, Roulet E, et al. **Acute brain perfusion disorders in children assessed by quantitative perfusion computed tomography in the emergency setting.** *Pediatr Emerg Care* 2005;21:149–60 Medline
36. Wintermark M, Lepori D, Cotting J, et al. **Brain perfusion in children: evolution with age assessed by quantitative perfusion computed tomography.** *Pediatrics* 2004;113:1642–52 CrossRef Medline
37. Jöbsis FF. **Noninvasive, infrared monitoring of cerebral and myocardial oxygen sufficiency and circulatory parameters.** *Science* 1977;198:1264–67 CrossRef Medline
38. Wyatt JS, Cope M, Delpy DT, et al. **Quantification of cerebral oxygenation and haemodynamics in sick newborn infants by near infrared spectrophotometry.** *Lancet* 1986;2:1063–66 Medline
39. Edwards AD, Wyatt JS, Richardson C, et al. **Cotside measurement of cerebral blood flow in ill newborn infants by near infrared spectroscopy.** *Lancet* 1988;2:770–71 Medline
40. Meek JH, Tyszczuk L, Elwell CE, et al. **Low cerebral blood flow is a risk factor for severe intraventricular haemorrhage.** *Arch Dis Child Fetal Neonatal Ed* 1999;81:F15–18 CrossRef Medline
41. Roche-Labarbe N, Carp SA, Surova A, et al. **Noninvasive optical measures of CBV, StO(2), CBF index, and rCMRO(2) in human premature neonates' brains in the first six weeks of life.** *Hum Brain Mapp* 2010;31:341–52 CrossRef Medline
42. Tsuji M, Saul JP, du Plessis A, et al. **Cerebral intravascular oxygenation correlates with mean arterial pressure in critically ill premature infants.** *Pediatrics* 2000;106:625–32 CrossRef Medline
43. Wong FY, Leung TS, Austin T, et al. **Impaired autoregulation in preterm infants identified by using spatially resolved spectroscopy.** *Pediatrics* 2008;121:e604–11 CrossRef Medline
44. Meek JH, Elwell CE, McCormick DC, et al. **Abnormal cerebral haemodynamics in perinatally asphyxiated neonates related to outcome.** *Arch Dis Child Fetal Neonatal Ed* 1999;81:F110–15 CrossRef Medline
45. Toet MC, Lemmers PM, van Schelven LJ, et al. **Cerebral oxygenation and electrical activity after birth asphyxia: their relation to outcome.** *Pediatrics* 2006;117:333–39 CrossRef Medline
46. Zaramella P, Saraceni E, Freato F, et al. **Can tissue oxygenation index (TOI) and cotside neurophysiological variables predict outcome in depressed/asphyxiated newborn infants?** *Early Hum Dev* 2007;83:483–89 CrossRef Medline
47. Wintermark P, Hansen A, Warfield SK, et al. **Near-infrared spectroscopy versus magnetic resonance imaging to study brain perfusion in newborns with hypoxic-ischemic encephalopathy treated with hypothermia.** *Neuroimage* 2014;85:287–93 CrossRef Medline
48. Singh H, Cooper RJ, Wai Lee C, et al. **Mapping cortical haemodynamics during neonatal seizures using diffuse optical tomography: a case study.** *Neuroimage Clin* 2014;5:256–65 CrossRef Medline
49. Kehrer M, Krägeloh-Mann I, Goelz R, et al. **The development of cerebral perfusion in healthy preterm and term neonates.** *Neuropediatrics* 2003;34:281–86 CrossRef Medline
50. Kehrer M, Goelz R, Krägeloh-Mann I, et al. **Measurement of volume of cerebral blood flow in healthy preterm and term neonates with ultrasound.** *Lancet* 2002;360:1749–50 CrossRef Medline
51. Ehehalt S, Kehrer M, Goelz R, et al. **Cerebral blood flow volume measurements with ultrasound: interobserver reproducibility in preterm and term neonates.** *Ultrasound Med Biol* 2005;31:191–96 CrossRef Medline
52. Ilves P, Lintrop M, Talvik I, et al. **Developmental changes in cerebral and visceral blood flow velocity in healthy neonates and infants.** *J Ultrasound Med* 2008;27:199–207 Medline
53. Kehrer M, Schöning M. **A longitudinal study of cerebral blood flow**

over the first 30 months. *Pediatr Res* 2009;66:560–64 CrossRef Medline
54. Eyding J, Wilkening W, Postert T. **Brain perfusion and ultrasonic imaging techniques.** *Eur J Ultrasound* 2002;16:91–104 CrossRef Medline
55. Kiselev VG. **On the theoretical basis of perfusion measurements by dynamic susceptibility contrast MRI.** *Magn Reson Med* 2001;46:1113–22 CrossRef Medline
56. Huisman TA, Sorensen AG. **Perfusion-weighted magnetic resonance imaging of the brain: techniques and application in children.** *Eur Radiol* 2004;14:59–72 CrossRef Medline
57. Tanner SF, Cornette L, Ramenghi LA, et al. **Cerebral perfusion in infants and neonates: preliminary results obtained using dynamic susceptibility contrast enhanced magnetic resonance imaging.** *Arch Dis Child Fetal Neonatal Ed* 2003;88:F525–30 CrossRef Medline
58. Wintermark P, Moessinger AC, Gudinchet F, et al. **Perfusion-weighted magnetic resonance imaging patterns of hypoxic-ischemic encephalopathy in term neonates.** *J Magn Reson Imaging* 2008;28:1019–25 CrossRef Medline
59. Wintermark P, Moessinger AC, Gudinchet F, et al. **Temporal evolution of MR perfusion in neonatal hypoxic-ischemic encephalopathy.** *J Magn Reson Imaging* 2008;27:1229–34 CrossRef Medline
60. Varela M, Groves AM, Arichi T, et al. **Mean cerebral blood flow measurements using phase contrast MRI in the first year of life.** *NMR Biomed* 2012;25:1063–72 CrossRef Medline
61. Benders MJ, Hendrikse J, De Vries LS, et al. **Phase-contrast magnetic resonance angiography measurements of global cerebral blood flow in the neonate.** *Pediatr Res* 2011;69:544–47 CrossRef Medline
62. Ferré JC, Bannier E, Raoult H, et al. **Arterial spin labeling (ASL) perfusion: techniques and clinical use.** *Diagn Interv Imaging* 2013;94:1211–23 CrossRef Medline
63. Alsop DC, Detre JA, Golay X, et al. **Recommended implementation of arterial spin-labeled perfusion MRI for clinical applications: a consensus of the ISMRM perfusion study group and the European consortium for ASL in dementia.** *Magn Reson Med* 2015;73:102–16 CrossRef Medline
64. Boudes E, Gilbert G, Leppert IR, et al. **Measurement of brain perfusion in newborns: pulsed arterial spin labeling (PASL) versus pseudo-continuous arterial spin labeling (pCASL).** *Neuroimage Clin* 2014;6:126–33 CrossRef Medline
65. Wang J, Licht DJ, Jahng G-H, et al. **Pediatric perfusion imaging using pulsed arterial spin labeling.** *J Magn Reson Imaging* 2003;18:404–13 CrossRef Medline
66. Madan N, Grant PE. **MR perfusion imaging in pediatrics.** In: Barker PB, Golay X, Zaharchuk G, eds. *Clinical Perfusion MRI: Techniques and Applications.* Cambridge: Cambridge University Press; 2013:326–48
67. Kehrer M, Blumenstock G, Ehehalt S, et al. **Development of cerebral blood flow volume in preterm neonates during the first two weeks of life.** *Pediatr Res* 2005;58:927–30 CrossRef Medline
68. Ferré JC, Petr J, Barillot C, et al. **Optimal individual inversion time in brain arterial spin labeling perfusion magnetic resonance imaging: correlation with carotid hemodynamics measured with cine phase-contrast magnetic resonance imaging.** *J Comput Assist Tomogr* 2013;37:247–51 CrossRef Medline
69. Wu WC, St. Lawrence KS, Licht DJ, et al. **Quantification issues in arterial spin labeling perfusion magnetic resonance imaging.** *Top Magn Reson Imaging* 2010;21:65–73 CrossRef Medline
70. Varela M, Hajnal JV, Petersen ET, et al. **A method for rapid in vivo measurement of blood T1.** *NMR Biomed* 2011;24:80–88 CrossRef Medline
71. Miranda MJ, Olofsson K, Sidaros K. **Noninvasive measurements of regional cerebral perfusion in preterm and term neonates by magnetic resonance arterial spin labeling.** *Pediatr Res* 2006;60:359–63 CrossRef Medline
72. De Vis JB, Petersen ET, de Vries LS, et al. **Regional changes in brain perfusion during brain maturation measured non-invasively with arterial spin labeling MRI in neonates.** *Eur J Radiol* 2013;82:538–43 CrossRef Medline
73. Duncan AF, Caprihan A, Montague EQ, et al. **Regional cerebral blood flow in children from 3 to 5 months of age.** *AJNR Am J Neuroradiol* 2014;35:593–98 CrossRef Medline
74. Wintermark P, Hansen A, Gregas MC, et al. **Brain perfusion in asphyxiated newborns treated with therapeutic hypothermia.** *AJNR Am J Neuroradiol* 2011;32:2023–29 CrossRef Medline
75. Pienaar R, Paldino MJ, Madan N, et al. **A quantitative method for correlating observations of decreased apparent diffusion coefficient with elevated cerebral blood perfusion in newborns presenting cerebral ischemic insults.** *Neuroimage* 2012;63:1510–18 CrossRef Medline
76. Massaro AN, Bouyssi-Kobar M, Chang T, et al. **Brain perfusion in encephalopathic newborns after therapeutic hypothermia.** *AJNR Am J Neuroradiol* 2013;34:1649–55 CrossRef Medline
77. De Vis JB, Hendrikse J, Petersen ET, et al. **Arterial spin-labelling perfusion MRI and outcome in neonates with hypoxic-ischemic encephalopathy.** *Eur Radiol* 2015;25:113–21 CrossRef Medline

“Arterial spin labeling in clinical pediatric imaging. DII 2016”

Diagnostic and Interventional Imaging (2016) **97**, 151—158

REVIEW /*Neuroradiology*

Arterial spin labeling in clinical pediatric imaging

M. Proisy[a,b,*], **B. Bruneau**[a], **C. Rozel**[a], **C. Tréguier**[a], **K. Chouklati**[a], **L. Riffaud**[c], **P. Darnault**[a], **J.-C. Ferré**[b,d]

[a] *Department of Radiology, hôpital Sud, CHU de Rennes, 16, boulevard de Bulgarie, BP 90347, 35203 Rennes cedex 2, France*
[b] *Inserm VisAGeS unité/projet U746, UMR 6074, Irisa, université Rennes 1, 35043 Rennes cedex, France*
[c] *Department of Pediatric Neurosurgery, CHU de Rennes, 2, rue Henri-Le-Guillou, 35033 Rennes cedex 9, France*
[d] *Department of Radiology, hôpital Pontchaillou, CHU de Rennes, 2, rue Henri-Le-Guilloux, 35033 Rennes cedex 9, France*

KEYWORDS
Arterial spin labeling;
Children;
Brain perfusion;
MRI

Abstract Arterial spin labeling (ASL) perfusion-weighted magnetic resonance imaging is the only approach that enables direct and non-invasive quantitative measurement of cerebral blood flow in the brain regions without administration of contrast material and without radiation. ASL is thus a promising perfusion imaging method for assessing cerebral blood flow in the pediatric population. Concerning newborns, there are current limitations because of their smaller brain size and lower brain perfusion. This article reviews and illustrates the use of ASL in pediatric clinical practice and discusses emerging cerebral perfusion imaging applications for children due to the highly convenient implementation of the ASL sequence.

Many approaches exist to measure brain perfusion such as positron emission tomography (PET), dynamic susceptibility contrast magnetic resonance imaging (DSC MRI) and computed tomography perfusion (CTP). However, these techniques require administration of contrast material and/or exposure to ionizing radiation. Non-invasive and non-radiating

Abbreviations: AIS, Arterial ischemic stroke; ASL, Arterial spin labeling; CASL, continuous ASL; PASL, pulsed ASL; pCASL, pseudo-continuous ASL; ATT, Arterial transit time; AVM, Arteriovenous malformation; CBF, Cerebral blood flow; CTP, Computed tomography perfusion; DSC, Dynamic susceptibility contrast; DWI, Diffusion-weighted imaging; MRI, Magnetic resonance imaging; PC MRI, Phase contrast MRI; PET, Positron emission tomography; PLD, Post labeling delay; PRES, Posterior reversible encephalopathy syndrome; SNR, Signal-to-noise ratio; T1b, Relaxation time constant of arterial blood.

* Corresponding author at: Department of Radiology, hôpital Sud, CHU de Rennes, 16, boulevard de Bulgarie, BP 90347, 35203 Rennes cedex 2, France.
E-mail address: maia.proisy@chu-rennes.fr (M. Proisy).

http://dx.doi.org/10.1016/j.diii.2015.09.001

methods such as Doppler ultrasonography and phase-contrast MRI (PC MRI) do not provide regional brain perfusion measurements, but only an overview based on cervical arterial flow. The emergence of arterial spin labeling (ASL) as a technique that provides both non-invasive and regional cerebral blood flow quantification offers new opportunities for assessing brain perfusion in neonates and children. ASL is currently moving from the field of research into that of routine clinical practice. A few studies have been conducted in pediatric patients and new clinical applications are emerging. These all make ASL a promising perfusion imaging method for assessing cerebral blood flow (CBF) in children [1].

The purpose of this article was to review and illustrate the use of ASL in pediatric clinical practice.

Technical principles

ASL is a non-invasive technique that uses endogenous blood water as a freely diffusible tracer. A previous article in this journal presents the principles of the technique [2]. The protons in arterial blood are magnetically labeled with a radiofrequency inversion pulse applied below the imaging slice in the neck vessels. Several labeling methods exist including continuous ASL (CASL), pulsed ASL (PASL) and pseudo-continuous ASL (pCASL). In CASL, a long flow-induced inversion pulse is applied. In PASL a short inversion pulse is applied to a larger region of the neck. pCASL is a hybrid method that utilizes a train of short RF pulses to mimic the effect of CASL. Because of several benefits the use of pCASL labeling is now recommended [3].

A labeled image is acquired after a minimum transit time for the labeled spins to reach the imaging slice, known as the inversion time or post labeling delay (PLD) (Fig. 1). A control image is acquired without prior labeling. Subtraction of the two images generates a perfusion-weighted image. Because the signal difference is only 0.5—1.5% of the full signal, multiple repetitions are needed to improve the signal-to-noise ratio (SNR). Subsequently, in order to obtain a quantitative perfusion map a quantitative model is required to calculate the ratio between the perfusion-weighted image signal and CBF. A number of parameters influence CBF quantification such as labeling efficiency, longitudinal magnetization of arterial blood, arterial blood and tissue relaxation time constant (T1b and T1t), arterial transit time (ATT), and blood-tissue partition coefficient. These parameters can be assumed or measured and may differ from adult literature values.

Initially proposed in 1996, CBF quantification using the ASL method has been improved with the addition of multiple parameters [4]. This method now has several research and clinical applications in adults [5,6]. However, a number of studies have demonstrated the challenges of optimizing ASL acquisition for subjects across a wide range of vascular and perfusion characteristics [3].

Given the non-invasiveness of the technique, which involves neither venous cannulation nor radiation, it is particularly suitable for children. In addition, ASL offers within-session repeatability and achieves absolute quantification of CBF.

The main drawback of the ASL method is a low SNR. However, there is a physiological improvement in SNR in children compared to healthy adults, mainly due to a higher

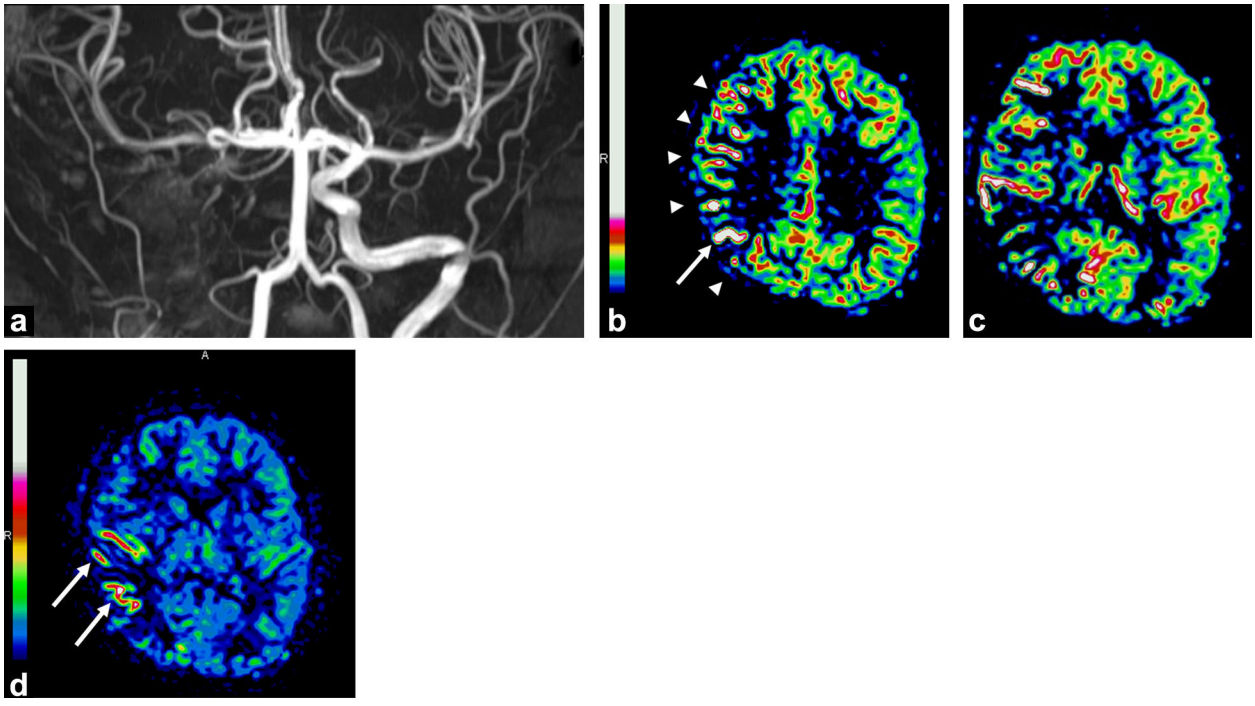

Figure 1. 11-year-old boy with recent surgical right internal carotid occlusion. MR angiogram shows right internal carotid occlusion (a). DWI shows no evidence of ischemia. ASL maps (b—d) show the transit time effect with pseudohypoperfusion of the right hemisphere (arrowheads) as well as linear high signal intensity representing slow flow in cortical vessels (arrows).

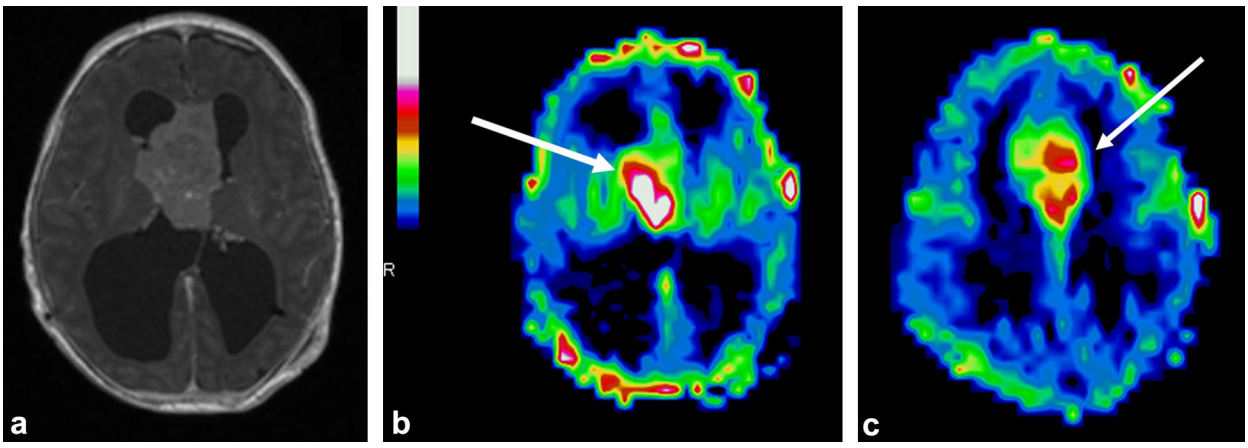

Figure 2. 3-day-old boy with hydrocephalus secondary to an interventricular tumor. T1-weighted MR image in the transverse plane after IV of gadolinium chelate shows an interventricular tumor (a). ASL perfusion maps (b and c) reveal hyperperfusion of the tumor with a ratio of 2.5 between the tumor and cortical perfusion. Tumor biopsy reveals high grade astrocytoma.

mean CBF and higher blood flow velocity in carotid arteries [6,7]. Indeed it results in reduced relaxation of the labeling effect and reduced transit effect in pediatric perfusion images. Moreover the higher water content of brain in children results in increased equilibrium MR signal and thereby improves pediatric ASL signal through increased tracer concentration and lifetime. Then pediatric perfusion images provides much stronger perfusion signal and provide much stronger delineation of cortical and subcortical structures compared with adult perfusion images [1].

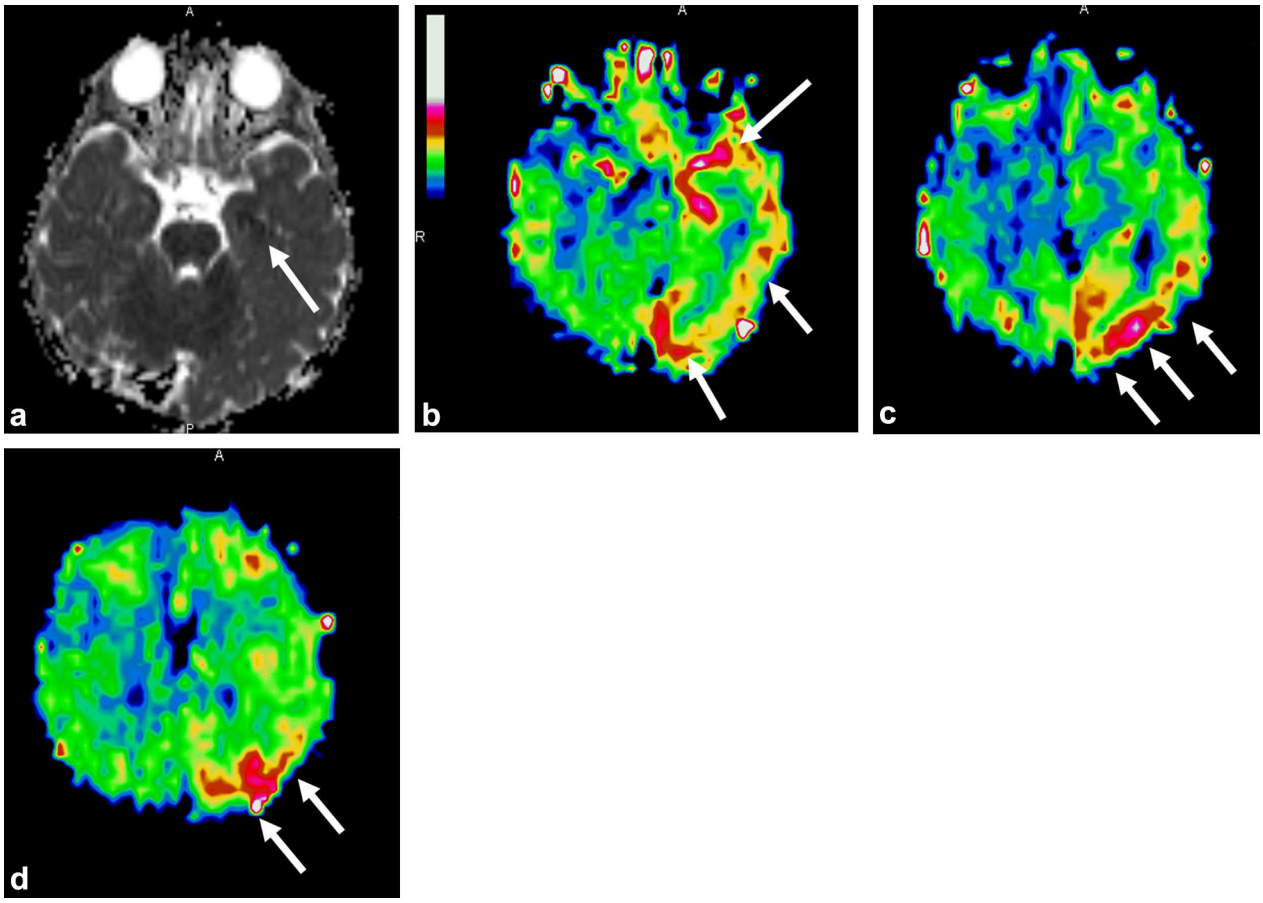

Figure 3. 14-month-old boy presenting with fever, right unilateral clonic seizures and ipsilateral hemiplegia that lasted for more than 1 hour. Postictal EEG showed slow focal and persistent left cerebral hemisphere activity 24 hours after the seizure. MRI performed during the postictal state shows no abnormality on conventional imaging. Apparent diffusion coefficient map (a) reveals restricted focal left hippocampal diffusion (*arrow*). ASL perfusion map (b–d) reveals a larger abnormal area of hyperperfusion in the left temporal and parieto-occipital lobes (*arrows*).

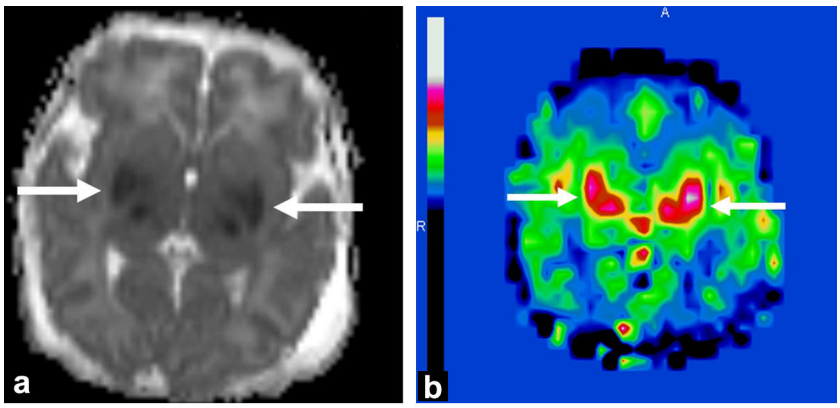

Figure 4. Asphyxiated neonate treated with hypothermia showing basal ganglia injury on MRI obtained on day 3 of life. ADC map (a) shows restricted diffusion in the bilateral thalami and lentiform nuclei (*arrows*). ASL perfusion map (b) reveals higher perfusion within the same areas (*arrows*).

Technical issues in pediatric imaging

Interpretation of perfusion data in children is further complicated by age-related changes (Table 1) and sedation-related changes in CBF. Indeed there is a need for perfusion map templates for healthy children to determine a normal perfusion map with regard to normal age-related changes in cerebral perfusion. CBF has been shown to be very low in neonates and then to rapidly increase during the first 6 month of life [8] and to continue slightly increase to be maximal between 5 and 10 years, according to study and cerebral perfusion imaging techniques [7,9,10] and depending on the cortical region [11]. Then CBF shows a negative correlation with age decreasing rapidly during adolescence

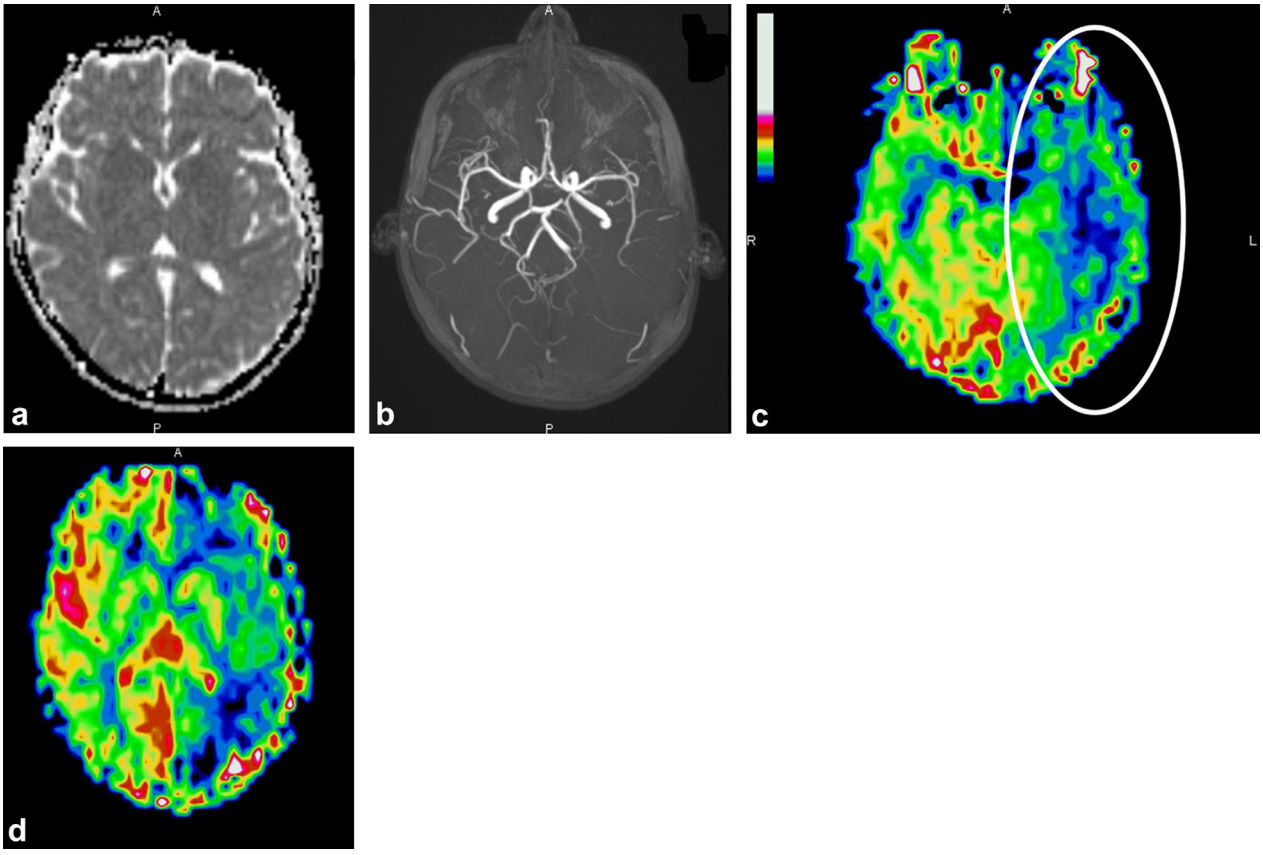

Figure 5. 12-year-old boy with no prior history of cephalalgia presenting a visual impairment followed by acute left temporal cephalalgia. Neurological examination reveals distal right arm deficit and paraesthesia and aphasia. Conventional MRI performed 10 hours after the onset of symptoms was normal with no restricted diffusion on the ADC map (a) and MR angiography was also normal (b). ASL perfusion map (c and d) was the single abnormal sequence, and showed hypoperfusion in the left temporal and parietal cerebral areas (*circle*). A diagnosis of first migraine attack with aura was made with total resolution of symptoms after ibuprofen administration.

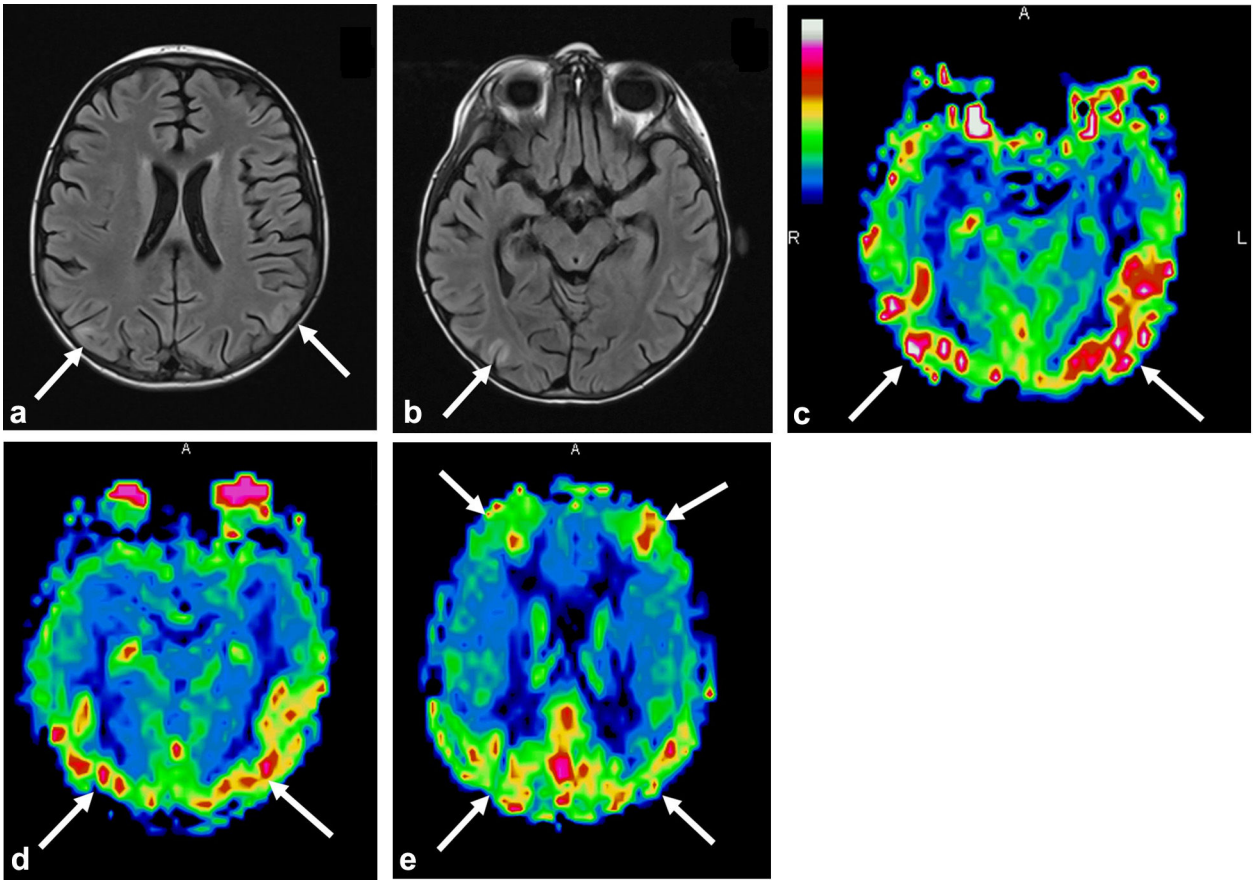

Figure 6. 9-year-old boy with a history of undetermined severe vascularitis presenting with seizures and hypertension: a and b: FLAIR images in the transverse plane demonstrate typical posterior involvement of posterior reversible encephalopathy syndrome with focal areas of high cortical signal intensity (*arrows*); c—e: ASL perfusion map shows more extensive hyperperfusion within the same areas (*arrows*).

until a plateau is reached around 25 to 30 years [7,12,13]. However, to our knowledge, there are no studies that have reported ASL CBF measurement in children with a specific age range of 5 month to 6 years.

A substantial proportion of pediatric patients receive anesthesia or sedation for MRI, which may have impact on cerebral perfusion [14]. Given general unknown effects of sedatives on ASL imaging, sedation status remains an important consideration in pediatric imaging.

Another point is the lack of standardization of acquisition parameters and image processing methods. Standardization of acquisition and post-processing methods is paramount to enable ASL to mature from a experimental method to a widespread clinical tool [15]. In clinical practice, CBF maps are automatically generated by the manufacturer workstation with assumed or measured quantification parameters. However, it is not clear whether values estimated in adults and applied to a neonatal and pediatric population allow

Table 1 Age-related evolution of CBF values in grey and white matter using ASL technique.

Age range	Global CBF	Mean GM CBF	Mean WM CBF	Labelling method	References
Healthy term neonate	13—27	16 (cortex) 30 (basal ganglia)	10	PASL pCASL pCASL	Miranda et al., 2006 [9], Pienaar et al., 2012 [10], Massaro et al., 2013 [11]
3—5 months	24—56	25—60	15—30	PASL PASL	Duncan et al., 2014 [12], Varela et al., 2015 [13]
4—12 years		97 ± 5	26 ± 1	CASL	Biagi et al., 2007 [7]
7—17 years	74	82.4	41.5	pCASL	Jain et al., 2012 [14]
13—19 years		79 ± 3	22 ± 1	CASL	Biagi et al., 2007 [7]
Up to 20 years		58 ± 4	20 ± 1	CASL	Biagi et al., 2007 [7]

CBF: Cerebral Blood Flow values in mL/100 g/minute; GM: grey matter; WM: white matter.

population-specific rather than subject-specific values to be used. Then pediatric specific standardization is needed to provide reproducible and comparable quantitative measurements of cerebral perfusion. As an example Varela et al. have shown that the accuracy of ASL CBF measurements in infants is improved with the use of infant-specific auxiliary parameters, particularly blood and tissue T1, which are much more variable in the imaged infants than in adults [16]. Another study demonstrated the accuracy and longitudinal repeatability of pCASL sequence in a sample of 22 children aged from 7 to 17 years with particular attention paid to incorporating developmental changes in blood T1 [17].

Clinical applications

Pediatric neurovascular diseases

Arterial ischemic stroke

Brain infarct may show both hyperperfusion and hypoperfusion during the acute stage in children. In 10 children with arterial ischemic stroke during the acute stage, Chen et al. have reported that CBF maps showed 5 lesions with hypoperfusion, 2 with hyperperfusion, 2 with normal perfusion and a complex lesion in one patient [18]. Perfusion-diffusion mismatch is a central concept in the imaging of ischemic stroke in adults [19]. However, post-ischemic hyperperfusion in stroke is well known. Moreover, the etiology of arterial ischemic stroke differs between adults and children and clots are less frequent in children than in adults. Other causes of focal autoregulatory dysfunction include posterior reversible encephalopathy syndrome (PRES) with initial vasoconstriction and hypoperfusion followed by rebound hyperperfusion [6].

Moyamoya disease

A good correlation between ASL perfusion-weighted MRI and $H_2[^{15}O]$-PET [20] and DSC MRI [21] has been shown in children with Moyamoya disease. However, one of the main limitations of the ASL technique is that the time between labeling in the feeding arteries and the arrival of labeled blood in tissue (i.e., ATT) can have a significant effect on the ASL signal. In cerebrovascular disorders such as Moyamoya disease, the ATT may be prolonged leading to focal intravascular signal artifacts. Moreover, CBF may be underestimated in regions with delayed arterial transit time. Multi-delay ASL can improve CBF quantification and could be used as a prognostic imaging biomarker in patients with Moyamoya disease. By incorporating delayed ATT into the calculation of CBF, multi-delay ASL is able to provide imaging consistent with CT perfusion in Moyamoya disease [22]. Yet artefacts may be useful as they can predict the presence and intensity of the collateral arterial network in Moyamoya disease [23].

Sickle cell disease

Several studies have investigated the value of ASL for measuring regional CBF in children with sickle cell disease in order to identify the existence of altered CBF in areas unaffected on conventional images [24]. There is a need for a reliable screening method to identify patients at risk of silent infarct. However, it is important to be aware of the difficulties involved in interpreting CBF asymmetries as reported in several studies. There are technical issues with ASL in children with sickle cell disease. For example, chronic anemia and compensatory increases in blood velocity and flow reduce the arterial transit time and labeling efficiency. Moreover, hematocrit levels affect the longitudinal relaxation time of arterial blood and this affects quantification. Gevers et al. took these technical aspects into account and did not find any correlation between CBF asymmetries and silent infarct in 12 children [25]. Care should be taken in interpreting ASL-CBF measurements in sickle cell disease patients.

Vascular malformations

One study demonstrates nidus location and patency in a cohort of 21 pediatric patients with brain arteriovenous malformation. This paper shows that the mean CBF in the arteriovenous malformation is twice those of normal contralateral cortical CBF [26]. Moreover quantification of nidal CBF may enable objective monitoring of arteriovenous malformation obliteration after treatment. Another related technique is unenhanced time-resolved spin-labeled MR angiographic imaging that has been shown to be a reliable clinical tool for cerebral arteriovenous malformation characterization in adult population [27,28].

Pediatric brain tumors

A few studies have addressed the issue of perfusion of brain tumors in pediatric patients (Fig. 2). Tumor evaluation with ASL has been studied, and correlations between flow and tumor grade have been established. ASL may play a complementary role to DSC MRI for investigation of pediatric brain tumors given that it can provide information on capillary perfusion [29]. Yeom et al. have studied the main ASL perfusion patterns among various pathologic types of brain tumors in a series of 54 children [30]. As found in adults, the maximum relative tumor blood flow (rTBF) of high-grade tumors was significantly higher than that of low-grade tumors. However, rTBF cannot separate high-grade from low-grade tumor at the individual level. There was no correlation between rTBF values and patterns of contrast enhancement. Moreover, posterior fossa tumors should be interpreted with caution due to posterior fossa susceptibility artifacts.

Another study focused on choroid plexus neoplasms in 13 children (7 papillomas and 6 carcinomas) [31]. This study shows that relative CBF values were significantly higher in carcinomas than in papillomas when using ASL. ASL is therefore a promising technique to discriminate between choroid plexus carcinomas and papillomas, which is difficult with conventional imaging techniques.

Epilepsy

Localized areas of decreased CBF have been found in children with focal cortical dysplasia during the interictal period [32]. This hypoperfusion was associated with structural MRI abnormalities and PET hypometabolism in 5/6 cases. CBF was significantly lower in the lesion than in the normal cortex [32]. One paper reported multiple hypo perfused areas

correlating with MRI tubers and ^{18}FDG hypometabolic areas in three patients with tuberous sclerosis [33]. On the other hand, ictal cortical hyperperfusion is believed to be a useful marker for identifying epileptogenic areas and has been observed with ASL imaging [34]. ASL imaging in a 25-year-old man with partial epilepsy status showed strong focal hyperperfusion of the region corresponding to the anatomical and physiological epileptic focus and also provided a clear contrast with the relative hypoperfusion in the interictal state [34]. The ASL sequence could be added at the end of the morphological MRI for epilepsy investigation and this would provide non-invasive functional information and help to detect the pathological area (Fig. 3).

Hydrocephalus

The distinction between ventriculomegaly and hydrocephalus with increased intracranial pressure is important. Yeom et al. were the first to assess cerebral perfusion using ASL in children with hydrocephalus [35]. Patients with symptomatic hydrocephalus had lower CBF than healthy controls for all brain regions. The median CBF increased after alleviation of obstructive hydrocephalus in all subjects. The results were consistent with another study reported using nuclear medicine methods [36]. Thus ASL measurement of CBF may be used as a potential non-invasive method to assess intracranial pressure, although additional data are needed.

Neonatal perfusion imaging

Brain perfusion plays a key role in the pathogenesis of brain damage in high-risk neonates (both preterm and full-term asphyxiated infants) (Fig. 4). It is challenging to perform ASL MRI in neonates due both to their low physiological baseline CBF compared to older children and adults and the method's low SNR. Technical adjustments to imaging parameters are needed to address the fundamental differences between pediatric and adult populations. Moreover, ASL is highly sensitive to motion. Yet some studies have been conducted in asphyxiated neonates, showing an early hyperperfusion in brain regions subsequently exhibiting injury [37]. Regions with low ADC values are highly correlated with increased co-located regions of increased ASL CBF intensity in 9 newborns aged between 0 and 3 days presenting with ischemia [38]. Moreover, ASL may be used as a spectroscopy biomarker to predict neurodevelopmental outcome. De Vis et al. have shown that a higher ASL perfusion value in 28 neonates with hypoxic ischemic encephalopathy was associated with a worse neurodevelopmental outcome at 9 or 18 months of age [39]. Technical and image processing improvements are needed to extend the use of ASL to neonates.

Emerging applications

ASL imaging can easily be performed during conventional MRI procedures without any side effects at the penalty of a longer examination time of approximately 5 minutes. Cerebral perfusion may therefore be assessed in numerous clinical applications (Figs. 5 and 6). By way of example, the use of ASL MRI can not only rule out differential diagnosis but also provide evidence for positive diagnosis of migraine by showing focal CBF abnormalities whereas conventional MRI is normal [40]. Another example is the use of ASL in metabolic disorders such as in stroke-like episodes of MELAS, showing hyperperfusion in the acute phase [41]. Another field of research is the investigation of cerebral perfusion before and after surgery in neurosurgical pathologies such as craniosynostosis and arachnoid cyst, as a better understanding of the physiopathology of these diseases and the functional impact of surgery can be gained.

Conclusion

The main advantage of ASL perfusion-weighted MR sequences in pediatric practice is their radiation-free and non-invasive nature. Moreover, there is a physiological improvement in SNR in children compared to healthy adults owing to a greater mean cerebral blood flow. Concerning newborns, there are current limitations because of their smaller brain size and lower brain perfusion. There are many emerging cerebral perfusion imaging applications for children due to the highly convenient implementation of the ASL sequence.

Acknowledgements

This work was carried out with the support of Société française de radiologie (2012 Research Grant). The authors thank Mrs. Tracey Westcott for editorial assistance.

Disclosure of interest

The authors declare that they have no conflicts of interest concerning this article.

References

[1] Wang J, Licht DJ. Pediatric perfusion MR imaging using arterial spin labeling. Neuroimaging Clin N Am 2006;16:149—67.
[2] Ferré JC, Bannier E, Raoult H, Mineur G, Carsin-Nicol B, Gauvrit JY. Arterial spin labeling (ASL) perfusion: techniques and clinical use. Diagn Interv Imaging 2013;94:1211—23.
[3] Alsop DC, Detre JA, Golay X, Günther M, Hendrikse J, Hernandez-Garcia L, et al. Recommended implementation of arterial spin-labeled perfusion MRI for clinical applications: A consensus of the ISMRM perfusion study group and the European consortium for ASL in dementia. Magn Reson Med 2014, http://dx.doi.org/10.1002/mrm.25197.
[4] Buxton RB, Frank LR, Wong EC, Siewert B, Warach S, Edelman RR. A general kinetic model for quantitative perfusion imaging with arterial spin labeling. Magn Reson Med 1998;40:383—96.
[5] Deibler AR, Pollock JM, Kraft RA, Tan H, Burdette JH, Maldjian JA. Arterial spin-labeling in routine clinical practice, part 2: hypoperfusion patterns. AJNR Am J Neuroradiol 2008;29:1235—41.
[6] Deibler AR, Pollock JM, Kraft RA, Tan H, Burdette JH, Maldjian JA. Arterial spin-labeling in routine clinical practice, part 3: hyperperfusion patterns. AJNR Am J Neuroradiol 2008;29:1428—35.
[7] Biagi L, Abbruzzese A, Bianchi MC, Alsop DC, Del Guerra A, Tosetti M. Age dependence of cerebral perfusion assessed by

magnetic resonance continuous arterial spin labeling. J Magn Reson Imaging 2007;25:696—702.
[8] Duncan AF, Caprihan A, Montague EQ, Lowe J, Schrader R, Phillips JP. Regional cerebral blood flow in children from 3 to 5 months of age. AJNR Am J Neuroradiol 2014;35:593—8.
[9] Wintermark M, Lepori D, Cotting J, Roulet E, van Melle G, Meuli R, et al. Brain perfusion in children: evolution with age assessed by quantitative perfusion computed tomography. Pediatrics 2004;113:1642—52.
[10] Chiron C, Raynaud C, Mazière B, Zilbovicius M, Laflamme L, Masure M-C, et al. Changes in regional cerebral blood flow during brain maturation in children and adolescents. J Nucl Med 1992;33:696—703.
[11] Taki Y, Hashizume H, Sassa Y, Takeuchi H, Wu K, Asano M, et al. Correlation between gray matter density-adjusted brain perfusion and age using brain MR images of 202 healthy children. Hum Brain Mapp 2011;32:1973—85.
[12] Hales PW, Kawadler JM, Aylett SE, Kirkham FJ, Clark CA. Arterial spin labeling characterization of cerebral perfusion during normal maturation from late childhood into adulthood: normal ''reference range'' values and their use in clinical studies. J Cereb Blood Flow Metab 2014;34:776—84.
[13] Avants BB, Duda JT, Kilroy E, Krasileva K, Jann K, Kandel BT, et al. The pediatric template of brain perfusion. Sci Data 2015;2:150003.
[14] Harreld JH, Helton KJ, Kaddoum RN, Reddick WE, Li Y, Glass JO, et al. The effects of propofol on cerebral perfusion MRI in children. Neuroradiology 2013;55:1049—56.
[15] Golay X, Guenther M. Arterial spin labelling: final steps to make it a clinical reality. Magma N Y N 2012;25:79—82.
[16] Varela M, Petersen ET, Golay X, Hajnal JV. Cerebral blood flow measurements in infants using look-locker arterial spin labeling. J Magn Reson Imaging 2015;41:1591—600.
[17] Jain V, Duda J, Avants B, Giannetta M, Xie SX, Roberts T, et al. Longitudinal reproducibility and accuracy of pseudo-continuous arterial spin-labeled perfusion MR imaging in typically developing children. Radiology 2012;263:527—36.
[18] Chen J, Licht DJ, Smith SE, Agner SC, Mason S, Wang S, et al. Arterial spin labeling perfusion MRI in pediatric arterial ischemic stroke: initial experiences. J Magn Reson Imaging 2009;29:282—90.
[19] Gory B, Riva R, Turjman F. Endovascular treatment in patients with acute ischemic stroke: technical aspects and results. Diagn Interv Imaging 2014;95:561—8.
[20] Goetti R, Warnock G, Kuhn FP, Guggenberger R, O'Gorman R, Buck A, et al. Quantitative cerebral perfusion imaging in children and young adults with Moyamoya disease: comparison of arterial spin-labeling-MRI and $H_2[^{15}O]$-PET. AJNR Am J Neuroradiol 2014;35:1022—8.
[21] Goetti R, O'Gorman R, Khan N, Kellenberger CJ, Scheer I. Arterial spin labelling MRI for assessment of cerebral perfusion in children with moyamoya disease: comparison with dynamic susceptibility contrast MRI. Neuroradiology 2013;55:639—47.
[22] Wang R, Yu S, Alger JR, Zuo Z, Chen J, Wang R, et al. Multi-delay arterial spin labeling perfusion MRI in moyamoya disease—comparison with CT perfusion imaging. Eur Radiol 2014;24:1135—44.
[23] Zaharchuk G, Do HM, Marks MP, Rosenberg J, Moseley ME, Steinberg GK. Arterial spin-labeling MRI can identify the presence and intensity of collateral perfusion in patients with moyamoya disease. Stroke 2011;42:2485—91.
[24] Oguz KK, Golay X, Pizzini FB, Freer CA, Winrow N, Ichord R, et al. Sickle cell disease: continuous arterial spin-labeling perfusion MR imaging in children. Radiology 2003;227:567—74.
[25] Gevers S, Nederveen AJ, Fijnvandraat K, van den Berg SM, van Ooij P, Heijtel DF, et al. Arterial spin labeling measurement of cerebral perfusion in children with sickle cell disease. J Magn Reson Imaging 2012;35:779—87.
[26] Blauwblomme T, Naggara O, Brunelle F, Grévent D, Puget S, Di Rocco F, et al. Arterial spin labeling magnetic resonance imaging: toward noninvasive diagnosis and follow-up of pediatric brain arteriovenous malformations. J Neurosurg Pediatr 2015;15:451—8.
[27] Raoult H, Bannier E, Maurel P, Neyton C, Ferré J-C, Schmitt P, et al. Hemodynamic quantification in brain arteriovenous malformations with time-resolved spin-labeled magnetic resonance angiography. Stroke 2014;45:2461—4.
[28] Raoult H, Bannier E, Robert B, Barillot C, Schmitt P, Gauvrit JY. Time-resolved spin-labeled MR angiography for the depiction of cerebral arteriovenous malformations: a comparison of techniques. Radiology 2014;271:524—33.
[29] Madan N, Grant PE. MR perfusion imaging in pediatrics. In: Barker PB, Golay X, Zaharchuk G, editors. Clinical perfusion MRI: techniques and applications. Cambridge, UK: Cambridge University Press; 2013. p. 326—48.
[30] Yeom KW, Mitchell LA, Lober RM, Barnes PD, Vogel H, Fisher PG, et al. Arterial spin-labeled perfusion of pediatric brain tumors. AJNR Am J Neuroradiol 2014;35:395—401.
[31] Dangouloff-Ros V, Grevent D, Pagès M, Blauwblomme T, Calmon R, Elie C, et al. Choroid plexus neoplasms: toward a distinction between carcinoma and papilloma using arterial spin-labeling. AJNR Am J Neuroradiol 2015, http://dx.doi.org/10.3174/ajnr.A4332.
[32] Blauwblomme T, Boddaert N, Chémaly N, Chiron C, Pages M, Varlet P, et al. Arterial Spin labeling MRI: a step forward in non-invasive delineation of focal cortical dysplasia in children. Epilepsy Res 2014;108:1932—9.
[33] Wissmeyer M, Altrichter S, Pereira VM, Viallon M, Federspiel A, Seeck M, et al. Arterial spin-labeling MRI perfusion in tuberous sclerosis: correlation with PET. J Neuroradiol 2010;37:127—30.
[34] Oishi M, Ishida G, Morii K, Hasegawa K, Sato M, Fujii Y. Ictal focal hyperperfusion demonstrated by arterial spin-labeling perfusion MRI in partial epilepsy status. Neuroradiology 2012;54:653—6.
[35] Yeom KW, Lober RM, Alexander A, Cheshier SH, Edwards MSB. Hydrocephalus decreases arterial spin-labeled cerebral perfusion. AJNR Am J Neuroradiol 2014;35:1433—9.
[36] Shinoda M, Yamaguchi T, Tanaka Y, Sato O, Kobayashi S, Suzuki Y. Single photon emission computerized tomography in childhood hydrocephalus. Childs Nerv Syst 1992;8:219—21.
[37] Wintermark P, Hansen A, Gregas MC, Soul J, Labrecque M, Robertson RL, et al. Brain perfusion in asphyxiated newborns treated with therapeutic hypothermia. AJNR Am J Neuroradiol 2011;32:2023—9.
[38] Pienaar R, Paldino MJ, Madan N, Krishnamoorthy KS, Alsop DC, Dehaes M, et al. A quantitative method for correlating observations of decreased apparent diffusion coefficient with elevated cerebral blood perfusion in newborns presenting cerebral ischemic insults. Neuroimage 2012;63:1510—8.
[39] De Vis JB, Hendrikse J, Petersen ET, de Vries LS, van Bel F, Alderliesten T, et al. Arterial spin-labelling perfusion MRI and outcome in neonates with hypoxic-ischemic encephalopathy. Eur Radiol 2015;25:113—21.
[40] Kossorotoff M, Calmon R, Grevent D, Gitiaux C, Desguerre I, Heilbronner C, et al. Arterial spin labeling (ASL) magnetic resonance imaging in acute confusional migraine of childhood. J Neuroradiol 2013;40:142—4.
[41] Wang Z, Xiao J, Xie S, Zhao D, Liu X, Zhang J, et al. MR evaluation of cerebral oxygen metabolism and blood flow in stroke-like episodes of MELAS. J Neurol Sci 2012;323:173—7.

Chapitre 2 – Technique ASL

Principes techniques

Le principe général de l'ASL repose sur la réalisation de deux acquisitions : une acquisition avec marquage magnétique des protons artériels (par une impulsion radiofréquence au niveau des vaisseaux du cou), et une acquisition de contrôle. La soustraction de l'acquisition avec marquage et de l'acquisition contrôle permet d'obtenir une image pondérée en perfusion (Detre et al., 1992; Williams et al., 1992) (Fig. 1).

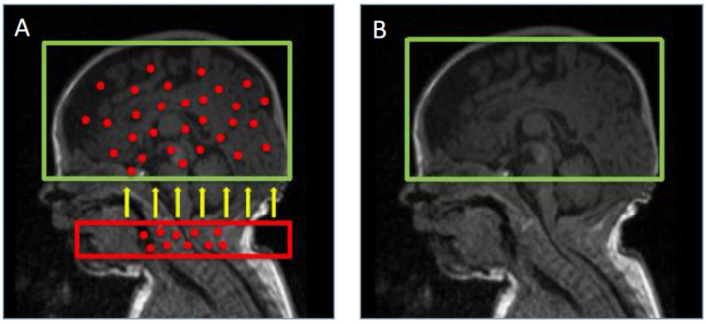

Figure 1 : Schéma représentant le principe général de la séquence ASL. A : acquisition de l'image marquée. B : Acquisition de l'image contrôle.

Marquage des protons

Il existe deux principales méthodes de marquage : le marquage continu (CASL) et le marquage pulsé (PASL). La CASL est la méthode de marquage développée initialement, consistant en une impulsion radiofréquence continue et sélective, appliquée au niveau des vaisseaux du cou. La PASL utilise des impulsions radiofréquences très courtes sur une plus large zone de marquage. Le marquage pseudo-continu (pCASL) est une méthode hybride qui utilise un train d'impulsions radiofréquence de très courte durée. L'avantage de la séquence de pCASL est un meilleur SNR que la PASL, avec une meilleure efficacité de marquage, et une mise en œuvre plus facile que la CASL. C'est actuellement la méthode de choix (Alsop et al., 2015).

L'image marquée est obtenue après un délai suffisant pour permettre aux protons marqués d'atteindre la zone d'intérêt (boite d'acquisition sur le cerveau). Ce délai est appelé délai post-marquage (PLD = post labeling delay ou TI = Inversion Time selon le type de marquage) (Fig. 2). L'acquisition des images est principalement réalisée en *echo planar imaging* (EPI), mais des séquences 3D ont été développées pour améliorer la qualité des images.

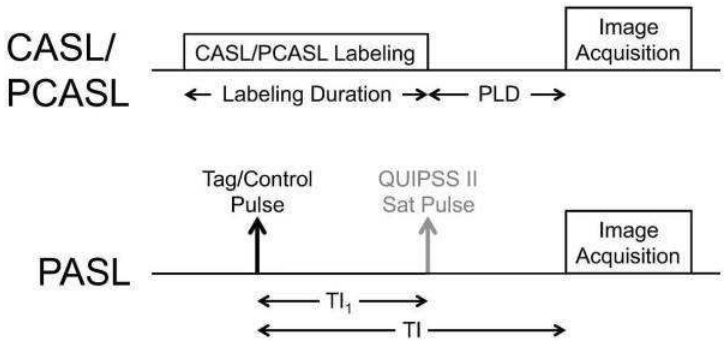

Figure 2: Schéma extrait de (Alsop et al., 2015) représentant le délai entre le marquage et l'acquisition des images pour les séquences de type CASL/PCASL et PASL. Pour la séquence QUIPSS II PASL, TI1 est la durée du bolus et équivalent au temps de marquage de la CASL/PCASL. Le délai post-marquage (PLD) de la CASL/PCASL est équivalent à la quantité (TI-TI1) dans la QUIPSS II PASL.

Obtention de la cartographie de perfusion

La soustraction de l'image contrôle et de l'image marquée donne une image pondérée en perfusion. La différence de signal est de l'ordre de seulement 0.5 – 1.5% du signal total. C'est pourquoi il est nécessaire de répéter plusieurs fois l'acquisition du couple image marquée – image contrôle (plusieurs dizaines de répétitions) afin d'augmenter le rapport signal/bruit. La moyenne des soustractions permet d'obtenir une cartographie de perfusion.

Afin d'obtenir une cartographie de perfusion quantitative du CBF (en mL/100g de tissu/min), il faut appliquer un modèle de quantification à partir de la cartographie pondérée en perfusion (Buxton et al., 1998; Wong et al., 1998) (Fig. 3). Les paramètres qui interviennent dans la quantification du CBF sont la densité de protons des tissus, les temps de relaxation T1 du tissu et du sang marqué ($T1_t$ et $T1_{blood}$), le temps de transit entre la zone de marquage et la zone d'intérêt (PLD ou TI et TI_1)), l'efficacité de marquage (α), le coefficient de partition du cerveau et du sang (λ). Ces paramètres peuvent être mesurés ou estimés, en utilisant des

valeurs de la littérature. Une vigilance particulière doit être portée à cette étape, notamment dans les populations pédiatriques normale et/ou malades, où certains de ces paramètres peuvent être modifiés (De Vis et al., 2014; Gevers et al., 2012).

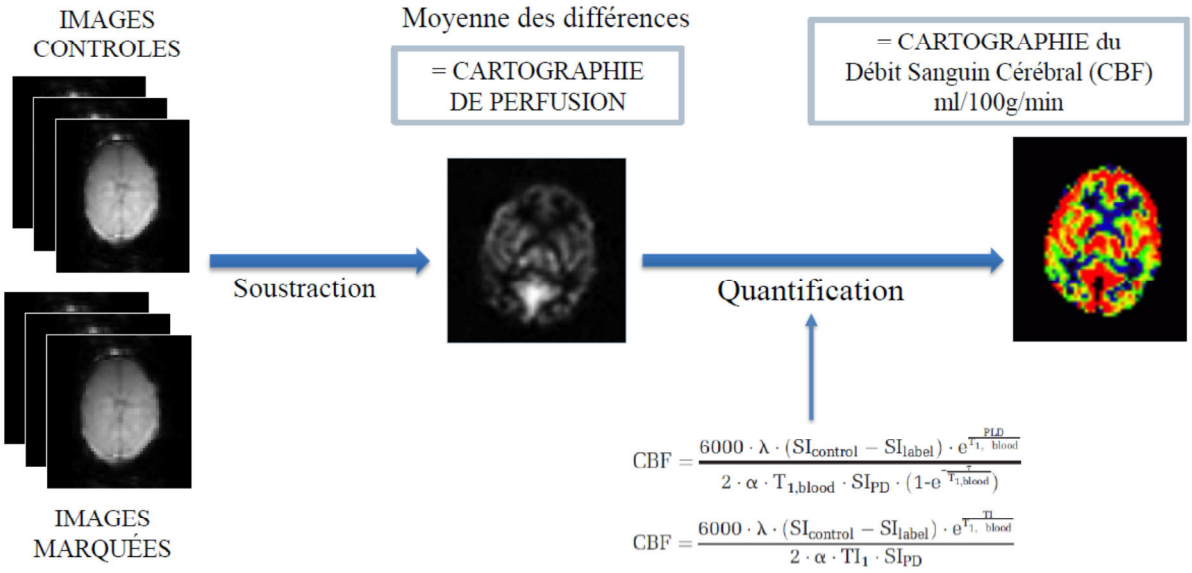

Figure 3: Schéma résumant le principe technique de la séquence de perfusion cérébrale ASL en IRM. Les formules de quantification sont différentes selon qu'il s'agit d'une séquence de pCASL ou PASL (Buxton et al., 1998; Wong et al., 1998). λ représente le coefficient de partition cerveau/sang, $SI_{controle}$ et SI_{label} correspondent à la moyenne du signal des images marquées et des images contrôles, $T1_{blood}$ est le temps de relaxation longitudinal du sang, SI_{PD} est l'intensité du signal d'une image en densité de proton, α est l'efficacité du marquage et τ est la durée du marquage.

Paramètres d'acquisition et de quantification : particularités pédiatriques

1/ Positionnement de la boite ou du plan de marquage

La boite de marquage pour une séquence de PASL est habituellement de 10cm d'épaisseur, adaptée à la taille du cou d'un adulte. Cependant elle est trop recouvrante chez un nouveau-né et descend jusqu'au thorax (Fig. 4). Nous n'avons pas la possibilité de modifier ce paramètre sur notre machine. A notre connaissance il n'existe pas d'étude dans la littérature étudiant l'impact sur la qualité du marquage et des cartographies de perfusion, bien qu'il soit recommandé de l'adapter à la taille de l'enfant (Wang and Licht, 2006).

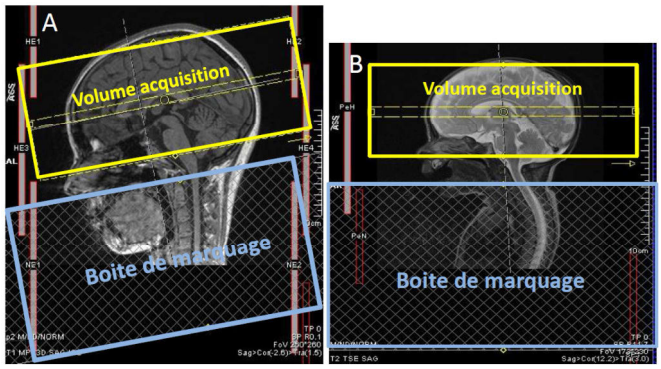

Figure 4 : Images représentant le positionnement de la boite de marquage d'une séquence de PASL chez un enfant (A) et chez un nouveau-né.

Concernant la séquence de pCASL, il s'agit plus d'une adaptation du positionnement du plan de marquage. Effectivement, pour un meilleur marquage le plan doit être perpendiculaire aux troncs supra-aortiques. Pour éviter la réalisation d'une Angio MR pour le positionnement, l'utilisation de critères anatomiques tels que 85mm sous le plan commissure antérieure-commissure postérieure (CA-CP) (Aslan et al., 2010) est utilisé chez l'adulte. Cependant cette mesure n'est pas adaptée aux enfants. Un autre choix est de placer le plan de marquage sous le bord inférieur du cervelet (Dai et al., 2012). L'étude récente d'Ouyang et al. (Ouyang et al., 2017) est une des rares à avoir étudié et détaillé ce paramètre chez des nouveau-nés. Leur choix s'est porté sur le positionnement à la partie inférieure du pont, et non du cervelet, en raison d'un meilleur contraste substance grise - substance blanche et de la réduction des artefacts sur la cartographie de perfusion (Fig. 5).

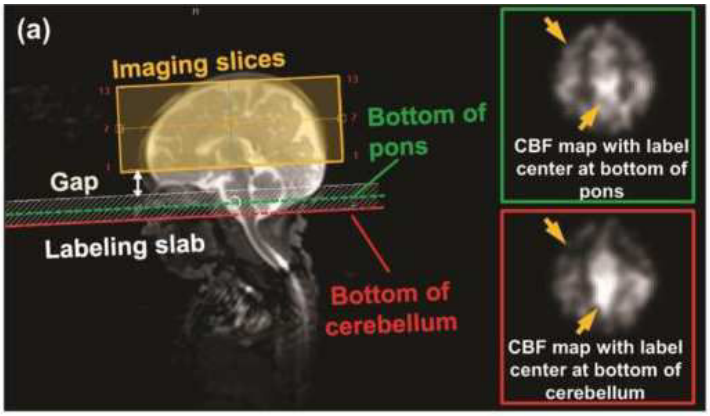

Figure 5 : Image extrait de (Ouyang et al., 2017) illustrant la sélection du positionnement du plan de marquage pour leur séquence de pCASL. Le plan de marquage était positionné parallèlement au plan CA-CP. Le choix du positionnement du milieu du plan de marquage était la partie inférieure du pont (ligne verte) plutôt que la partie inférieure du cervelet (ligne rouge).

2/ Nombre de répétitions

Le choix du nombre de répétitions est un compromis entre le temps d'acquisition, la qualité de l'image et la durée de l'acquisition. Il n'existe pas de spécifié pédiatrique, mis à part que les enfants sont plus sujets à bouger et donc plus la séquence est courte plus le risque d'artefacts de mouvement diminue.

3/ PLD ou TI

Le délai entre le marquage des spins et l'acquisition des images marquées doit être adapté à la vitesse de circulation des protons et au temps qu'ils mettent à atteindre le tissu ciblé. Pour l'analyse du CBF, il s'agit du temps pour atteindre la microcirculation cérébrale, afin d'obtenir le meilleur signal de perfusion et le moins de signal dans les gros vaisseaux (artefacts artériels à type de spot en hypersignal si l'acquisition est trop précoce). Le cas idéal est lorsque le PLD est juste un peu plus long que le temps de transit artériel (ATT) du sujet. Or l'ATT est directement lié à l'âge, et au territoire artériel. Des valeurs de TI ou PLD ont été données à titre indicatif, selon les populations, dans l'article de référence faisant une synthèse sur l'ASL (Alsop et al., 2015) (Fig. 6). Il est cependant primordial de comprendre, que selon les sujets et selon les pathologies, un faible signal ASL peut correspondre à la combinaison d'une hypoperfusion (CBF bas) et d'un ATT augmenté, et non spécifiquement d'un CBF bas uniquement. C'est une des raisons pour laquelle des séquences multi-TI ont été développées.

Parameter	Value
PCASL labeling duration	1800 ms
PCASL PLD: neonates	2000 ms
PCASL PLD: children	1500 ms
PCASL PLD: healthy subjects <70 y	1800 ms
PCASL PLD: healthy subjects >70 y	2000 ms
PCASL PLD: adult clinical patients	2000 ms
PCASL: average labeling gradient	1 mT/m
PCASL: slice-selective labeling gradient	10 mT/m
PCASL: average B_1	1.5 μT
PASL TI_1	800 ms
PASL TI	Use PCASL PLD (from above)
PASL labeling slab thickness	15–20 cm

Figure 6 : Paramètres de marquage recommandés (Alsop et al., 2015).

Des tests ont été effectués au cours de ce travail afin d'ajuster le TI ou PLD optimal en fonction de l'âge des enfants, de la machine et de la séquence utilisée.

- Choix du TI sur la nouvelle Siemens Aera 1.5T à l'Hôpital Sud en 2013 avec séquences PASL PICORE QIITIPS :

- Test de TI entre 1500ms et 1800ms sur environ 10 enfants
- Tests de TI entre 2000ms et 2200ms sur environ 10 nouveau-nés (moins de 6 mois)
- Analyse visuelle des cartographies de perfusion avec grille de lecture (Tableau 1) par MP et JCF
- Choix final de TI 1800ms pour les enfants de plus de 6 mois et 2000ms pour les moins de 6 mois

- Choix du PLD pour l'étude Etude PERINE (Effet des expositions prénatales à des neurotoxiques sur le cerveau en développement : une étude IRM ; promoteur : CHU de Rennes, Investigateur principal : Dr Fabienne Pelé – service d'épidémiologie et de Santé publique) :

- IRM 3T Verio Siemens, séquences de pCASL 2D
- Phase Pilote : test sur 10 enfants des PLD 1200ms, 1350ms et 1500ms pour chaque enfant
- Scoring visuel avec grille de lecture
- Choix final du PLD 1350ms
- Inclusion de 100 enfants

- Des tests ont également été effectués en 2015 sur des séquences WIP pCASL 2D, finalement non utilisées par la suite

Gray matter (GM) and white matter (WM) signal quality was scored on a 3-point scale:

1 = highest signal intensity,

2 = acceptable signal,

3 = poor signal.

Arterial and venous vascular artifacts (VAs), as unwanted vessels signal using a priori anatomical information, were rated on a 3-point scale:

1 = no or minor artifacts,

2 = moderate artifacts not preventing image interpretation,

3 = marked artifacts rendering images unreadable.

The VA compromise (VAC) was the compromise toward the least possible arterial and venous artifacts.

The overall quality (OQ) was the compromise between the best possible GM and WM signal and the least possible VAs.

The VAC and OQ were scored on a 3-point scale:

1 = best compromise,

2 = acceptable compromise

3 = poor compromise

Tableau 1 : Grille de lecture avec critères de qualité utilisée pour l'analyse visuelle des cartographies de perfusion ASL issu de (Ferré et al., 2012). 5 items côtés chacun entre 1 et 3.

4/ Quantification : le T1 du sang

Parmi les différents paramètres utilisés pour la quantification, le T1 du sang ou $T1_{blood}$ est une particularité pédiatrique, en particulier chez les nouveau-nés. Effectivement ce paramètre est en général supposé être de 1650 ms à 3T et 1350 ms à 1.5T (Alsop et al., 2015). Ces calculs ont été effectués chez l'adulte. Or l'hématocrite chez les nouveaux nés est connue pour varier sur un large écart, et ceci d'un jour à l'autre. Il existe une relation linéaire entre le $T1_{blood}$ et l'hématocrite, et une formule a été validée à 3T pour les nouveau-nés (Varela et al., 2011). L'utilisation d'un $T1_{blood}$ adapté à chaque nouveau-né permet d'obtenir des valeurs de CBF plus justes et de limiter les erreurs de quantification (Varela et al., 2015). Les changements de valeurs de perfusion induit par le $T1_{blood}$ sont de l'ordre de 11% (De Vis et al., 2014).

5/ Paramètres utilisés dans la littérature chez les nouveau-nés

Les paramètres d'acquisition utilisés chez les nouveau-nés dans la littérature sont détaillés dans le tableau 2.

	Âge à l'IRM (jours)	Population	inclus (n)	exclus (n)	IRM		Séquence	résolution ou épaisseur coupe	T1b (ms)	TI	LD/PLD
Wintermark, AJNR 2011	1 et 2-3	HIE	18	NR	3T	Siemens	**PASL (QUIPSS II)**	4,9 mm	1500	1400	--
Pienaar, Neuroimage, 2012	0 à 3	ischémie (HIE et AVC)	9		1.5T	GE	**pCASL 2D**	3,75 mm3	NR	--	1200/1000
		normaux en diffusion	6								
De Vis, Eur Radiol 2015	2 à 7	HIE avec mauvaise évolution	8	NR	3T	Philips	**PASL (PULSAR)**	4 x 4 x 7 mm;	calculé	1500	--
		HIE avec évolution favorable	20	NR				gap 1 mm			
Massaro, AJNR 2013	7 à 10	HIE	18	NR	3T	GE	**pCASL 3D**	3 mm	1600	--	1500/1025
	7 à 10	contrôles	18								
Miranda, Pediatric Research 2006	63	prématurés normaux <32SA	32	NR	3T	Siemens	**PASL (PICORE)**	5 mm; gap 0,5	1500	1500	--
	2	à terme normaux	17								
Wintermark, Neuroimage 2013	1 et/ou 2	HIE (IRM et NIRS)	7	NR	3T	Siemens	**PASL (QUIPSS II)**	4,9 mm	1500	1400	--
Boudes, Neuroimage: Clinical 2014	1 et/ou 2-3	HIE	61	15	3T	Philips	**PASL (EPISTAR)**	6 mm	1800	1800	
	1 et/ou 2-3				3T	Philips	**pCASL 2D**	6 mm	1800		1650/1800
Varela, JMRI 2014	32-78 SA		7	5	3T	Philips	**PASL (QUASAR)**	3 x 3 x 5.5 mm	calculé	--	--
Watson, Stroke 2016	< 28 SA	AVC	25	8	3T	Siemens	**pCASL 2D**	3 x 3 x 5 mm	NR		1600/1500
Tortora, Neuroimage: Clinical 2017	TEA	prématurés normaux <32SA	49	12	3T	Philips	**PASL (EPISTAR)**	6 mm	calculé	1250	--
	5	à terme	15	4							--
Ouyang, Neuroimage 2017	32- 45 SA	prématurés	12	4	3T	Philips	**pCASL 3D GRASE**	3.5 x 3.5 x 4 mm	calculé	--	2500
			10	8			**pCASL 2D**	3.5 x 3.5 x 3.5 mm			

Tableau 2 : Résumé des paramètres utilisés dans les études de la littérature portant sur l'étude de la perfusion cérébrale par ASL chez les nouveau-nés. NR = non renseigné; HIE = Hypoxic-Ischemic encephalopathy ou encéphalopathie hypoxo-ischémique ; TEA = Term Equivalent Age ou équivalent de terme; SA = semaines d'aménorrhée; TI = temps d'inversion; LD = labeling delay ou durée de marquage; PLD = post-labeling delay ou délais post-marquage. T1b = T1 du sang, calculé = selon la méthode de (Varela et al., 2011) ou (Liu et al., 2016)

(Boudes et al., 2014; De Vis et al., 2015; Massaro et al., 2013; Miranda et al., 2006; Ouyang et al., 2017; Pienaar et al., 2012; Tortora et al., 2017; Varela et al., 2015; Watson et al., 2016; Wintermark et al., 2011, 2014)

Chaine de traitement automatisée : l'outil AutoASL

Le traitement des images d'ASL et des images morphologiques (3D-T1, utile pour la segmentation) nécessite l'utilisation de logiciels de traitement d'image. Une chaine de traitement automatisée nommée autoASL, basée sur l'utilisation du logiciel SPM8 (Wellcome Trust Centre for Neuroimaging, University College of London, UK) et Matlab® (The MathWorks, Inc.), a été développée au sein de l'équipe Visage (https://team.inria.fr/visages/).

L'installation, la compréhension et l'utilisation de SPM8, MATLAB® et de l'outil AutoASL, ont fait partie intégrale de ce travail de thèse.

De même la préparation des images a été une étape préalable primordiale, avec l'aide de Mme Elise Banier (Ingénieur de recherche - Plateforme Neurinfo ; Equipe Visages), car nécessitant la mise en place d'un circuit, qui était inexistant pour les acquisitions réalisées sur l'IRM pédiatrique de l'Hôpital Sud. A savoir, au final :

1. Anonymisation des images DICOM
2. Transfert sur le PACS recherche du CHU
3. Transfert sur le PACS Neurinfo
4. Import sur la plateforme Shanoir (https://project.inria.fr/shanoir/) et conversion au format Nifti

   NB : Essais d'installation du logiciel Shanoir Uploader pour éviter les étapes 1-2-3, non concluante à ce jour
5. Téléchargement des images Nifti et organisation standardisée des fichiers

La Figure 7 résume les différentes étapes de traitement des images anatomiques et de perfusion, avant analyse statistique, réalisées par l'outil AutoASL (Annexe 1) et que nous explicitons ci-dessous. A noter que certaines étapes sont optionnelles et/ou ajustables.

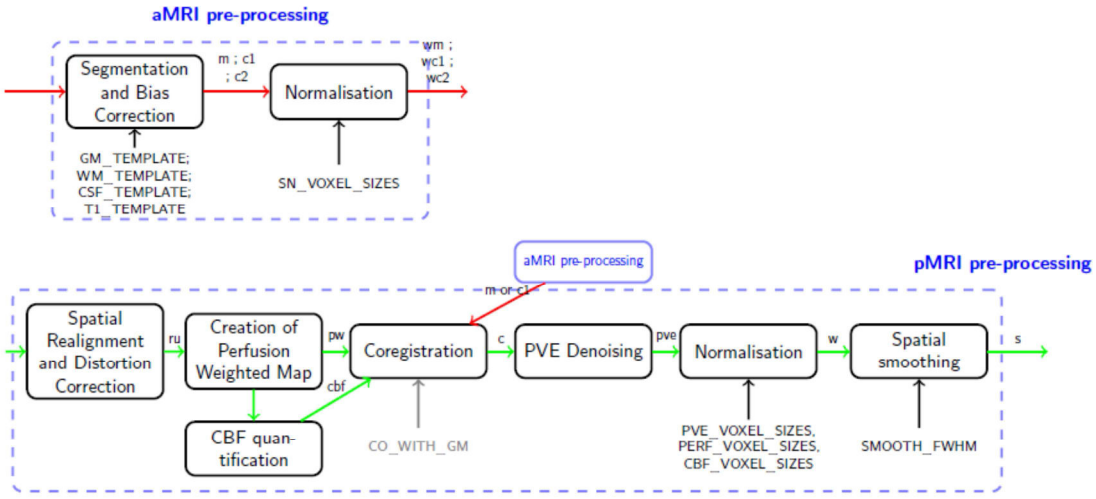

Figure 7 : Schéma extrait du Manuel d'utilisation AutoASL représentant les étapes du traitement des images anatomiques et de perfusion ASL avant analyse statistique.

1/ Prétraitement des images anatomiques

Premièrement, une correction des artefacts d'hétérogénéité en intensité est réalisée par SPM sur les images 3D T1, afin d'améliorer l'étape de segmentation. Ensuite une segmentation de la substance grise, substance blanche et liquide céphalo-rachidien est effectuée en utilisant le template par défaut de SPM8 (Montreal Neurological Institute (MNI) ICMB152). Une normalisation spatiale (optionnelle) est ensuite réalisée pour recaler le 3D T1 dans l'espace du template du MNI.

2/ Prétraitement des images de perfusion ASL

- Il est réalisé un recalage rigide des volumes ASL du même sujet pour correction de mouvement, réalisé en deux étapes : réalignement des images contrôles et des images marquées sur le premier volume, puis recalage des séries sur la moyenne des images alignées a la première étape.
- Ensuite, la création des images pondérées en perfusion se fait par soustraction des paires, après avoir mis de côté la première image, correspondant au M0. Un co-recalage au 3D T1 est effectué avec une transformation rigide. Cette transformation est estimée par maximisation de l'information mutuelle entre la moyenne des images contrôles (moyennes des images contrôles réalignées) et la cartographie 3D T1 de substance grise. L'utilisation du recalage par maximisation de l'information mutuelle

est effectué pour un meilleur recalage car la résolution et la distribution des intensités de l'ASL est différente que celle du 3DT1.

- La cartographie de perfusion est obtenue par soustraction de la moyenne des répétitions des images non marquées et des images marquées.
- La conversion de la cartographie de perfusion en une cartographie quantitative se fait en appliquant un modèle cinétique standard, selon le type de séquence ASL, et en choisissant les paramètres de quantification.
- L'étape de correction de volume partiel (« PVE denoising ») est optionnelle et utilise la méthode de Petr par défaut. La résolution de la séquence ASL étant relativement faible, l'utilisation de correction de volume partiel permet d'éviter une sous-estimation du CBF dans la substance grise par contamination par des voxels de substance blanche.
- La normalisation spatiale des différentes cartographies ASL obtenues (cartographie de perfusion, cartographie CBF, cartographie de PVE) est optionnelle
- Enfin un filtre de lissage (« spatial smoothing ») de type 3D gaussien est appliqué au préalable d'une analyse statistique voxel-à-voxel.

Chapitre 3 – Travaux chez l'enfant

Le cerveau est un organe qui subit des changements tout au long de la vie. Il existe une croissance et une maturation complexe du cerveau. Les processus de myélinisation et de giration sont particulièrement visibles en IRM dans les deux premières années de vie. Même si le cerveau a une apparence grossièrement identique en terme de signal à celui de l'adulte à partir de 1 an en imagerie IRM pondérée T1 et 2 ans en pondération T2, les différences structurelles existent encore ensuite. Par exemple, les proportions de volumes de substance blanche et substance grise vont évoluer au cours de l'enfance et de l'adolescence, de manière non linéaire et différente selon les lobes (Giedd et al., 1999; Lange et al., 1997; Sowell et al., 1999). Le cortex cérébral va s'épaissir au cours de la croissance dans les 10 premières années de vie. Pour toutes ces évolutions physiologiques, il est problématique d'utiliser des volumes de référence de populations adultes pour le traitement d'images pédiatriques (Richards et al., 2016; Richards and Xie, 2015).

Comme développé dans le chapitre 1, la perfusion cérébrale évolue également au cours de l'enfance et est particulièrement basse chez les nouveau-nés pour ensuite atteindre un pic entre 4 et 10 ans, selon les études.

Nous nous intéresserons dans ce chapitre aux enfants âgés de 6 mois à 16 ans, et nous aborderons les problématiques propres aux nouveau-nés dans le chapitre 4.

Adaptation de la chaine de traitement

L'outil AutoASL a été créé initialement à des fins de recherche pour une utilisation sur des imageries IRM adultes. L'utilisation pour des données pédiatriques n'avait pas encore été évaluée avant ce travail de thèse. Il a donc fallu dans un premier temps adapter l'outil aux données pédiatriques. Ce travail a été fait en collaboration avec Isabelle Corouge (Ingénieure de Recherche Université de Rennes 1, Plateforme Neurinfo ; Equipe Visages), et Aline Carsin-Vu (Interne en médecine au CHU de Reims, DES Radiologie) dans le cadre d'un Master 2 SIBM (Université de Rennes 1) sous la direction du Pr Jean-Christophe Ferré et de moi-même.

Voici un résumé des principales adaptations da la chaine de traitement.

1. Extraction du cerveau

L'extraction du cerveau de la boite crânienne est une étape préalable indispensable au traitement des images anatomiques. En particulier cette étape améliore la segmentation entre les structures cérébrales. La plupart des méthodes d'extraction du cerveau ont été développées chez des adultes, or la boite crânienne ainsi que le cerveau des enfants ont une forme différente et les tissus ont des intensités de signal différentes.

La comparaison de l'extraction sur 10 sujets en utilisant l'outil BET de FSL (Smith, 2002) (https://fsl.fmrib.ox.ac.uk/fsl/fslwiki/FSL) et VolBrain (http://volbrain.upv.es/index.php) a permis de retenir l'extraction avec BET FSL qui était de meilleure qualité (cerveau érodé avec Volbrain).

2. Segmentation des images anatomiques – Templates pédiatriques

L'utilisation de cartes de probabilité de substance grise, substance blanche et liquide céphalo-rachidien, adaptées à la population étudiée, permet d'améliorer la segmentation des tissus. L'atlas utilisé par défaut dans SPM8 a été construit sur des images IRM normales d'une population d'adultes jeunes. Nous avons testé plusieurs atlas pédiatriques afin d'en choisir un pour l'intégrer dans la chaine de traitement, afin d'éviter une classification erronée des tissus cérébraux.

Les atlas testés sur 12 enfants entre 6 mois et 15 ans étaient : NIHPD (Evans and Brain Development Cooperative Group, 2006; Fonov et al., 2011), le template of South Carolina (Richards et al., 2016; Sanchez et al., 2012a, 2012b), le template TOM (Wilke et al., 2008) et le template MNI adulte.

Il existait des erreurs de segmentation avec le template de South Carolina. Les autres étaient équivalents, sans erreur de segmentation. Les valeurs de CBF obtenues sur 2 groupes de 4 sujets (enfants et adolescents) étaient assez équivalentes, mis à part pour la substance blanche. Notre choix final s'est porté sur les atlas du NIHPD avec 3 tranches d'âges (4.5 - 8.5 ans, 7.5-13.5 ans et 13 -18.5 ans).

3. Correction de mouvement des images ASL

Cette étape n'a pas de spécificités techniques pédiatriques, mais on sait que les enfants sont tout de même plus sujet à bouger lors de la réalisation de l'examen IRM, ce qui rend cette étape d'autant plus importante.

Nous avons comparé 2 techniques sur 16 sujets. La première technique était l'utilisation des premiers résultats du traitement des données ASL. Effectivement il s'agit des résultats du recalage (6 paramètres, rigide) des volumes ASL acquis chez un même sujet, comme décrit dans le précédent chapitre. Les schémas fournis permettent de repérer les paires les plus bougées et de les supprimer manuellement. Nos critères de suppression ont été fixés comme suit : translation supérieure à 0.4mm dans une direction ou une rotation de plus de 0.3 degré.

La deuxième technique consistait à utiliser le M-estimator de Huber (Maumet et al., 2014) qui permet d'accorder un poids moindre aux valeurs les plus extrêmes dans l'estimation de la carte pondérée en perfusion. Effectivement le signal de perfusion est une moyenne des répétitions. Or une moyenne conventionnelle est sensible aux valeurs aberrantes. L'utilisation du M-estimator de Huber permet de minimiser le poids d'une valeur aberrante (par exemple d'une répétition bougée, loin de la moyenne).

Notre choix final s'est porté sur l'utilisation de la seconde méthode qui est automatisée, avec de bons résultats, et qui étaient équivalents pour les deux techniques.

4. Analyse par ROI

Nous avons défini les lobes (frontal, temporal, parietal, occipital, limbique et insula) et les hémisphères en regroupant les ROI de l'atlas Automated Anatomical Labeling (AAL) (Tzourio-Mazoyer et al., 2002). AAL est un logiciel intégré dans SPM permettant de segmenter différentes régions anatomiques du cerveau dans l'espace du MNI. Nous avons réalisé l'analyse par ROI pour chaque sujet, après normalisation spatiale dans l'espace du template.

Les valeurs moyennes de CBF étaient obtenues dans chaque ROI après exclusion des voxels ayant une probabilité de substance grise de moins de 0.8.

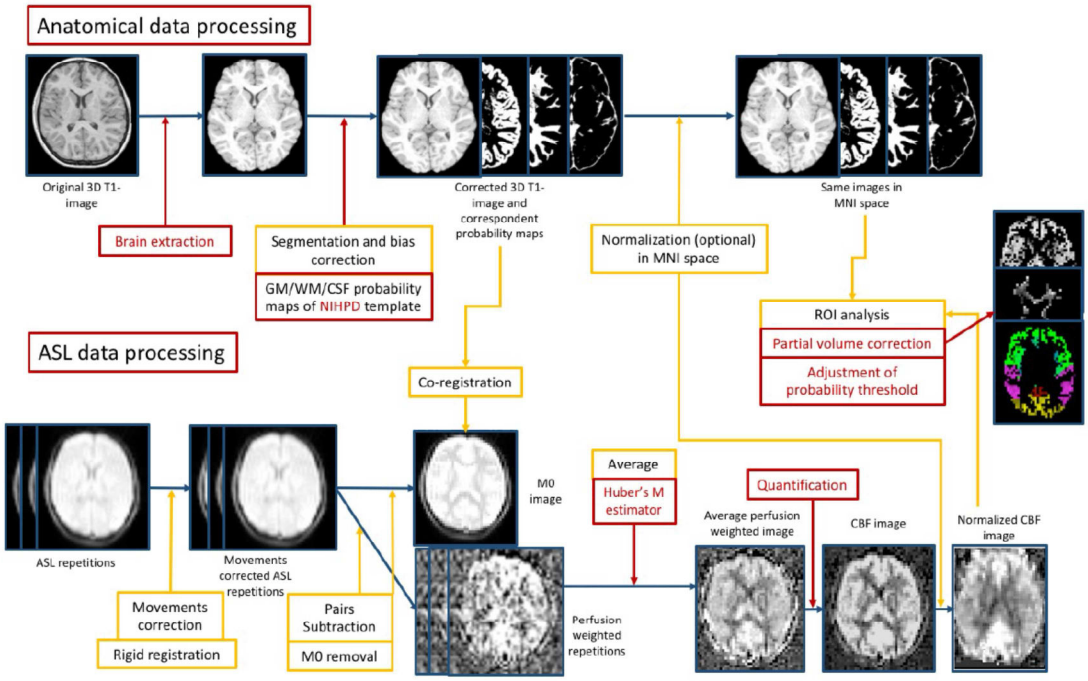

Figure 8 : Schéma issu du mémoire de master 2 SIBM du Dr Aline Carsin-Vu, représentant le post-traitement des images anatomiques et de perfusion ASL par la chaine AutoASL et SPM8, et son adaptation aux données pédiatriques.

Applications cliniques

Grâce à l'élaboration de la chaine de traitement, nous avons pu faire un traitement d'images et une analyse statistique dans le cadre de travaux de recherche clinique en imagerie pédiatrique, menés tous deux par des internes de médecine (Dr Aline Carsin-Vu ayant soutenu sa thèse le 04-05-2017 à Reims et Dr Domitille Cadiot ayant soutenu le 12-06-2017 à Rennes), sous ma direction, et ayant fait l'objet de publications (Cadiot et al., 2018; Carsin-Vu et al., 2018). Le traitement des images concernant le travail d'Aline Carsin-Vu avait été effectué préalablement lors de son master 2. J'ai effectué moi-même le traitement des images et l'analyse par ROI pour le travail sur les migraines.

“Measurement of pediatric regional cerebral blood flow from 6 months to 15 years of age in a clinical population. EJR 2018”

Résumé

L’objectif était d’examiner l’évolution du débit sanguin cérébral (CBF) dans la matière grise (GM) entre 6 mois et 15 mois ans et de fournir des valeurs de CBF pour le cerveau, le GM, la substance blanche (WM), les hémisphères et les lobes.

Nous avons inclus rétrospectivement tous les examens IRM avec séquence ASL réalisés dans un contexte clinique entre 2013 et 2016 dans notre institution. Cette étude a obtenue l’accord du comité d’éthique et le recueil de l’accord des parents a été obtenu pour chaque enfant. Nous avons exclu les sujets présentant une affection pouvant affecter la perfusion cérébrale. Pour chaque sujet, les valeurs moyennes de CBF ont été calculées dans le cerveau, la GM, la WM, et les hémisphères et lobes. Les fonctions polynomiales de premier, deuxième et troisième ordre modélisant le CBF en fonction de l’âge dans la SG ont été comparées à l’aide du critère d’information d’Akaike (AIC) et de tests de rapports de vraisemblance (LRT).

Au final 84 enfants ont été inclus (44 filles / 40 garçons). Les valeurs moyennes de CBF étaient de 64,2 ± 13,8 mL/100g/min dans la GM et de 29,3 ± 10,0 mL/100g/min dans la WM. La fonction polynomiale modélisant au mieux l’évolution du CBF dans la GM était une fonction polynomiale cubique avec un pic vers l’âge de 3-4 ans (AIC = 672.7, contre AIC = 673.9 avec une fonction de premier ordre et AIC = 674.1 avec une fonction quadratique). Les LRT n’ont pas retrouvé de différence significative entre les 3 fonctions polynomiale, ne permettant pas d’affirmer la supériorité de la fonction quadratique (p = 0.18) ou cubique (p = 0.06) sur la fonction de premier ordre. Aucun effet de l’anesthésie générale (p = 0,34) ou du sexe (p = 0,16) n’a été observée sur les valeurs de CBF.

En conclusion, cette étude fournie des valeurs de CBF en ASL dans le cerveau, la GM, la WM, les hémisphères et lobes sur une large tranche d'âge pédiatrique, montrant approximativement une évolution en forme de U inversée dans la perfusion de la GM au cours de l'enfance.

European Journal of Radiology 101 (2018) 38–44

Contents lists available at ScienceDirect

European Journal of Radiology

journal homepage: www.elsevier.com/locate/ejrad

Research article

Measurement of pediatric regional cerebral blood flow from 6 months to 15 years of age in a clinical population

Aline Carsin-Vu[a,b,c,d,e,*], Isabelle Corouge[a,b,c,d], Olivier Commowick[a,b,c,d], Guillaume Bouzillé[f,g], Christian Barillot[a,b,c,d], Jean-Christophe Ferré[a,b,c,d,h], Maia Proisy[a,b,c,d,h]

[a] Univ Rennes1, Faculté de Médecine, F-35043 Rennes, France
[b] INSERM, U 1228, ERL VISAGES, F-35042 Rennes, France
[c] CNRS, IRISA, UMR 6074, F-35042 Rennes, France
[d] INRIA, VISAGES Project-Team, F-35042 Rennes, France
[e] CHU Reims, Département de Radiologie, F-51092 Reims, France
[f] INSERM, U 1414, CIC, F-35033 Rennes, France
[g] CHU Rennes, Centre de Données Cliniques, F-35033 Rennes, France
[h] CHU Rennes, Département de Radiologie, F-35033 Rennes, France

ARTICLE INFO

Keywords:
Arterial spin labeling (ASL)
Pediatric brain imaging
Cerebral blood flow (CBF)

ABSTRACT

Objectives: To investigate changes in cerebral blood flow (CBF) in gray matter (GM) between 6 months and 15 years of age and to provide CBF values for the brain, GM, white matter (WM), hemispheres and lobes.
Methods: Between 2013 and 2016, we retrospectively included all clinical MRI examinations with arterial spin labeling (ASL). We excluded subjects with a condition potentially affecting brain perfusion. For each subject, mean values of CBF in the brain, GM, WM, hemispheres and lobes were calculated. GM CBF was fitted using linear, quadratic and cubic polynomial regression against age. Regression models were compared with Akaike's information criterion (AIC), and Likelihood Ratio tests.
Results: 84 children were included (44 females/40 males). Mean CBF values were 64.2 ± 13.8 mL/100 g/min in GM, and 29.3 ± 10.0 mL/100 g/min in WM. The best-fit model of brain perfusion was the cubic polynomial function (AIC = 672.7, versus respectively AIC = 673.9 and AIC = 674.1 with the linear negative function and the quadratic polynomial function). A statistically significant difference between the tested models demonstrating the superiority of the quadratic (p = 0.18) or cubic polynomial model (p = 0.06), over the negative linear regression model was not found. No effect of general anesthesia (p = 0.34) or of gender (p = 0.16) was found.
Conclusion: we provided values for ASL CBF in the brain, GM, WM, hemispheres, and lobes over a wide pediatric age range, approximately showing inverted U-shaped changes in GM perfusion over the course of childhood.

1. Introduction

Arterial Spin Labeling (ASL), developed in the early 1990s, is an innovative magnetic resonance imaging (MRI) sequence that uses magnetically labeled protons of blood water as an endogenous contrast agent [1]. It enables imaging of brain perfusion and quantification of cerebral blood flow (CBF) without intravenous injection or irradiation, unlike nuclear medicine or MRI-based perfusion techniques involving injection of a paramagnetic contrast agent. Consequently, ASL is particularly well suited for investigating pediatric brain perfusion.

From birth to adulthood, the brain undergoes many overall and regional developmental changes. The ability to study these transformations would allow a better understanding of brain development. A possible way to do this could be the quantification of CBF using ASL due to its non-invasive nature and the close relationship between cerebral metabolism and perfusion [2]. ASL is also increasingly used in pathological contexts [3], particularly for newborn hypoxic-ischemic encephalopathy [4], cerebrovascular diseases [5], epilepsy, brain tumor grading and tumor identification [3,6].

ASL is not yet widely used as a routine perfusion method. One of the

Abbreviations: (p)ASL, (pulsed) arterial spin labeling; MRI, magnetic resonance imaging; CBF, cerebral blood flow; GM, gray matter; WM, white matter; CSF, cerebrospinal fluid; ROIs, regions of interest; AAL, automated anatomical labeling; AIC, Akaike's information criterion; LRT, likelihood ratio tests

* Corresponding author at: INRIA, VISAGES Project-Team, F-35042 Rennes, France.
E-mail addresses: acarsinvu@gmail.com (A. Carsin-Vu), isabelle.corouge@irisa.fr (I. Corouge), olivier.commowick@irisa.fr (O. Commowick), guillaume.bouzille@chu-rennes.fr (G. Bouzillé), christian.barillot@irisa.fr (C. Barillot), jean-christophe.ferre@chu-rennes.fr (J.-C. Ferré), maia.proisy@chu-rennes.fr (M. Proisy).

https://doi.org/10.1016/j.ejrad.2018.02.003
Received 11 September 2017; Received in revised form 17 December 2017; Accepted 5 February 2018

reasons for this is the incomplete knowledge of normal pediatric ASL CBF values and the potential changes in brain perfusion over the course of childhood. This knowledge is a prerequisite for the pertinent detection of CBF abnormalities. Several teams have studied CBF in pediatric populations using ASL but these studies were often limited to specific age groups, around birth [7,8] or after 4 years of age [9–12]. To our knowledge, there is only one study that reports CBF values using ASL in four subjects aged between 6 months and 4 years [13]. In this age group, sedation or general anesthesia is virtually mandatory to obtain the child's compliance, and this could have distorted the results of the investigation. Consequently, there is a real need to investigate normal CBF values in a wide range of ages in order to develop clinical use of ASL in the pediatric population and to better understand brain development.

The aim of this study was to investigate changes in brain perfusion in gray matter from 6 months to 15 years of age, using ASL sequences, and to provide reference values for the brain, gray matter (GM), white matter (WM), hemispheres, and lobes in this age range. A secondary objective was to study the effect of general anesthesia and gender on CBF values.

2. Material and methods

2.1. Study population

We retrospectively reviewed all consecutive routine brain MRIs performed in our pediatric radiology department between January 2013 and June 2016 for which ASL images had been acquired. The main inclusion criteria were age between 6 months and 15 years and normal morphological MRI images. The main exclusion criteria were all factors that could have affected CBF such as a history of stroke, brain tumor, metabolic diseases, seizure or headache in the previous 2 days, prematurity, brain malformations or neurosurgery. MRI indications were resumed in Table 1. We excluded scans with artifacts or significant patient movement. The study was approved by the local Institutional Review Board. According to national legislation, written consent is not necessary for such retrospective studies, however all the parents were informed about the study and could choose not to include their child.

2.2. MRI protocol

All scans were performed on a 1.5 T Magnetom Aera (Siemens Healthcare, Erlangen, Germany) with a 12-channel head coil. The complete imaging protocol varied according to clinical features but 3D T1-weighted and pulsed ASL (pASL) images were acquired in all cases. The parameters of both image types were standardized.

The parameters of 3D sagittal MPRAGE T1-weighted morphological images were as follows: TR = 2090 ms, TE = 4.92 ms, TI = 1100 ms, 256 × 256 matrix, 0.5 × 0.5 × 1 mm^3 voxel size, FOV = 26 cm^2, 160 slices, TA = 200 s.

Table 1
MRI indications for all children.

MRI indications	*n*
Headache	24
Seizure	12
Brief minor neurological deficit without sequelae	10
Psychomotor retardation	9
Autism	8
Facial Port-Wine Stain	8
Paresthesia	4
Behavioral disorders	3
Others[a]	6
Total	84

Note: All MRI images must be normal and were performed outside an acute context; *n* number of patients.

[a] Others: cervical bone malformation, drug intoxication, psychological problem, uveitis, weight loss, chronic fatigue.

The parameters of pASL axial images with the PICORE Q2TIPS labeling scheme [14] were as follows: TR = 3200 ms, TE = 12 ms, TI_1/TI_2 = 700/1800 ms, 64 × 64 matrix, 4 × 4 × 8 mm^3 voxel size, FOV = 256 mm^2, TA = 336 s, 9 slices, 8 mm slice thickness, 2.0 mm slice gap, 61 repetitions. One M_0 reference image (magnetization of brain tissue at the equilibrium used to normalize the difference perfusion map) and 30 control/label image pairs were acquired.

Depending on the age and behavior of children, sedation or general anesthesia was administered before performing the scan as required. A pediatrician performed sedation with permanent monitoring of oxygen saturation. The general anesthesia protocol was standardized using sevoflurane. A controlled ventilation system and an end-tidal carbon dioxide monitor were used to maintain normocapnia.

2.3. Data processing

Processing of both 3D-T1 and ASL images was performed using custom-built ASL processing tools based on SPM8 (Wellcome Trust Centre for Neuroimaging, Institute of Neurology, University College, London, UK) and MATLAB® 2014b (The MathWorks Inc., Natick, Massachusetts, USA).

2.3.1. Anatomical data processing

Brain data were extracted with the FSL Brain Extraction Tool (Analysis Group, FMRIB, Oxford, UK) [15]. A bias intensity correction of each T1-weighted sequence was performed using SPM. Then the sequence was segmented into GM, WM and cerebrospinal fluid (CSF) probability maps using NIHPD pediatric brain atlases [16]. Spatial normalization parameters, estimated by the same unified segmentation model SPM routine, were applied to register the 3D T1 volumes to the atlas space.

2.3.2. ASL data processing

The first step was a 6-parameter (rigid body) registration of the ASL volumes acquired from the same subject using a least-squares approach to reduce subject motion between repetitions [17]. Then the M0 image was separated from other ASL volumes; label and control volumes were pair-wise subtracted. The perfusion signal was usually obtained by averaging across the repetitions. However, a conventional mean is sensitive to outliers. To create a perfusion-weighted map, we replaced the conventional mean by a Huber-M-estimator, that minimizes the weight of a repetition far removed from the mean [18]. Then the perfusion-weighted map was co-registered to the 3D T1 gray matter map using a rigid transform and by maximizing Normalized Mutual Information. The averaged perfusion-weighted map was converted into a quantitative ASL CBF map by applying the following single compartment model [13,19]:

$$CBF = \frac{6000 \times \lambda \times \Delta M \times e^{\frac{(TI_2 + idx_{sl} \times TI_{sl})}{T_{1b}}}}{2 \times \alpha \times TI_1 \times M_{0b}} [mL/100g/min]$$

The factor of 6000 converts the unit from mL/g/s to mL/100 g/min. λ is the brain/blood partition coefficient in mL/g (0.9 mL/g) [20]. ΔM is the average difference in signal intensity between control and label acquisitions. TI_2, inversion time, is the time from the initial pulse to image acquisition (1800 ms) [20]. TI_2 is adjusted for each slice to take into consideration the time interval TI_{sl} (47 ms) between slice acquisitions in our 2D multislice ASL sequences. idx_{sl} is the slice index (0 for the first slice). Blood T1, T_{1b}, is the longitudinal relaxation time of blood in seconds (1350 ms). Alpha is labeling efficiency (98%) [20]. TI_1 is the duration between the inversion and saturation pulse (700 ms). M_{0b} is the longitudinal magnetization of blood at equilibrium and is estimated from the M0 map, the first volume of the ASL series.

Finally, the normalization step warped each individual quantitative

Table 2
CBF values for each age group in the brain, gray matter and white matter.

Age group	Brain CBF[a] Mean (± SE)	GM CBF[a] Mean (± SE)	WM CBF[a] Mean (± SE)	*n*	Sex ratio F/M	Sedation No/S/GA
6–11 months	53.3 (± 7.8)	58.6 (± 8.3)	29.2 (± 5.1)	4	2/2	0/4/0
12–23 months	61.7 (± 3.2)	68.2 (± 3.5)	39.3 (± 2.5)	14	5/9	0/14/0
2–3 years	68.5 (± 4.4)	76.5 (± 4.9)	40.2 (± 4.5)	8	3/5	0/7/1
4–5 years	56.6 (± 3.8)	64.9 (± 4.3)	26.0 (± 2.1)	13	4/9	1/2/10
6–7 years	62.4 (± 3.0)	71.4 (± 3.1)	30.5 (± 2.3)	8	4/4	6/0/2
8–9 years	54.9 (± 2.7)	63.9 (± 3.1)	25.8 (± 1.8)	11	6/5	10/0/1
10–11 years	53.4 (± 5.2)	62.4 (± 6.1)	23.9 (± 2.6)	7	5/2	7/0/0
12–13 years	43.3 (± 2.6)	51.0 (± 3.0)	21.7 (± 2.0)	11	7/4	9/0/2
14–15 years	50.1 (± 2.0)	59.3 (± 2.5)	24.8 (± 1.2)	8	8/0	8/0/0
Total	56.1 (± 1.4)	64.2 (± 1.5)	29.3 (± 1.1)	84	44/40	41/27/16

Note: CBF, cerebral blood flow; GM, gray matter; WM, white matter; *n* number of patients; SE, standard error of the means; F, female; M, male; S, sedative; GA, general anesthesia.
[a] CBF unit is mL/100 g/min.

ASL CBF map using the spatial normalization parameters estimated from the anatomical data normalization and a smoothing process applied a smoothing filter to the images.

2.3.3. Regions of interest (ROIs) analysis in brain tissues

By applying as masks the GM and WM probability map obtained during anatomical data processing, it was possible to create GM and WM ASL CBF maps for each subject in GM and WM. To avoid cross-contamination between brain tissue, we thresholded GM and WM probability maps at 80% and 99% respectively prior to masking [21]. Overall CBF values were obtained by averaging GM and WM CBF maps subsequent to masking. The quality of the segmentation was visually checked.

2.3.4. Regions of interest analysis (ROIs) in lobes and hemispheres

Lobe (frontal, temporal, parietal, occipital, limbic and insular) and hemisphere masks were defined using the Automated Anatomical Labeling (AAL) atlas [22]. Lobe definitions are summarized in the Appendix A. Hemispheres were defined by all the right and left regions available in AAL. CBF values were averaged in each lobe and hemisphere ROIs using masks created with AAL and the GM CBF map. Given that the ASL sequence may not completely cover supratentorial regions, the lobe GM CBF maps had to contain lobe volumes greater than 10 cm^3 in the insular lobe, 20 cm^3 in the limbic lobe, 35 cm^3 in the occipital lobe, 60 cm^3 in the parietal lobe, 40 cm^3 in the temporal lobe and 100 cm^3 in the frontal lobe to be taken into consideration. Threshold values were chosen by rounding half of the average of GM CBF map lobes volumes in our population. The quality of the segmentations was visually checked.

2.4. Statistical analysis

Quantitative (continuous) data were expressed as mean ± standard error of the means. Qualitative data were expressed as numbers and percentages.

We performed an analysis to study the relationships between grey matter CBF values and the potential associated factors. CBF values in GM were plotted against age and fitted using linear, quadratic and cubic polynomial regression. We evaluated the goodness of fit of the models with the use of Akaike's information criterion (AIC), defined as: $AIC = -2 \ln L + 2p$, where L is the penalized maximum likelihood and p is the number of parameters. The AIC has the advantage of minimizing potential overfitting issues caused by incorporating too many parameters in the models (the smaller the value of this statistic, the better the model). We used Pearson correlation tests for each model. We also performed Likelihood Ratio tests (LRT) between models. We investigated the influence of hemisphere side on CBF using a paired student's *t*-test. We used a student's *t*-test to study the association with gender and general anesthesia after ensuring that the variables were normally distributed. For multiple comparisons between GM CBF in lobes, data were analyzed with a two-factor repeated-measures analysis of variance (ANOVA) between lobes. Post hoc comparisons were performed by Tukey's honestly significant difference test to specify differences among mean GM CBF values in lobes. We considered a two-sided *p* value of less than 0.05 as statistically significant. We performed the statistical analysis using R© 3.2.4 statistical computing software (R Core Team (2017). R: A language and environment for statistical computing. R Foundation for Statistical Computing, Vienna, Austria. URL https://www.R-project.org/).

3. Results

3.1. Population

We reviewed approximatively 600 MRI scans, and 90 patients met our inclusion criteria. Six parents chose not to include their child. Eighty-four children were finally included, distributed equally: 44 females (52%), and 40 males (48%). Their mean age was 7.2 years (range: 6 months – 15 years and 10 months). The age distribution of the children is shown in Table 2. Forty-one children received no sedation (49%), 16 (19%) needed general anesthesia and 27 (32%) received a sedative.

3.2. Age-related changes in brain perfusion

CBF was 64.2 ± 1.5 mL/100 g/min in GM, and 29.3 ± 1.1 mL/100 g/min in WM. The CBF values in the brain, gray matter, white matter and hemispheres per age group class are summarized in Table 2.

CBF values in gray matter are plotted against age in Fig. 1. CBF in GM seemed to increase from 6 months to 3–4 years of age and declined thereafter (Figs. 1 and 2). The equations of the polynomial models fitted (linear, quadratic and cubic) to the GM CBF values with respect to age (years) were as follows:

1. linear model: $GM\ CBF = 71.50 - 1.01 \times age$
2. quadratic model: $GM\ CBF = 67.86 + 0.49 \times age - 0.09 \times age^2$
3. cubic model: $GM\ CBF = 60.74 + 5.82 \times age - 0.92 \times age^2 + 0.03 \times age^3$

The best-fit-model of brain perfusion was the cubic polynomial function (AIC = 672.7, versus AIC = 673.9 with the negative linear function and AIC = 674.1 with the quadratic polynomial function). However, we did not find a statistically significant difference between the three tested polynomial regression models that would have demonstrated the superiority of the quadratic or cubic polynomial model over the negative linear regression model (Table 3).

No significant difference was found between mean CBF of left and right hemispheres (GM CBF: right hemisphere 65.3 ± 1.6 mL/100 g/

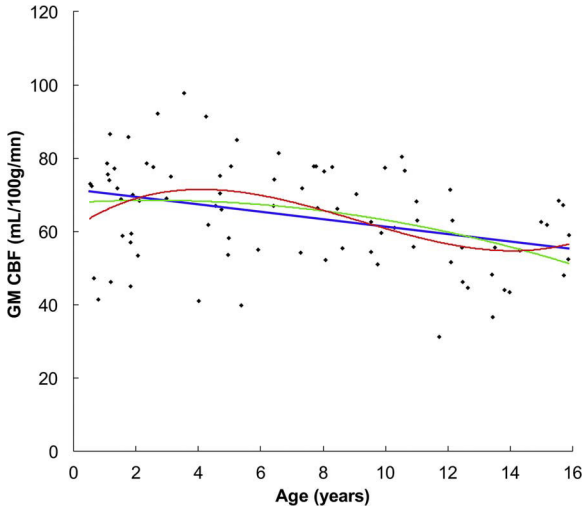

Fig. 1. Changes in gray matter CBF as a function of age. Gray matter CBF was fitted using negative linear (blue line), quadratic (green line) and cubic polynomial regression (red line).

min versus left hemisphere 64.8 ± 1.5 mL/100 g/min; p = 0.09); therefore, right and left hemispheres were combined for analysis per lobe. CBF values in lobes per age group are summarized in Table 4. CBF was often highest in the occipital lobe and lowest in the limbic and insular lobe in most age group. Two-factor repeated-measures ANOVA showed a significant effect of lobes in GM CBF between 6 months and 15 years of age ($p < 0.0001$). After ANOVA, the Tukey's honestly significant difference test only indicated significant differences of GM CBF between occipital lobe and parietal, frontal, insular or limbic lobe (respectively p = 0.01, p = 0.002, $p < 0.0001$, $p < 0.0001$) and between temporal lobe and limbic or insular lobe (respectively p = 0.002, p = 0.0002) (Fig. 3).

3.3. Effect of general anesthesia and gender on cerebral blood flow

In GM, CBF was not significantly different between females and males (62.1 ± 2 mL/100 g/min versus 66.4 ± 2.2 mL/100 g/min; p = 0.16). No significant effect of general anesthesia was found. Mean GM CBF was 64.9 ± 1.7 mL/100 g/min without general anesthesia and 61.2 ± 3.4 mL/100 g/min with general anesthesia, p = 0.34.

4. Discussion

Knowledge of normal pediatric CBF values is vital for improving our understanding of normal human brain development and the accuracy of diagnosis of pediatric brain pathologies. To the best of our knowledge, this study investigates normal pediatric CBF changes using ASL MRI perfusion over the widest age range reported in the literature to date, covering the period from infancy to adolescence. The obtained CBF values should be helpful in pathological context [3] such as migraine, Sickle cell disease…

The GM CBF measured by the ASL images tended to increase during the first years of life with a peak at 3–4 years, and to progressively decline afterwards, following an approximatively inverse U-shaped curve. During late adolescence, CBF seemed to display a small rebound. The superiority of the cubic polynomial function over the linear or quadratic function for fitting GM CBF with age was not significant, probably because of a lack of power due to our relatively small sample size. However, the third-order polynomial model had the smallest AIC, which means this model is likely to have the best performance for predicting future observations. Previous studies described similar inverse U-shaped changes in brain perfusion over the course of childhood generally, produced with several imaging techniques: SPECT using ^{133}Xe [23] in brain, perfusion CT [24] in GM and ASL MRI [10] in most lobes. In the latter study [10], the CBF peak occurred later but the age range of its population was higher (5–18 years). A parallel age-related evolution of local cerebral metabolic rate of glucose by PET was shown by Chugani et al. [25]. The teams studying ASL MRI with smaller age ranges found a similar CBF increase after birth [8] and CBF reduction after 7 years of life [9,11,12,26]. A small rebound of CBF values during late adolescence was also noticed by Taki et al. [10] in some brain regions. Considering the close relationship between CBF and glucose consumption, the CBF rising phase could correspond to the overproduction of neurons and synapses during the first years of life and the second phase to the decrease in the number of synapses per neuron [10,23,25].

On the basis of literature providing absolute values of CBF determined with the ASL images in children above 4 years of age, the mean GM CBF varies from 62 to 96.5 mL/100 g/min, and mean WM CBF varies from 22 to 41.58 mL/100 g/min [9,27,11,12]. Our GM CBF values were in the lower range, and WM CBF values were of the same order. The highest regional CBF values were found in occipital lobes, in common with Duncan et al. [8] and in the contrast to other studies [10,27]. Nevertheless, it is difficult to compare our regional CBF values to those in the literature because of differences in age groups and different methodological issues for brain region definition and ROI measurements (manual or automatic).

We did not find a significant effect of gender on brain perfusion during childhood, in common with Duncan et al. with ASL between 3 and 5 months of age, and Wintermark et al. with perfusion CT during childhood [8,24]. Nonetheless, Satterthwaite et al. [26] found a gender difference for CBF changes over time from mid puberty in many brain regions, particularly in hubs of the default mode network and executive system: female CBF described a plateau before an increase from around

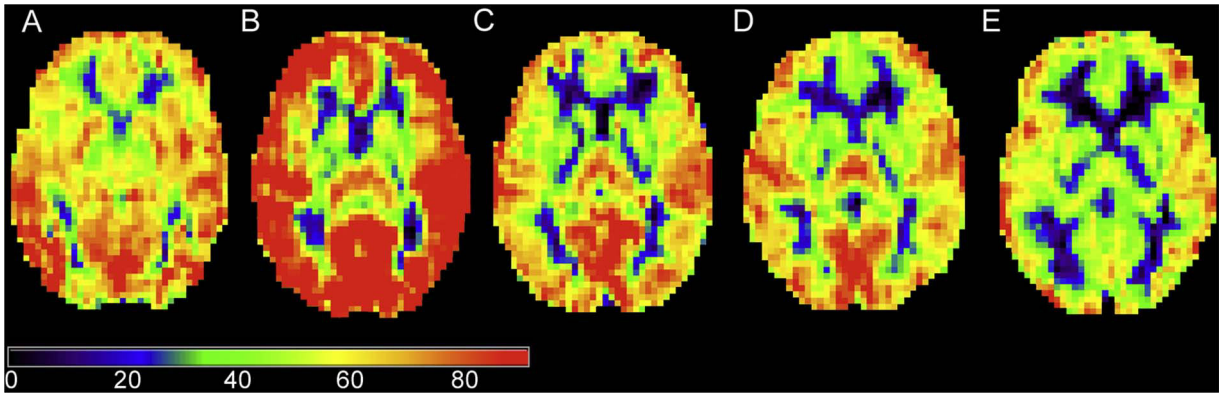

Fig. 2. Examples of representative single subject ASL CBF map as a function of age. (A) child aged 6 months. (B) child aged 4 years. (C) child aged 7 years. (D) child aged 11 years. (E) child aged 15 years.

Table 3
Results of the polynomial model comparison.

Model	Formula	$-2 \ln L$	AIC	LRT	LRT p value	r	r p value
Linear	$CBF_{GM} = 71.50 - 1.01 \times age$	668	673.9	11.15	< 0.001	0.35	0.001
Quadratic	$CBF_{GM} = 67.86 + 0.49 \times age - 0.09 \times age^2$	666	674.1	1.79	0.18	0.38	0.0003
Cubic	$CBF_{GM} = 60.74 + 5.82 \times age - 0.92 \times age^2 + 0.03 \times age^3$	663	672.7	3.42	0.06	0.42	< 0.0001

Note: CBF, cerebral blood flow; GM, gray matter; $-2 \ln L$, log-likelihood; AIC, Akaike information criterion; LRT, Likelihood Ratio test between model of order *k* and model of order *k-1* (e.g., for the linear model, the comparison is between linear model and model with intercept only); r, correlation coefficient.

Table 4
CBF values for each age group in lobes.

Age Group	Frontal lobe CBF[a] Mean (± SE) *n* = 82	Insular lobe CBF[a] Mean (± SE) *n* = 83	Limbic lobe CBF[a] Mean (± SE) *n* = 83	Occipital lobe CBF[a] Mean (± SE) *n* = 80	Parietal lobe CBF[a] Mean (± SE) *n* = 82	Temporal lobe CBF[a] Mean (± SE) *n* = 79
6–11 months	54.6 (± 8.7)	55.8 (± 7.7)	55.9 (± 8.6)	69.9 (± 6.2)	60.6 (± 10.3)	62.8 (± 8.8)
12–23 months	68.4 (± 3.9)	66.0 (± 4.0)	67.4 (± 3.9)	75.2 (± 3.3)	68.1 (± 3.8)	75.3 (± 4.1)
2–3 years	76.0 (± 4.9)	71.2 (± 4.4)	71.2 (± 5.0)	86.2 (± 5.3)	79.1 (± 6.2)	81.7 (± 5.0)
4–5 years	59.2 (± 4.6)	60.5 (± 4.9)	61.0 (± 4.3)	78.4 (± 5.9)	68.5 (± 4.7)	68.4 (± 4.6)
6–7 years	71.9 (± 3.2)	65.0 (± 4.1)	66.5 (± 2.3)	78.0 (± 4.1)	72.8 (± 4.3)	80.7 (± 4.4)
8–9 years	64.8 (± 3.8)	56.9 (± 3.2)	62.0 (± 3.3)	70.2 (± 2.7)	64.5 (± 3.8)	69.9 (± 3.9)
10–11 years	63.8 (± 7.1)	54.4 (± 6.5)	56.5 (± 5.9)	72.2 (± 4.9)	61.5 (± 7.2)	65.4 (± 6.5)
12–13 years	52.4 (± 3.1)	48.7 (± 3.2)	48.9 (± 3.1)	54.8 (± 3.6)	48.3 (± 3.2)	56.1 (± 4.0)
14–15 years	59.8 (± 2.3)	55.8 (± 2.5)	56.5 (± 2.9)	66.2 (± 3.8)	57.5 (± 3.4)	64.8 (± 3.3)
Total	63.5 (± 1.6)	59.7 (± 1.6)	61.1 (± 1.5)	72.4 (± 1.7)	64.6 (± 1.8)	70.3 (± 1.8)

Note: CBF, cerebral blood flow; *n*, number of patients; SE, standard error of the means.
[a] CBF unit is mL/100 g/min.

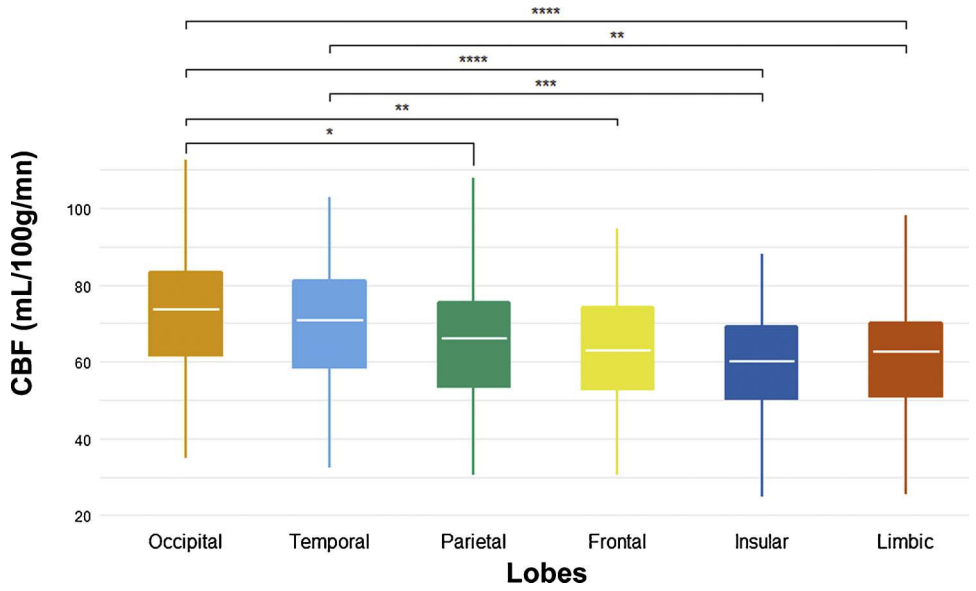

Fig. 3. Lobes CBF values in all population. Only the significant differences between lobes founded by the Tukey's honestly significant difference test are shown. The number of stars designated the level of significance (*: $p < 0.05$; **: $p < 0.01$; ***: $p < 0.001$; ****: $p < 0.0001$).

14–15 years, although male CBF continued to decrease until adulthood. The upper limit of our age group was in mid puberty and this could explain the absence of a significant gender influence.

Very few studies have investigated the influence of anesthesia on ASL CBF in a pediatric population. General anesthesia is known to usually induce depression of CBF and of metabolism [28]. Unlike a previous study [9], significant ASL CBF changes were not enhanced with general anesthesia in our study. The inhaled halogenated anesthetic, sevoflurane, is known to induce direct vasodilation of the cerebral vessels and could unbalance CBF reduction [29]. Furthermore, sevoflurane has a smaller vasodilation effect than other halogenated anesthetics and is less likely to induce brain luxury perfusion. These results suggest that sevoflurane should be preferred to other anesthetics in pediatric brain perfusion research.

Our workflow allowed fully automated processing of ASL data, adjusted to pediatric MRI conditions. A major feature of our processing workflow was the correction of subject motion, which is of particular importance in pediatric populations. A few abnormal or moved ASL repetitions could induce outlier values in the ASL CBF map. Sidaros et al. [30] showed that regular motion correction was often insufficient in an infant population, and could cause strong corolla-shaped artifacts. Furthermore, regular motion correction requires the definition of excessive motion and the suppression or the correction of moved repetitions. The use of a robust estimator of the mean like Huber's M-estimator overcomes the drawbacks of regular motion correction to avoid outliers and artifacts induced by uncorrected corrupted ASL repetitions [18].

Our workflow included a few limitations such as the use of NIHPD templates, which had an age range (4.5–18.5 years) different to that of our population. CBF measurements in white matter were higher for 1 year and 2–3 years age groups. Consequently, a cross-contamination between gray matter and white matter CBF values was possible, although no visual segmentation errors were found between 6 months and 4 years.

The aim of this work was to provide CBF reference values that could be used in clinical practice or in research studies. However, the different approaches of ASL (pulsed, continuous, pseudocontinuous), the different available quantification models and the varying values of quantification parameters make this goal difficult to achieve. Consequently, we chose literature values for some parameters (blood T1, brain/blood partition coefficient) and a single compartment quantification model in the quantification step, which was simpler to handle in clinical practice. These choices could have induced quantification errors, the aforementioned parameters being higher during childhood than in adulthood. Given that the use of adult values leads to underestimation of CBF for the brain/blood partition coefficient and overestimation of CBF for blood T1, the effects are antagonistic in the quantification step permitting the employment of adult values as suggested by Wang et al. and Alsop et al. [13,20].

All MRI examinations were acquired in a clinical setting. Therefore, subjects in our study were not strictly healthy children and it could have affected CBF values. However, exclusion criteria were defined so as to exclude all pathologies that may affect brain perfusion and morphological MRI examinations had to be normal. Moreover, it would have been ethically questionable to recruit healthy children for studies requiring general anesthesia or sedation.

In conclusion, we provided values of ASL CBF in the brain, gray matter, white matter, hemispheres, and lobes over a wide age range, showing approximatively inverted U-shaped changes in brain perfusion in gray matter over the course of childhood. No significant effect of gender or general anesthesia on pediatric ASL CBF was found, thus allowing the development of ASL to be considered in pediatric patients. Our CBF data shows inter-subject variability and are cross-sectional; a longitudinal study would allow better modeling of the relationship between age and brain perfusion from birth to adulthood.

Conflict of interest

The authors have no conflicts of interest.

Grant support

Aline Carsin-Vu received a research grant from the French Society of Radiology. The funding source was not involved in the study design; in the collection, analysis or interpretation of data; in the writing of the report.

Appendix A. Definition of lobes using AAL labels

Names of lobes	Names of labels in AAL	Number of RIGHT labels	Number of LEFT labels
Frontal	Precentral gyrus	2002	2001
	Superior frontal gyrus, dorsolateral	2102	2101
	Superior frontal gyrus, orbital part	2112	2111
	Middle frontal gyrus	2202	2201
	Middle frontal gyrus, orbital part	2212	2211
	Inferior frontal gyrus, opercular part	2302	2301
	Inferior frontal gyrus, triangular part	2312	2311
	Inferior frontal gyrus, orbital part	2322	2321
	Rolandic operculum	2332	2331
	Supplementary motor area	2402	2401
	Olfactory cortex	2502	2501
	Superior frontal gyrus, medial	2602	2601
	Superior frontal gyrus, medial orbital	2612	2611
	Gyrus rectus	2702	2701
	Paracentral Lobule	6402	6401
Temporal	Superior temporal gyrus	8112	8111
	Temporal pole: superior temporal gyrus	8122	8121
	Middle temporal gyrus	8202	8201
	Temporal pole: middle temporal gyrus	8212	8211
	Inferior temporal gyrus	8302	8301
	Heschl gyrus	8102	8101
Parietal	Superior parietal gyrus	6102	6101
	Inferior parietal gyrus	6202	6201
	Precuneus	6302	6301
	Angular gyrus	6222	6221
	Supramarginal gyrus	6212	6211
	Postcentral gyrus	6002	6001
Occipital	Superior occipital gyrus	5102	5101
	Middle occipital gyrus	5202	5201
	Inferior occipital gyrus	5302	5301
	Cuneus	5012	5011
	Calcarine fissure and surrounding cortex	5002	5001
	Lingual gyrus	5022	5021
	Fusiform gyrus	5402	5401
Limbic	Anterior cingulate and paracingulate gyri	4002	4001

	Median cingulate and paracingulate gyri	4012	4011
	Posterior cingulate gyrus	4022	4021
	Hippocampus	4102	4101
	Parahippocampal gyrus	4112	4111
Insular	Insula	3002	3001

References

[1] J.A. Detre, J.S. Leigh, D.S. Williams, A.P. Koretsky, Perfusion imaging, Magn. Reson. Med. 23 (1992) 37–45.

[2] L. Sokoloff, Localization of functional activity in the central nervous system by measurement of glucose utilization with radioactive deoxyglucose, J. Cereb. Blood Flow Metab. 1 (1981) 7–36.

[3] M. Proisy, B. Bruneau, C. Rozel, C. Tréguier, K. Chouklati, L. Riffaud, P. Darnault, J.-C. Ferré, Arterial spin labeling in clinical pediatric imaging, Diagn. Interv. Imaging 97 (2016) 151–158.

[4] P. Wintermark, A. Hansen, M.C. Gregas, J. Soul, M. Labrecque, R.L. Robertson, S.K. Warfield, Brain perfusion in asphyxiated newborns treated with therapeutic hypothermia, AJNR Am. J. Neuroradiol. 32 (2011) 2023–2029.

[5] J. Chen, D.J. Licht, S.E. Smith, S.C. Agner, S. Mason, S. Wang, D.W. Silvestre, J.A. Detre, R.A. Zimmerman, R.N. Ichord, J. Wang, Arterial spin labeling perfusion MRI in pediatric arterial ischemic stroke: initial experiences, J. Magn. Reson. 29 (2009) 282–290.

[6] V. Dangouloff-Ros, C. Deroulers, F. Foissac, M. Badoual, E. Shotar, D. Grévent, R. Calmon, M. Pagès, J. Grill, C. Dufour, T. Blauwblomme, S. Puget, M. Zerah, C. Sainte-Rose, F. Brunelle, P. Varlet, N. Boddaert, Arterial spin labeling to predict brain tumor grading in children: correlations between histopathologic vascular density and perfusion MR imaging, Radiology 281 (2016) 553–566.

[7] J.B. De Vis, E.T. Petersen, L.S. de Vries, F. Groenendaal, K.J. Kersbergen, T. Alderliesten, J. Hendrikse, M.J.N.L. Benders, Regional changes in brain perfusion during brain maturation measured non-invasively with Arterial Spin Labeling MRI in neonates, Eur. J. Radiol. 82 (2013) 538–543.

[8] A.F. Duncan, A. Caprihan, E.Q. Montague, J. Lowe, R. Schrader, J.P. Phillips, Regional cerebral blood flow in children from 3 to 5 months of age, AJNR Am. J. Neuroradiol. 35 (2014) 593–598.

[9] L. Biagi, A. Abbruzzese, M.C. Bianchi, D.C. Alsop, A. Del Guerra, M. Tosetti, Age dependence of cerebral perfusion assessed by magnetic resonance continuous arterial spin labeling, J. Magn. Reson. 25 (2007) 696–702.

[10] Y. Taki, H. Hashizume, Y. Sassa, H. Takeuchi, K. Wu, M. Asano, K. Asano, H. Fukuda, R. Kawashima, Correlation between gray matter density-adjusted brain perfusion and age using brain MR images of 202 healthy children, Hum. Brain Mapp. 32 (2011) 1973–1985.

[11] P.W. Hales, J.M. Kawadler, S.E. Aylett, F.J. Kirkham, C.A. Clark, Arterial spin labeling characterization of cerebral perfusion during normal maturation from late childhood into adulthood: normal "reference range" values and their use in clinical studies, J. Cereb. Blood Flow Metab. 34 (2014) 776–784.

[12] B.B. Avants, J.T. Duda, E. Kilroy, K. Krasileva, K. Jann, B.T. Kandel, N.J. Tustison, L. Yan, M. Jog, R. Smith, Y. Wang, M. Dapretto, D.J.J. Wang, The pediatric template of brain perfusion, Sci. Data 2 (2015) 150003.

[13] J. Wang, D.J. Licht, G.-H. Jahng, C.-S. Liu, J.T. Rubin, J. Haselgrove, R.A. Zimmerman, J.A. Detre, Pediatric perfusion imaging using pulsed arterial spin labeling, J. Magn. Reson. 18 (2003) 404–413.

[14] W.M. Luh, E.C. Wong, P.A. Bandettini, J.S. Hyde, QUIPSS II with thin-slice TI1 periodic saturation: a method for improving accuracy of quantitative perfusion imaging using pulsed arterial spin labeling, Magn. Reson. Med. 41 (1999) 1246–1254.

[15] S.M. Smith, Fast robust automated brain extraction, Hum. Brain Mapp. 17 (2002) 143–155.

[16] V. Fonov, A.C. Evans, K. Botteron, C.R. Almli, R.C. McKinstry, D.L. Collins, Brain Development Cooperative Group, Unbiased average age-appropriate atlases for pediatric studies, Neuroimage 54 (2011) 313–327.

[17] K.J. Friston, C.D. Frith, R.S. Frackowiak, R. Turner, Characterizing dynamic brain responses with fMRI: a multivariate approach, Neuroimage 2 (1995) 166–172.

[18] C. Maumet, P. Maurel, J.-C. Ferré, C. Barillot, Robust estimation of the cerebral blood flow in arterial spin labelling, Magn. Reson. Imaging 32 (2014) 497–504.

[19] J. Wang, D.C. Alsop, L. Li, J. Listerud, J.B. Gonzalez-At, M.D. Schnall, J.A. Detre, Comparison of quantitative perfusion imaging using arterial spin labeling at 1.5 and 4.0 Tesla, Magn. Reson. Med. 48 (2002) 242–254.

[20] D.C. Alsop, J.A. Detre, X. Golay, M. Günther, J. Hendrikse, L. Hernandez-Garcia, H. Lu, B.J. MacIntosh, L.M. Parkes, M. Smits, M.J.P. van Osch, D.J.J. Wang, E.C. Wong, G. Zaharchuk, Recommended implementation of arterial spin-labeled perfusion MRI for clinical applications: a consensus of the ISMRM perfusion study group and the European consortium for ASL in dementia, Magn. Reson. Med. 73 (2015) 102–116.

[21] H.J.M.M. Mutsaerts, E. Richard, D.F.R. Heijtel, M.J.P. van Osch, C.B.L.M. Majoie, A.J. Nederveen, Gray matter contamination in arterial spin labeling white matter perfusion measurements in patients with dementia, Neuroimage Clin. 4 (2014) 139–144.

[22] N. Tzourio-Mazoyer, B. Landeau, D. Papathanassiou, F. Crivello, O. Etard, N. Delcroix, B. Mazoyer, M. Joliot, Automated anatomical labeling of activations in SPM using a macroscopic anatomical parcellation of the MNI MRI single-subject brain, Neuroimage 15 (2002) 273–289.

[23] C. Chiron, C. Raynaud, B. Mazière, M. Zilbovicius, L. Laflamme, M.C. Masure, O. Dulac, M. Bourguignon, A. Syrota, Changes in regional cerebral blood flow during brain maturation in children and adolescents, J. Nucl. Med. 33 (1992) 696–703.

[24] M. Wintermark, D. Lepori, J. Cotting, E. Roulet, G. van Melle, R. Meuli, P. Maeder, L. Regli, F.R. Verdun, T. Deonna, P. Schnyder, F. Gudinchet, Brain perfusion in children: evolution with age assessed by quantitative perfusion computed tomography, Pediatrics 113 (2004) 1642–1652.

[25] H.T. Chugani, M.E. Phelps, J.C. Mazziotta, Positron emission tomography study of human brain functional development, Ann. Neurol. 22 (1987) 487–497.

[26] T.D. Satterthwaite, R.T. Shinohara, D.H. Wolf, R.D. Hopson, M.A. Elliott, S.N. Vandekar, K. Ruparel, M.E. Calkins, D.R. Roalf, E.D. Gennatas, C. Jackson, G. Erus, K. Prabhakaran, C. Davatzikos, J.A. Detre, H. Hakonarson, R.C. Gur, R.E. Gur, Impact of puberty on the evolution of cerebral perfusion during adolescence, Proc. Natl. Acad. Sci. U. S. A. 111 (2014) 8643–8648.

[27] V. Jain, J. Duda, B. Avants, M. Giannetta, S.X. Xie, T. Roberts, J.A. Detre, H. Hurt, F.W. Wehrli, D.J.J. Wang, Longitudinal reproducibility and accuracy of pseudo-continuous arterial spin-labeled perfusion MR imaging in typically developing children, Radiology 263 (2012) 527–536.

[28] L. Schlünzen, N. Juul, K.V. Hansen, G.E. Cold, Regional cerebral blood flow and glucose metabolism during propofol anaesthesia in healthy subjects studied with positron emission tomography, Acta Anaesthesiol. Scand. 56 (2012) 248–255.

[29] K.K. Kaisti, J.W. Långsjö, S. Aalto, V. Oikonen, H. Sipilä, M. Teräs, S. Hinkka, L. Metsähonkala, H. Scheinin, Effects of sevoflurane, propofol, and adjunct nitrous oxide on regional cerebral blood flow, oxygen consumption, and blood volume in humans, Anesthesiology 99 (2003) 603–613.

[30] K. Sidaros, K. Olofsson, M.J. Miranda, O.B. Paulson, Arterial spin labeling in the presence of severe motion, J. Cereb. Blood Flow Metab. 25 (2005) S382.

“Magnetic resonance imaging in children presenting migraine with aura: Association of hypoperfusion detected by arterial spin labelling and vasospasm on MR angiography findings. Cephalalgia 2018”

Résumé

Un enfant présentant une première crise de migraine avec aura bénéficie généralement d’une imagerie par résonance magnétique pour exclure un accident vasculaire cérébral. Le but de cette étude était de rapporter les résultats de la perfusion vasculaire et cérébrale chez les enfants souffrant de migraine avec aura en angio-MR en temps de vol (TOF-MRA) et imagerie de perfusion en ASL.

Nous avons rétrospectivement inclus tous les enfants ayant eu une IRM en urgence avec ASL et TOF-MRA, pour déficit neurologique aigu et dont le diagnostic final était celui de migraine avec aura. Les cartes de perfusion ASL et les images de TOF-MRA ont été évaluées indépendamment par des examinateurs en aveugles des données cliniques. Un CBF moyen a été obtenu pour chaque lobe cérébral après le post-traitement automatisé des images.

Dix-sept enfants ont finalement été inclus. Une hypoperfusion était visualisée dans un ou plusieurs lobes cérébraux sur les cartographies de perfusion chez 16/17 (94%) enfants. Un vasospasme intracrânien été retrouvé sur les images TOF-MRA chez 12/17 (71%) enfants. Toutes les images TOF-MRA anormales (100%) étaient associées à hypoperfusion homolatérale. Les valeurs moyennes de CBC étaient significativement plus faibles ($p < 0,05$) dans les lobes visuellement hypoperfusés que dans les lobes normalement perfusés.

En conclusion, l’ASL et l’angio-MR TOF sont deux séquences d'IRM totalement non invasives et faciles à utiliser pour les enfants en situation d'urgence. Une hypoperfusion associée à un vasospasme homolatéral peut suggérer un diagnostic de migraine avec aura.

Implications cliniques

- L’ASL est une technique de perfusion cérébrale totalement non invasive qui peut être facilement ajoutée en plus des séquences conventionnelles en IRM pour établir un diagnostic positif de migraine avec aura chez les enfants.
- La migraine avec aura est généralement caractérisée par une hypoperfusion cérébrale qui ne se limite pas à un territoire vasculaire, qui est souvent asymétrique et affecte préférentiellement les régions cérébrales postérieures.

- Le TOF-MRA peut montrer une visualisation légèrement réduite des branches artérielles distales liées à un vasospasme.
- Dans la pratique de routine, lors de l'étude du déficit neurologique avec maux de tête, la boîte d'acquisition de la TOF peut être positionnée légèrement plus haut que la position standard pour améliorer la visualisation des branches artérielles distales.
- L'association d'une hypoperfusion ASL et d'un vasospasme dans les branches distales des artères intracrâniennes en TOF-MRA peut faire renforcer un diagnostic clinique de migraine et soutient la théorie neurovasculaire de la migraine avec aura.

Original Article

Cephalalgia
An International Journal of Headache

International Headache Society

Cephalalgia
0(0) 1–10

DOI: 10.1177/0333102417723570
journals.sagepub.com/home/cep

SAGE

Magnetic resonance imaging in children presenting migraine with aura: Association of hypoperfusion detected by arterial spin labelling and vasospasm on MR angiography findings

Domitille Cadiot[1], Romain Longuet[2], Bertrand Bruneau[1], Catherine Treguier[1], Aline Carsin-Vu[3], Isabelle Corouge[3], Constantin Gomes[4] and Maïa Proisy[1,3]

Abstract

Objective: A child presenting with a first attack of migraine with aura usually undergoes magnetic resonance imaging (MRI) to rule out stroke. The purpose of this study was to report vascular and brain perfusion findings in children suffering from migraine with aura on time-of-flight MR angiography (TOF-MRA) and MR perfusion imaging using arterial spin labelling (ASL).

Methods: We retrospectively included all children who had undergone an emergency MRI examination with ASL and TOF-MRA sequences for acute neurological deficit and were given a final diagnosis of migraine with aura. The ASL perfusion maps and TOF-MRA images were independently assessed by reviewers blinded to clinical data. A mean cerebral blood flow (CBF) value was obtained for each cerebral lobe after automatic data post-processing.

Results: Seventeen children were finally included. Hypoperfusion was identified in one or more cerebral lobes on ASL perfusion maps by visual assessment in 16/17 (94%) children. Vasospasm was noted within the intracranial vasculature on the TOF-MRA images in 12/17 (71%) children. All (100%) of the abnormal TOF-MRA images were associated with homolateral hypoperfusion. Mean CBF values were significantly lower ($P < 0.05$) in visually hypoperfused lobes than in normally perfused lobes.

Conclusion: ASL and TOF-MRA are two totally non-invasive, easy-to-use MRI sequences for children in emergency settings. Hypoperfusion associated with homolateral vasospasm may suggest a diagnosis of migraine with aura .

Keywords

Perfusion imaging, migraine with aura, vasoconstriction, diagnostic imaging

Date received: 23 March 2017; revised: 26 May 2017; 5 June 2017; accepted: 8 June 2017

The prevalence of migraine in children is in the range of 2.7–17% (1). There are two major subtypes of migraine: with or without aura. Aura migraines are characterised by transient focal neurological symptoms associated with headache. Symptoms can be motor, visual, sensory, aphasia or decreased level of consciousness. They last for 5–60 min and are accompanied, or followed within 60 min, by headache. Most children with migraine experience aura-type migraines during their lifetime (1,2).

Migraine with aura presents as an acute neurological disorder mimicking stroke, especially the initial attacks. It calls for emergency imaging. But strokes are less

[1]CHU Rennes, Department of Radiology, Pediatric Imaging, Rennes, France
[2]CHU Rennes, Department of Pediatrics, Rennes, France
[3]INSERM U1228, Unité Visage, CNRS UMR 6074, Université de Rennes I, Rennes, France
[4]CHU Rennes, Department of Neurophysiology, Rennes, France

Corresponding author:
Domitille Cadiot, Department of Radiology, Pediatric Imaging Unit, Rennes University Hospital, CHU Hôpital Sud, 16 Boulevard de Bulgarie, 35200, Rennes, France.
Email: domitille.cadiot@chu-rennes.fr

common than migraine with aura in children (3,4). Magnetic resonance imaging (MRI) combined with diffusion-weighted imaging (DWI) sequences is the most sensitive radiological technique for ruling out stroke. The diagnosis of migraine is generally a clinical diagnosis, with normal findings on conventional imaging (structural imaging and DWI) if undertaken.

The pathophysiology of migraine attacks with aura is still unclear. Hypoperfusion was described in adult populations by Olesen in 1990 using intracarotid xenon-133 injection and single-photon emission computed tomography (SPECT) (5,6). Olesen described a hypoperfusion pattern during the aura phase of the migraine attack followed by a hyperperfusion pattern during the headache phase itself. More recently, two studies demonstrated cerebral hypoperfusion in 14/20 and 18/33 adult patients suffering from aura migraine with neurological deficit mimicking acute stroke by using susceptibility-based MR perfusion-weighted imaging following bolus injection (DSC-PWI) (7,8).

Among the various perfusion imaging techniques available, arterial spin labelling (ASL) is an emerging MRI sequence that can be easily performed during conventional MRI without contrast injection or any side effects (9). The only downside is a longer examination time of approximately 5 min. In children, a single study in the literature has shown the sensitivity of ASL in detecting perfusion abnormalities in a series of ten patients suffering from migraine with aura (10). Time-of-flight MR angiography (TOF-MRA) sequences provide visualisation of the intracranial arteries without contrast injection and are usually used if a stroke is suspected. Literature studies describing TOF-MRA findings in migraine with aura are rare. A reversible vasospasm has been reported in an 11-year-old girl (11) and more recently in a series of eight children suffering from acute hemiplegic migraine (12).

The aim of our study was to report ASL cerebral perfusion imaging and TOF-MRA findings in children with aura migraine.

Materials and methods

Patients

A retrospective analysis was conducted in our institution over a three-year period. We retrospectively included all children who had undergone emergency MRI with ASL and TOF-MRA sequences in our radiology department for acute neurological (visual, language, motor or sensory) deficit and whose final diagnosis was migraine with aura, according to the ICHD-3 beta criteria (13).

Children with a motor deficit were classified as having hemiplegic migraine, and children with a decreased level of consciousness and no motor deficit were classified as having brainstem aura.

Exclusion criteria were children with a complex neurological history (e.g. coma or epilepsy), an uncertain diagnosis of migraine with aura, an incomplete MR examination (no TOF-MRA or ASL) or uninterpretable TOF-MRA or ASL sequences.

Four of our patients underwent a control MRI examination.

Our study was approved by the local Ethics Committee. Parental consent was obtained.

Clinical data

The following demographic and clinical data were retrospectively collected from medical files: age; sex; past medical history including personal or family history of migraine; ongoing medical treatment; symptom onset; and duration. The neurological examination was assessed by a senior emergency paediatrician.

Imaging study

All children were imaged using a Siemens 1.5T Magnetom Aera scanner and a 16-channel head coil (Siemens; Erlangen, Germany). The brain MRI protocol included routine sequences as implemented in our standard protocol: axial fluid-attenuated inversion recovery (FLAIR); axial T2 gradient-echo; three-dimensional (3D)-T1; diffusion-weighted MRI; and TOF-MRA.

As the TOF-MRA sequence is performed to rule out stenosis or occlusion, standard TOF-MRA acquisition box placement is usually over the circle of Willis. We noticed two different acquisition box positions in our population due to practice variability: the standard position (stroke protocol) and a higher position where the distal arterial branches are best visualised.

The non-contrast perfusion two-dimensional (2D) pulsed ASL MRI sequence used was PICORE Q2TIPS (14). Imaging parameters were as follows: $TR/TE/TI_1/TI_2 = 3500/12/700/1800$ ms; voxel size $= 4 \times 4 \times 8$ mm; gap $= 2$ mm; 30 label/control pairs; total scan time $= 3$ min 20 s. One M0 reference image was acquired. Multi-slice single-shot echo-planar imaging (EPI) was used as readout. ASL perfusion images were automatically generated by the Siemens station and used for visual/qualitative analysis.

Additionally, post-processing of both 3D-T1 and ASL data was performed using AutoASL, a custom-built ASL processing tool based on SPM software (Wellcome Trust Centre for Neuroimaging, University College of London, UK) and Matlab® (The MathWorks, Inc.) to create a quantitative map of cerebral blood flow (CBF). Furthermore, brain

segmentation was automatically performed using templates. Regions of interest (ROI) were defined using the Automated Anatomical Labeling (AAL) atlas (15) to obtain a quantitative CBF value (mL/100 g/min) for each lobe.

Imaging analysis

All MR images were retrospectively analysed by two paediatric radiologists in consensus. The TOF-MRA and ASL images were evaluated separately. The reviewers were blinded to clinical data, including the side affected by the neurological symptoms.

First, the perfusion maps were analysed visually with the readers blinded to all other sequences, including MRA. Perfusion maps were classified as showing a normal perfusion pattern or abnormal perfusion pattern. Perfusion symmetry was also assessed. Perfusion abnormalities were classified as areas of hypoperfusion or hyperperfusion in each cerebral lobe: frontal (F); temporal (T); parietal (P); and occipital (O). Second, a mean CBF value (mL/100 g/min) was obtained for each lobe after data post-processing. Finally, the mean CBF and standard deviation (SD) were determined in the lobes that were visually hypoperfused and those that were visually normally perfused.

Syngo.via® (Siemens) was used to analyse the circle of Willis vessels on the 3D TOF stack. TOF-MRA images were analysed for each hemisphere and arterial territory of the circle of Willis: anterior cerebral artery (ACA); middle cerebral artery (MCA); and posterior cerebral artery (PCA). TOF-MRA findings were classified as follows: normal; vasoconstriction of the peripheral branches; vasodilation of the peripheral branches; or stenosis.

Statistical analysis

Quantitative variables were described by a mean ± SD or median (range). After verification of normality, the comparison of CBF values was analysed using Student's *t*-test. All statistics were performed with a 0.05 level of significance.

Results

Clinical and laboratory findings

Between January 2014 and November 2016, we finally included 17 children aged 11–16 years (mean age = 13.6 years ± 1.5). There were eight girls and nine boys.

Six children had a personal history of migraine, four of which also had a family history. For the 11 remaining children, there was either no history of migraine or no information available. Five of them (30%) had a history of CT scan performed for 'brain trauma' between six months and nine years previously (median time = 5 years).

The median time between arrival at the emergency room and the MRI examination was 1 h 51 min (range = 7 min–5 h 32 min). The median onset-to-MRI time was 6 h (range = 1 h 36 min–2 days) for onset of the aura and 6 h 15 min (range = 2 h 30 min–3 days) for headache. All children presented with headache before or during the MRI examination.

Symptoms included visual disturbance (n = 7), aphasia/dysarthria (n = 12), sensory deficit (n = 10), motor deficit (n = 2), sensory and motor deficit (n = 3) and decreased level of consciousness (n = 3). Some children had several symptoms simultaneously.

The population characteristics are summarised in Table 1. Only six children had a prior migraine history and therefore met the International Classification of Headache Disorders criteria for migraine with aura (13). When excluding the criterion defining the number of earlier episodes, ten children met the criteria for migraine with typical aura, five children for hemiplegic migraine and two children for brainstem aura.

Three patients also underwent electroencephalography (EEG) examinations. Two of them had abnormal EEG results showing hemispheric slowing contralateral to the side of hemiplegia (patients 9 and 13). One patient had a normal EEG (patient 10).

Four children underwent follow-up MRI between 1 day and 3 h (27 h) and 3 days and 2 h (74 h) after the acute neurological episode. Symptoms had

Table 1. Population characteristics.

Population	17
Girls/Boys	8/9
Mean age (years)	13.6 ± 1.5
Arrival to MRI time (median, range)	Median 1 h 51 min (7 min–5 h 32 min)
Clinical presentation	
Sensory deficit	10/17 (59%)
Motor deficit	2/17 (12%)
Sensory and motor deficit	3/17 (18%)
Decreased level of consciousness	3/17 (18%)
Dysarthria, aphasia	12/17 (71%)
Visual disturbance	7/17 (41%)
Headache	17/17 (100%)
Aura to MRI time (median, range)	6 h 00 min (1 h 36 min–2 days)
Headache to MRI time (median, range)	6 h 15 min (2 h 30 min–3 days)

disappeared when follow-up MRI was performed and the neurological examination was normal. The same MRI protocol including TOF-MRA and ASL was used.

Neuroimaging findings

Standard conventional MR sequences were normal for every patient, particularly the DWI and FLAIR sequences.

Perfusion maps

In 16 patients (16/17 [94%]), alteration of cerebral perfusion was found by visual assessment. It was always hypoperfusion (100%), which was unilateral in 13/16 (81%) and bilateral in 3/16 (19%) patients. Among the patients with unilateral hypoperfusion, left hemisphere involvement was predominant (10/13 patients, 77%) compared with right hemisphere involvement (3/13 patients, 23%).

Bilateral and symmetrical hypoperfusion was found in two patients (patients 13 and 15). Bilateral and asymmetrical hypoperfusion with left-side predominance was found in one case (patient 6).

When hypoperfusion involved the left hemisphere, four (FTOP; $n = 7$) and three (TPO; $n = 3$) lobes were affected. When hypoperfusion involved the right hemisphere, four (FTOP; $n = 1$), two (TO; $n = 1$) and one (P; $n = 1$) lobes were affected.

CBF values

The mean CBF value in the visually hypoperfused lobes was 40.3 ± 6.4, 44.9 ± 8.4, 45.0 ± 9.5 and 35.9 ± 6.5 mL/100g/min in the frontal, temporal, occipital and parietal lobes, respectively. The mean CBF value in the normally perfused lobes was 53.6 ± 13.1, 59.5 ± 12.1, 59.9 ± 9.5 and 51.9 ± 9.5 mL/100g/min in the frontal, temporal, occipital and parietal lobes, respectively. There was a significant difference between all the lobes with $P = 0.036$, $P = 0.008$, $P = 0.005$ and $P < 0.001$, respectively (Figure 1).

The mean difference in CBF values when asymmetrical cerebral perfusion was observed by visual assessment was 32.7 ± 8.6, 30.2 ± 9.2, 28.8 ± 12.7 and 28.4 ± 11.9% in the frontal, temporal, occipital and parietal lobes, respectively. The mean difference in CBF values when there was a symmetrical perfusion map on visual assessment was 6.8 ± 2.7; 7.0 ± 4.2; 11.6 ± 10.3 and 7.4 ± 3.8% in the frontal, temporal, occipital and parietal lobes, respectively. There was a significant difference between all the lobes with $P < 0.001$, $P = 0.001$, $P = 0.044$ and $P = 0.003$, respectively.

TOF-MRA

Finally 9/17 (53%) MRI examinations had a higher acquisition box and the findings were all abnormal. All normal TOF-MRA (5/17, 30%) images had standard acquisition box placement which did not allow visualisation of the distal arterial branches.

Twelve TOF-MRA images displayed abnormalities (12/17, 71%). These were vasospasm with decreased visualisation of the peripheral branches in all cases. Neither stenosis nor occlusion was found.

The arteries affected were both MCA and PCA in seven children (7/12, 58%) and MCA or PCA alone in three children (3/12, 25%). There was bilateral involvement (PCA or/and MCA) in two children (2/12, 17%).

ASL/TOF-MRA mapping

Perfusion map abnormality (16/17) was greater than TOF-MRA abnormality (12/17). All vascular abnormalities found on the TOF-MRA sequence matched the homolateral hypoperfusion on the ASL sequence (12/16, 75%).

Representative hypoperfusion and homolateral vasospasm are shown in Figure 2. An example of an abnormal perfusion map and normal TOF-MRA image is shown in Figure 3.

MRI/clinical mapping

Among the children presenting with focal neurological deficit (15/17), contralateral hypoperfusion was seen on the perfusion maps in 14/15 cases. One child had a normal perfusion map (patient 7), but we note that for this patient's MRI was performed two days after the onset of symptoms. One patient (patient 13) had bilateral temporo-occipital hypoperfusion but presented with left sensory-motor deficit.

Among the two patients with no focal neurological deficit, one (patient 8) had visual symptoms and right hemisphere hypoperfusion, and the other (patient 15) had a decreased level of consciousness with a Glasgow Coma Scale score of 13 and diffuse symmetrical cerebral hypoperfusion with diffuse vasoconstriction on TOF-MRA.

The times and clinical and neuroimaging findings are provided for each patient in Table 2.

Follow-up MRI

Four patients underwent follow-up MRI 27–74 h after the onset of neurological symptoms. No perfusion abnormality was detected on imaging in three out of four cases and the TOF-MRA images were normal in

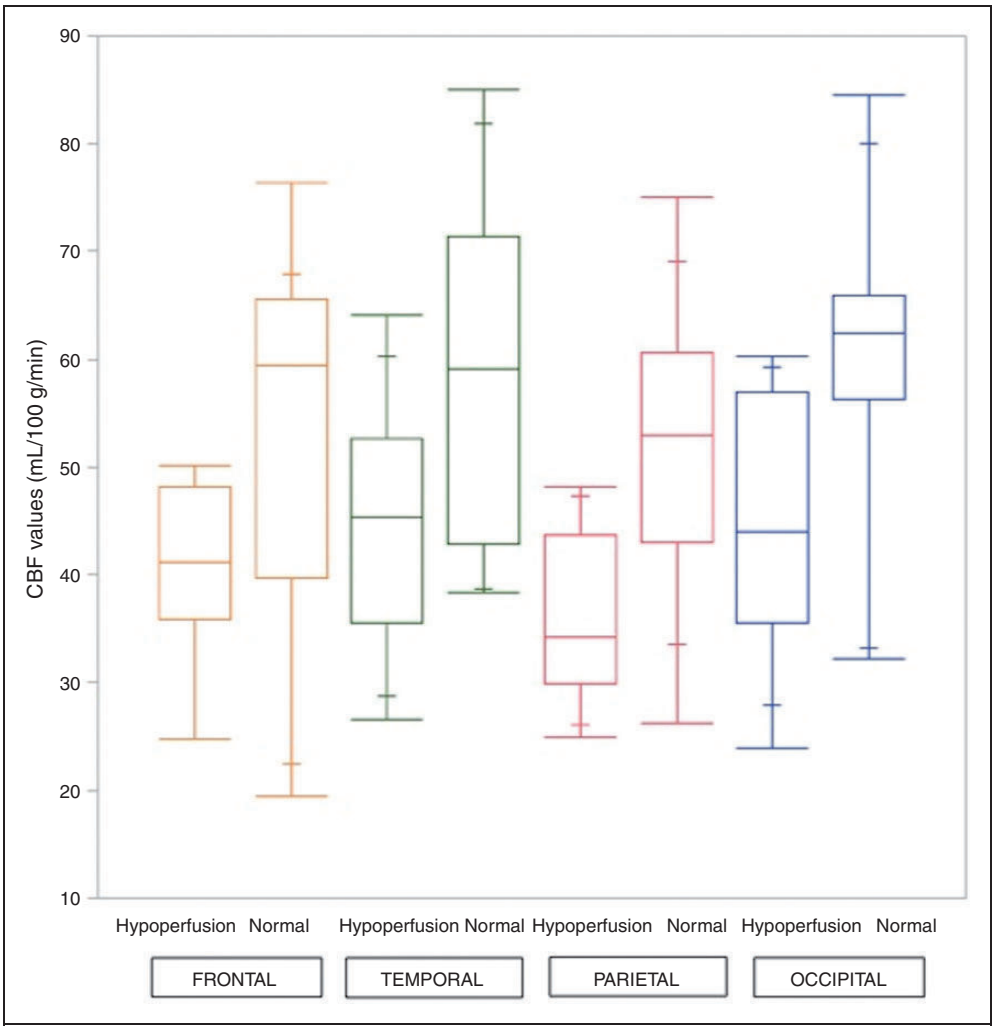

Figure 1. Box plot of CBF values in the frontal, temporal, parietal and occipital lobes. There is a significant difference ($P < 0.05$) between mean CBF in hypoperfused and normally perfused lobes assessed visually on ASL perfusion maps.

all four cases. Representative normal follow-up MRI is shown in Figure 2.

For one child (patient 3, time = 28 h), visual hyperperfusion was observed in the cerebral regions that were initially hypoperfused (four lobes).

Discussion

The main finding of our study was that all but one (94%) child presented with regional cerebral hypoperfusion on MR perfusion imaging with ASL, which was frequently associated (75%) with a minor vasospasm of the intracranial arteries on the TOF-MRA images. To our knowledge, this is the first study in the literature to report both perfusion abnormalities and angiography findings in children with atypical aura.

ASL is a non-invasive perfusion technique which does not require injection of contrast material, unlike DSC PWI. In recent years, the technique has therefore become more widely used for paediatric patients. In addition, it offers the capability to quantify absolute CBF. In our study, the mean CBF values were significantly different between the visually hypoperfused and normally perfused lobes.

The pathophysiology of migraine with aura is still poorly understood. The neuronal theory, introduced by Lashley and Leao in 1946 (16,17) describes a phenomenon known as cortical spreading depression (CSD), triggered by initial cortical hyperexcitability and moving from the posterior (occipital) regions to the anterior regions. Vascular phenomena have been shown with different perfusion imaging techniques in adults, in connection with CSD (6,18). In 1990, Olesen demonstrated parieto-occipital oligemia using an intra-carotid xenon-133 injection triggering migraine aura and similar to cortical spreading depression.

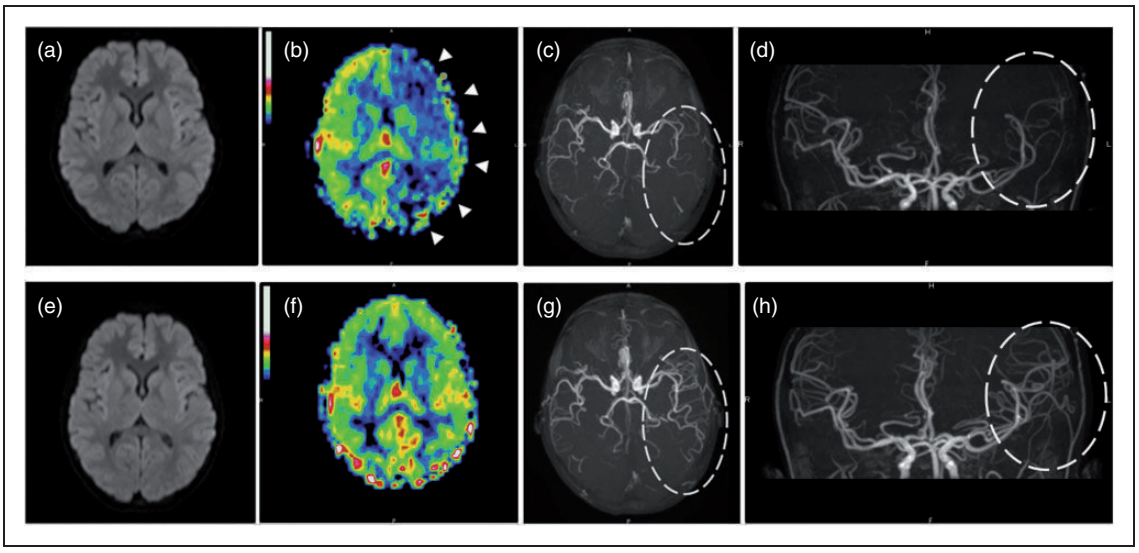

Figure 2. A 13-year-old girl presenting with acute right sensory deficit, dysarthria and decreased level of consciousness. Initial MRI (a–d) performed 9 h 16 min after the onset of aura shows no ischemia on DWI (a), left hypoperfusion in the frontal, temporal, parietal and occipital lobes (arrow heads) on the ASL perfusion map (b), and vasospasm of the distal branches of the left middle cerebral arteries and posterior cerebral arteries (ellipse) on axial (c) and coronal (d) 3D TOF-MRA. Follow-up MRI (e–h) performed one day later shows no ischemia on DWI (e), normalisation of the ASL perfusion map (f), and resolution of vasospasm (ellipse) on axial (g) and coronal (h) 3D TOF-MRA.

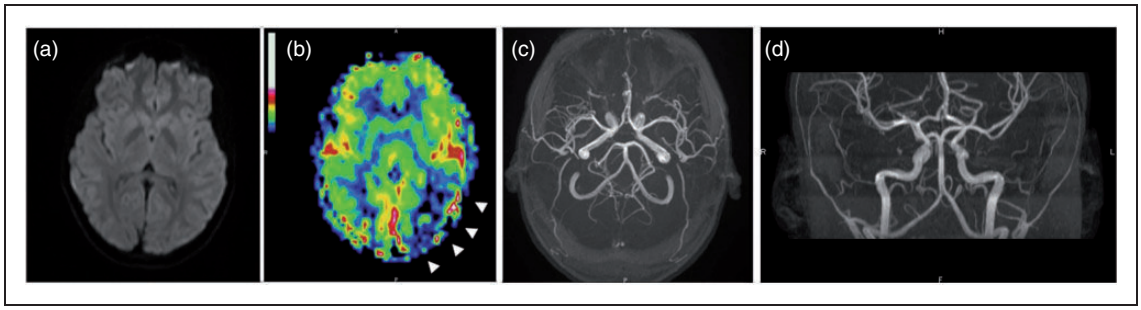

Figure 3. A 14-year-old boy presenting with acute dysarthria and right sensory deficit. Initial emergency MRI shows no ischemia on DWI (a), left temporo-occipital hypoperfusion (arrow heads) on the ASL perfusion map (b), and no vascular abnormalities on axial (c) and coronal (d) 3D TOF-MRA. Note that the low position of the TOF-MRA box does not allow visualisation of the distal intracranial arteries, meaning that distal vasospasm may go underdiagnosed in this case.

More recently, blood-oxygenation-level-dependent (BOLD) functional imaging confirmed the association of a BOLD signal decrease initiated in the occipital cortex contralateral to the aura but without reaching the ischemic threshold (19). This phenomenon is characterised by anterior propagation limited by fissures, not confined to vascular territories, and similar to the cortical spreading depression described by Leao. Perfusion changes vary over time and hypoperfusion tends to occur during the aura phase and hyperperfusion during headache, although the headache phase can begin during hypoperfusion. These abnormalities can vary greatly from one patient and generation to another.

In our study, MRI was performed very early on (median time of 6 h after the onset of neurological symptoms) which probably explains why the abnormalities observed were always hypoperfusion. The only MRI examination with no perfusion abnormality was performed two days after the onset of aura, and we may assume that the abnormalities had already regressed. Hyperperfusion observed on the control scan of one child was consistent with the literature data. This late hyperperfusion was shown in several studies within 17–72 h after the onset of symptoms (10,20,21).

Moreover, we observed that the perfusion abnormalities were predominant in the posterior (parieto-occipital) regions, without being confined to a particular

Table 2. Clinical symptoms and MR imaging findings. Frontal (F), Temporal (T), Parietal (P), Occipital (O), Left (L), Right (R), middle cerebral artery (MCA), posterior cerebral artery (PCA), distal branches (distal), vasoconstriction (VC), nausea (N), vomiting (V).

				Clinical findings							Hypoperfusion	
Patient	Age (years)	Aura to MRI time (h:min)	Headache to MRI time	Headache	Visual disturbance	Sensory deficit	Motor deficit	Aphasia/ Dysarthria	Decreased level of consciousness	Other	ASL	TOF
1	14	4:53	5:53	F bilateral	No	Right	No	Yes	No	X	FTPO L	VC MCA L VC PCA L distal
2	13	3:57	3:57	T bilateral	Yes	Right	No	Yes	No	X	FTPO L	VC MCA L VC PCA L distal
3	16	1:36	2:36	T R	No	Right	No	Yes	No	X	FTPO L	VC MCA L VC PCA L distal
4	13	3:36	3:36	FTOP L	No	Right	No	No	No	X	FTPO L	Normal
5	13	X	X	X	No	Right	No	Yes	No	X	TPO L	Normal
6	14	3:40	3:40	X	Yes	Right	No	Yes	No	N/V	FTPO L O R	Normal
7	13	10:23	10:23	T L	Yes	Right	No	No	No	X	FTPO L	VC MCA L VC PCA L distal
8	11	7:04	7:04	Retro orbital R	Yes	No	No	No	No	N/V Photophonophobia	FTPO R	VC MCA R VC PCA R distal
9	13	9:16	9:16	X	No	Right	No	Yes	Yes	N/V	FTPO L	VC MCA L VC PCA L distal
10	16	2:30	2:30	F R	No	Left	No	Yes	No	N/V Photophonophobia	TO R	Normal
11	13	X	X	X	No	Right	Right	Yes	Yes	X	TPO L	VC MCA L distal
12	12	2:31	3:46	X	No	No	Right	Yes	No	X	FTPO L	VC PCA L distal
13	15	10:00	10:00	P bilateral	No	Left	Left	Yes	No	X	TO R TO L	VC MCA distal bilateral
14	16	2 days	3 days	O bilateral	Yes	No	Left	No	No	X	normal	Normal
15	15	6:37	6:37	X	Yes	No	No	Yes	Yes	N/V Photophonophobia	FTPO L FTOP R	VC MCA VC PCA distal bilateral
16	13	4:30	4:30	X	No	Left	No	Yes	No	X	P R	VC MCA R distal
17	12	9:14	8:44	X	Yes	Right	Right	No	No	N/V	TPO L	VC MCA L VC PCA L distal

vascular territory, and were mostly asymmetrical. The data are similar to the findings for DSC PWI in adults (7,8) and concordant with the theory that CSD begins in the posterior (occipital) region with anterior propagation of the cortical depression broken up by fissures. This distribution of perfusion abnormalities is also consistent with the clinical data reported for adults (22), in that the symptoms are most often unilateral, with a visual impact in the majority of cases. Lastly, in our study we noted that the perfusion abnormalities mostly affected the left hemisphere, and that when the right hemisphere was affected it was to a lesser extent. To our knowledge, left predominance of symptoms is not reported in the literature.

Cerebral perfusion abnormalities are generally due to a vascular abnormality. A study on adult patients with migraine without aura revealed a discreet intracranial vasodilation (23). These data concord with the hyperperfusion phenomenon described during the headache phase. Data regarding MRA findings in migraine with aura are sparse and limited (8,12). Safier et al. report the largest series in the literature which includes eight children with suspected acute hemiplegic migraine. They found vasospasm within the middle cerebral artery branches during attacks in seven patients which had resolved on follow-up imaging. No concomitant perfusion imaging was performed in the study. Our findings corroborate this study and show that the vasospasm observed is associated with homolateral hypoperfusion in ASL, in line with the clinical findings. To our knowledge, there are only two literature reports describing concomitant perfusion and angiographic abnormalities. Forster et al. (8) reported side-to-side differences in peripheral branch visualisation in seven of 33 adult patients with migraine with aura. The patients in their study had undergone MRI for suspected stroke. We may therefore assume that TOF box placement was slightly low as in the standard stroke protocol, and that abnormal TOF findings had been underestimated. In their case report, in addition to cerebral hypoperfusion Kim et al. described homolateral vasoconstriction of the distal branches of the MCA and PCA (24).

This study therefore contributes to a positive diagnosis of migraine with aura. The normalisation of follow-up MRI (perfusion and TOF-MRA) performed on some of our patients confirmed the transient nature of these alterations related to migraine aura. The rest of the morphological imaging should of course be normal in the acute phase, notably the diffusion imaging. In addition, clinical data are also essential for ruling out a different diagnosis. Particularly with vascular abnormalities in a patient with headaches, the main differential diagnosis is reversible cerebral vasoconstriction syndrome (RCVS). The onset of headaches is generally sudden (peak intensity within 1 min) and they can persist for one to four weeks. Besides the clinical data, the angiographic data are also different. Angiography generally shows diffuse bilateral vasoconstriction, with clear irregularities in size presenting as segmental narrowing and dilation ('strings of beads' or 'sausage-string pattern') (25,26).

On retrospective review of the clinical history of all our patients, we noticed that 30% of children had suffered a head injury between six months and nine years previously, requiring admission to the paediatric emergency department of our institution. A brain scan had been indicated and the result was normal for all children. This may be a coincidence but the literature reports a link between migraine and children with juvenile head trauma syndrome (JHTS) (27). CSD shows similar involvement in the JHTS and migraine mechanisms according to Haas (28). To our knowledge, no previous study has revealed MRI abnormalities in children suffering from JHTS during the acute phase to be similar to those observed during migraine aura, thereby confirming the theory of a common CSD mechanism.

Our study has certain limitations. The first is its retrospective, single-centre design and small sample size (17 children). This relates to the fact that MRI is not systematically indicated in the diagnostic workup of migraine patients in an emergency setting. It was the first attack for 11 children, and/or aura symptoms were particularly intense, which is one reason why MRI was performed. The ICHD criteria were therefore not fully met as regards the number of attacks. However, the final diagnosis was probable migraine.

TOF-MRA acquisition box position variability is a limiting factor. The five TOF-MRA sequences described as normal were systematically TOF-MRA sequences with a too low standard position not allowing adequate visualisation of the distal arterial branches. It is therefore likely that distal vascular abnormalities were underestimated in these children. This observation helped us to adapt our practice, however, and for investigation of headache in particular, we now use an acquisition box in an intermediate position to allow correct visualisation of the circle of Willis as well as the distal arterial branches.

The absolute CBF values cannot be interpreted alone due to inter-subject variations, which depend on age and brain regions (29), preventing a normal or abnormal perfusion cutoff value from being defined. In addition, there may be bilateral perfusion abnormalities that prevent intra-subject comparison. Visual analysis of perfusion mapping is therefore essential. Besides, this is the analysis method used in daily clinical practice.

Conclusion

The association of perfusion abnormalities on ASL in brain regions not corresponding to vascular territories, and vascular vasospasm in TOF-MRA, can aid diagnosis of migraine with aura. These two sequences are totally non-invasive and easy to perform in routine practice in children and can provide additional information for understanding the pathophysiology of this complicated disorder.

Clinical implications

- ASL is a totally non-invasive cerebral perfusion technique that can be easily used in addition to conventional MRI to establish a positive diagnosis of migraine with aura in children.
- Migraine with aura is typically characterised by cerebral hypoperfusion that is not limited to a specific vascular territory, is often asymmetrical and preferentially affects the posterior brain regions.
- TOF-MRA can show slightly reduced visualisation of the distal arterial branches relating to a vasospasm.
- In routine practice, when investigating neurological deficit with headache, the TOF acquisition box can be positioned slightly higher than the standard position to improve visualisation of the distal arterial branches.
- The association of hypoperfusion on ASL and vasospasm in the distal branches of the intracranial arteries on TOF-MRA can aid MRI diagnosis of migraine and supports the neurovascular theory of migraine with aura.

Acknowledgements

The authors thank Mrs Tracey Westcott for her editorial assistance, and Mr Geoffrey Groussard for his statistical assistance.

Declaration of conflicting interests

The authors declared no potential conflicts of interest with respect to the research, authorship, and/or publication of this article.

Funding

The authors received no financial support for the research, authorship, and/or publication of this article.

References

1. Laurell K, Larsson B and Eeg-Olofsson O. Prevalence of headache in Swedish schoolchildren, with a focus on tension-type headache. *Cephalalgia* 2004; 24: 380–388.
2. Bille B. A 40-year follow-up of school children with migraine. *Cephalalgia* 1997; 17: 488–491.
3. Mackay MT, Monagle P and Babl FE. Brain attacks and stroke in children. *J Paediatr Child Health* 2016; 52: 158–163.
4. Mackay MT, Chua ZK, Lee M, et al. Stroke and nonstroke brain attacks in children. *Neurol* 2014; 82: 1434–1440.
5. Olesen J, Larsen B and Lauritzen M. Focal hyperemia followed by spreading oligemia and impaired activation of rCBF in classic migraine. *Ann Neurol* 1981; 9: 344–352.
6. Olesen J, Friberg L, Olsen TS, et al. Timing and topography of cerebral blood flow, aura, and headache during migraine attacks. *Ann Neurol* 1990; 28: 791–798.
7. Floery D, Vosko MR, Fellner FA, et al. Acute-onset migrainous aura mimicking acute stroke: MR perfusion imaging features. *AJNR Am J Neuroradiol* 2012; 33: 1546–1552.
8. Förster A, Wenz H, Kerl HU, et al. Perfusion patterns in migraine with aura. *Cephalalgia* 2014; 34: 870–876.
9. Proisy M, Bruneau B, Rozel C, et al. Arterial spin labeling in clinical pediatric imaging. *Diagn Interventional Imaging* 2016; 97: 151–158.
10. Boulouis G, Shotar E, Dangouloff-Ros V, et al. Magnetic resonance imaging arterial-spin-labelling perfusion alterations in childhood migraine with atypical aura: a case-control study. *Dev Med Child Neurol* 2016; 58: 965–969.
11. Prodan CI, Holland NR, Lenaerts ME, et al. Magnetic resonance angiogram evidence of vasospasm in familial hemiplegic migraine. *J Child Neurol* 2002; 17: 470–472.
12. Safier R, Cleves-Bayon C, Vaisleib I, et al. Magnetic resonance angiography evidence of vasospasm in children with suspected acute hemiplegic migraine. *J Child Neurol* 2014; 29: 789–792.
13. Headache Classification Committee of the International Headache Society (IHS). The International Classification of Headache Disorders, 3rd edition (beta version). *Cephalalgia* 2013; 33: 629–808.
14. Luh WM, Wong EC, Bandettini PA, et al. QUIPSS II with thin-slice TI1 periodic saturation: a method for improving accuracy of quantitative perfusion imaging using pulsed arterial spin labeling. *Magn Reson Med* 1999; 41: 1246–1254.
15. Tzourio-Mazoyer N, Landeau B, Papathanassiou D, et al. Automated anatomical labeling of activations in SPM using a macroscopic anatomical parcellation of the MNI MRI single-subject brain. *Neuroimage* 2002; 15: 273–289.
16. Lashley KS. Patterns of cerebral integration indicated by the scotomas of migraine. *Arch Neurol Psychiatry* 1941; 46: 331–339.
17. Leao AP. Spreading depression of activity in the cerebral cortex. *J Neurophysiol* 1944; 7: 359–390.
18. Lauritzen M. Pathophysiology of the migraine aura. The spreading depression theory. *Brain* 1994; 117: 199–210.

19. Hadjikhani N, del Rio MS, Wu O, et al. Mechanisms of migraine aura revealed by functional MRI in human visual cortex. *Proc Natl Acad SCI U S A* 2001; 98: 4687–4692.
20. Mourand I, De Champfleur NM, Carra-Dallière C, et al. Perfusion-weighted MR imaging in persistent hemiplegic migraine. *Neuroradiology* 2011; 54: 255–260.
21. Masuzaki M, Utsunomiya H, Yasumoto S, et al. A case of hemiplegic migraine in childhood: transient unilateral hyperperfusion revealed by perfusion MR imaging and MR angiography. AJNR *Am J Neuroradiol* 2001; 22: 1795–1797.
22. Jensen K, Tfelt-Hansen P, Lauritzen M, et al. Classic migraine. *Acta Neurol Scand* 1986; 73: 359–362.
23. Amin FM, Asghar MS, Hougaard A, et al. Magnetic resonance angiography of intracranial and extracranial arteries in patients with spontaneous migraine without aura: a cross-sectional study. *Lancet Neurol* 2013; 12: 454–461.
24. Kim S, Kang M and Choi S. A case report of sporadic hemiplegic migraine associated cerebral hypoperfusion: comparison of arterial spin labeling and dynamic susceptibility contrast perfusion MR imaging. *Eur J Pediatr* 2016; 175: 295–298.
25. Ducros A. Reversible cerebral vasoconstriction syndrome. *Lancet Neurol* 2012; 11: 906–917.
26. Ducros A, Boukobza M, Porcher R, et al. The clinical and radiological spectrum of reversible cerebral vasoconstriction syndrome. A prospective series of 67 patients. *Brain* 2007; 130: 3091–3101.
27. Van der Veek EMJ, Oosterhoff M and Vos PE. The juvenile head trauma syndrome: a trauma triggered migraine. *Neuropediatrics* 2015; 46: 116–122.
28. Haas DC, Pineda GS and Lourie H. Juvenile head trauma syndromes and their relationship to migraine. *Arch Neurol* 1975; 32: 727–730.
29. Taki Y, Hashizume H, Sassa Y, et al. Correlation between gray matter density-adjusted brain perfusion and age using brain MR images of 202 healthy children. *Hum Brain Mapp* 2011; 32: 1973–1985.

Chapitre 4 – Travaux chez le nouveau-né

Comme expliqué précédemment, le cerveau des nouveau-nés a un signal et une morphologie très différente de l'enfant plus grand. En particulier, la myélinisation est incomplète et entraine une inversion du contraste substance grise – substance blanche. Le cortex cérébral est très fin. Les problématiques de traitement des images sont donc encore différentes de celles concernant les enfants plus grands.

L'adaptation de l'outil AutoASL aux données pédiatriques (Chapitre 3) nécessitait encore des adaptations pour une utilisation sur une population de nouveau-nés. Ce travail a été réalisé en étroite collaboration avec Isabelle Corouge (Ingénieure de Recherche Université de Rennes 1, Plateforme Neurinfo ; Equipe Visages), et Antoine Leghouy (Doctorant Irisa, financé par l'ANR MAIA 2015, Projet ANR-15-CE23-009; Investigateur principal Pr François Rousseau).

La démarche de l'adaptation de la chaine de traitement des images est expliquée ci-dessous, en complément du chapitre 2.3. Processing of imaging data, dans la section Matériel et Méthodes de l'article intitulé "Changes in brain perfusion in successive arterial spin labelling MRI scans in neonates with hypoxic-ischaemic encephalopathy" (section suivante). Les Figures 1 à 3 du même article résument le traitement des images sous forme de schéma.

Adaptation de la chaine de traitement

1/Extraction du cerveau

Dans un premier temps l'extraction du cerveau a été réalisée avec bet FSL (Smith, 2002) (https://fsl.fmrib.ox.ac.uk/fsl/fslwiki/FSL) comme utilisé avec succès chez les enfants. Cependant le résultat était insuffisant. Cet échec de l'extraction est en lien avec des contrastes différents chez le nouveau-né.

La réalisation d'un atlas personnalisé a été réalisée à partir des données ALBERT disponibles en ligne (Gousias et al., 2012). Il s'agit de 20 IRM de nouveau-nés, pondération T1 et T2, avec segmentation manuelle de 50 régions anatomiques. Pour créer notre atlas personnalisé du cerveau, nous avons fusionné les segmentations, puis appliqué un spécial « closing » (dilatation, remplissage des trous et érosion) en utilisant le logiciel Anima

(https://github.com/Inria-Visages/Anima-Public/) et des algorithmes de recalage affine puis diffeomorphique basé sur le « block-matching » (Commowick et al., 2012) (Fig. 9 et 10) (Chapitre 2.3.1 *Construction of custom atlas*).

Figure 9 : création d'un masque du cerveau à partir des segmentations des données ALBERT (Gousias et al., 2012).

L'obtention de ces masques a permis une extraction automatisée des cerveaux très satisfaisante et une amélioration de la segmentation (étape suivante) (Fig. 11). Quelques échecs étaient parfois liés à la présence d'hématomes extra-crâniens liés à l'accouchement nécessitant une correction manuelle.

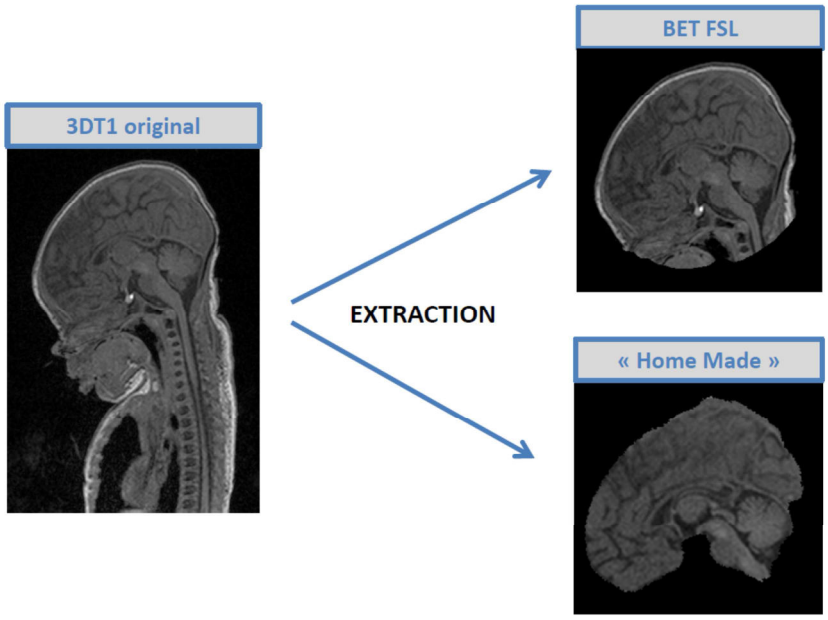

Figure 10 : Extraction du cerveau à partir du 3DT1 original par deux méthodes différentes

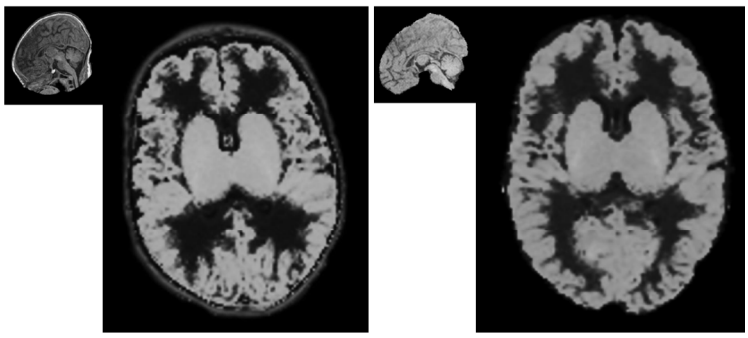

Figure 11 : Impact de l'extraction du cerveau sur l'étape de segmentation

2/Segmentation de la substance grise – substance blanche

Les atlas du NIHPD utilisés précédemment n'incluaient pas de tranche d'âge néonatale. Les tests effectués avec cet atlas sur des cerveaux de nouveau-nés montraient un échec de la segmentation, comme attendu. Nous avons donc cherché à utiliser des atlas (cartes de probabilité des tissus) adaptés aux nouveau-nés.

Nous avons utilisé les atlas de l'Imperial College London (Serag et al., 2012). Il s'agit d'atlas 4D cartes de probabilités créées à partir de 204 prématurés (nouveau-nés imagés entre 28 et 44 semaines d'aménorrhées). Nous avons fait le choix du volume 17 (dernier volume) correspondant à un âge post-menstruel à terme et regroupé les cartes de probabilités du cortex cérébral, substance grise profonde et tronc cérébral pour faire un atlas de la substance grise globale. Les cartes de probabilités de substance blanche et liquide céphalo-rachidien n'ont pas été modifiées.

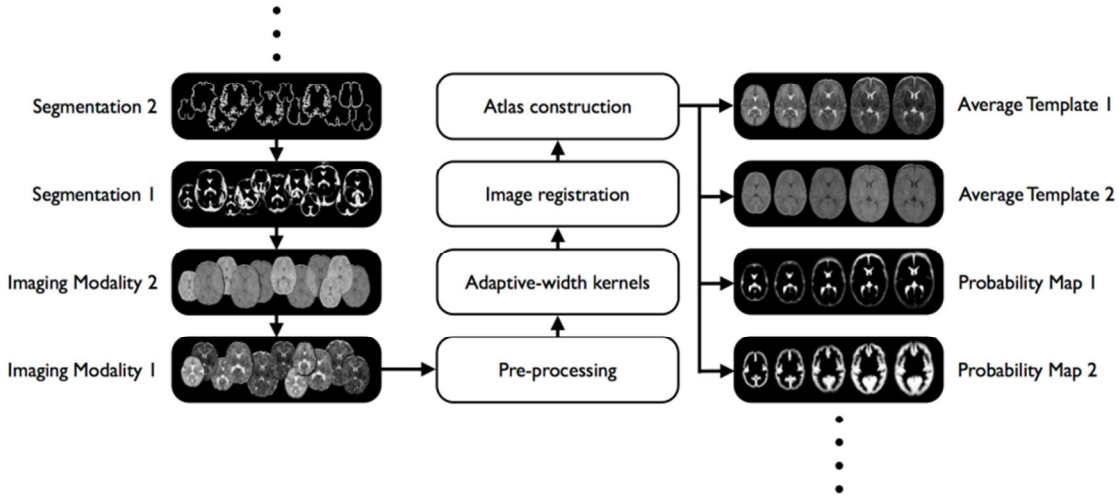

Figure 12 : Méthodologie de la construction de l'atlas 4D de Serag et al.

L'utilisation de ces atlas était très satisfaisante pour certains sujets et totalement erronée pour d'autres, malgré une extraction du cerveau et des images morphologiques de qualité égales. Nous avons alors relié le problème à l'alignement des images pour certains sujets (Fig. 13). Un repositionnement manuel avec l'outil « display option » de SPM8 nous a permis de recentrer le 3DT1 proche des coordonnées 0.0.0 comme les cartes de probabilité, améliorant ainsi l'étape de segmentation réalisée par SPM. Ce réalignement a été réalisé manuellement pour plusieurs sujets, permettant de constater une nette amélioration des résultats de segmentation (Fig. 14). Afin de limiter les manipulations manuelles, pour rendre la chaine de traitement la plus automatisée possible, nous avons décidé de réaligner systématiquement les 3DT1 en effectuant un recalage rigide sur le template (Chapitre 2.3.1 *Reorientation and Tissu segmentation*).

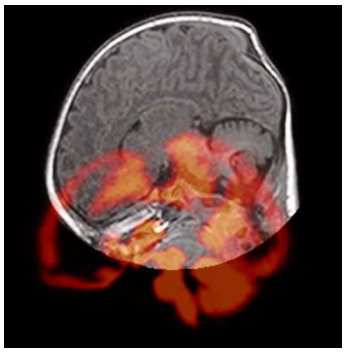

Figure 13 : Représentation du mauvais « alignement » du 3DT1 avec la carte de probabilité de substance grise chez un sujet, et de la nécessité de réorienter la carte de probabilité dans deux directions sur cette image (translation verticale et rotation).

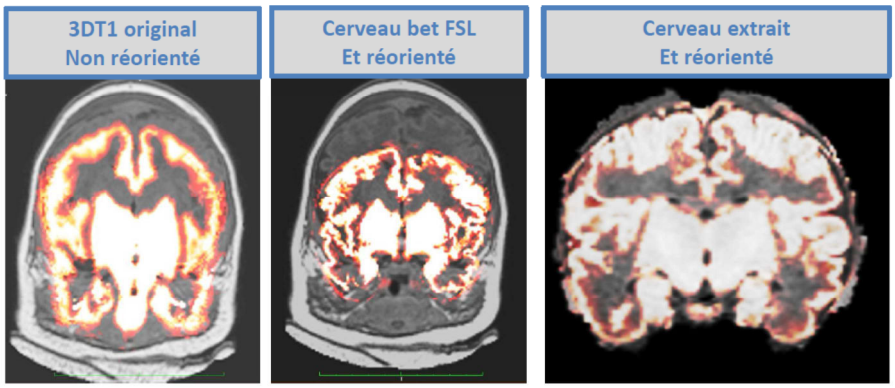

Figure 14 : Impact de la réorientation et de l'extraction sur la qualité de la segmentation de la substance grise.

3/Correction de mouvement et analyse qualité

Une analyse visuelle de la qualité des cartographies de perfusion pour chaque sujet a été réalisée avant et après correction de mouvement. Pour chaque sujet les images natives contrôles et marquées ont été regardées et les paires bougées ont été supprimées manuellement avant la soustraction des images. La qualité des cartographies de perfusion analysée à nouveau après suppression des paires bougées n'était globalement pas améliorée. Une analyse qualité a aussi été réalisée de manière automatisée avec le calcul des valeurs négatives sur les cartographies de perfusion, dans le cerveau entier, la GM et la WM, à la fin du traitement des données ASL (Tableau 3).

Enfin, comme décrit aux chapitres 2 et 3, nous avons utilisé le recalage rigide des volumes ASL du même sujet pour correction de mouvement puis le M-estimator de Huber.

Sujet	Qualité J3	Paires bougées	Qualité après correction	% valeurs nég cerveau	% valeurs nég SG	Qualité J10	Paires bougées	Qualité après correction	% valeurs nég cerveau	% valeurs nég SG
201_HY_1	1	0		29,3	21,04	3	9	2	20,88	19,93
202_RJ_0	1	0		9,08	5,98	2	3	2	23,9	13,02
203_RB_1	1	0		12,45	8,4	3	3	2	6,97	6,74
204_DM_1	1	0		12,19	6,58	--	--		--	--
205_PA_0	3	0		45,86	41,84	--	--		--	--
206_AI_0	1	0		24,19	14,91	2	0		34,6	28,76
207_MR_1	1	0		14,54	9,61	1	2	2	17,92	11,14
208_VL_0	1	0		33,17	25,09	--	--			
209_RN_1	3	0		37,36	26,66	3	12	2	11,88	6,84
210_HS_0	1	14	1	1,46	1,03	1	0		3,88	3,52
211_MT_1	3	0		51,85	45,63	2	9	2	17,33	12,75
212_BL_1	2	0		40,56	38,56	1	0		27,07	15,59
213_SM_0	3	0		58,79	55,75	2	6	2	23,73	17,86
214_BS_0	2	0		29,04	19,04	2	0		19,61	12,87
215_GL_0	2	0		19,33	16,47	2	0		36,39	27,22
216_RC_1	2	0		53,75	46,02	2	0		7,37	4,18
217_BN_1	1	0		11,08	7,87	2	0		37,16	30,71
218_KD_1	3	0		43,35	41,79	1	0		4,18	1,13
219_GA_0	1	0		21,23	6,84	2	3	2	16,37	9,03
220_LTL_1	1	0		4,88	2,64	1	0		8,8	2,1
221_HT_1	1	2	1	12,7	13,55	--	--		--	--
222_RL_0	3	0		71,64	66,12	2	15	2	12,84	9,66
223_MDK_1	3	0		54,16	48,58	2	8	2	13,68	7,75
224_CY_1	2	0		20,26	11,13	3	»30	3	24,76	19,02
225_HC_0	2	5	2	14,69	5,43	2	0		18,21	10,57
226_PL_1	1	3	1	7,44	2,68	2	0		7,13	7,45
227_VJS_1	2	0		39,61	25,32	1	4	1	9,41	2,58
228_BA_0	1	0		7,67	5,88	--	--		--	--

Tableau 3 : Analyse de la qualité des cartographies de perfusion pour chaque sujet. Analyse visuelle (scoring de 1 à 3 : bon, moyen, mauvais) et paires bougées exclues manuellement. Pourcentage de valeurs négatives calculé avec le logiciel autoASL dans le cerveau entier et la substance grise. En rouge les valeurs supérieures à un seuil arbitraire de 30% pour le cerveau entier et 22% pour la substance grise. Seuil utilisé pour exclure les sujets et correspondant globalement aux cartographies de mauvaise qualité en analyse visuelle (6 discordants).

4/Analyse par ROI

Avant la mise au point de la chaine de traitement, une segmentation manuelle des noyaux gris centraux, lobes et hémisphères a été réalisée avec le logiciel ITK-SNAP (http://www.itksnap.org) (Yushkevich et al., 2006) dans le cadre d'un master 1 (Mme Amélie Nicolas, interne en Radiologie au CHU de Rennes). Par la suite, la mise en place de la chaine de traitement automatisée a permis de créer des ROIs à partir des données ALBERT. Les régions ALBERT étant au nombre de 50, elles ont été regroupées pour former des ROI plus larges (Annexe 1).

Les ROIs ont été appliqués sur les cartographies de perfusion pour obtenir une moyenne, un écart-type, valeur minimale et maximale, et un volume. Les valeurs moyennes de CBF étaient obtenues dans chaque ROI après exclusion des voxels ayant une probabilité de substance grise de moins de 0.7, et de moins de 0.85 pour le cerveau entier. Les voxels négatifs n'ont pas été exclus (Chapitre 2.3.3 *Calculation of CBF statistics over ROIs*). Apres analyse statistique sur échantillons appariés, il n'existait pas de différence significative entre les NGC ALBERT et les NGC manuelles (tableau 4) ou entre les ROIs droite – gauche pour chaque région excepté pour les NGC ALBERT (tableau 5). En raison du rejet de la normalité de la majorité des échantillons par test de Shapiro-Wilk, et en raison de la taille des échantillons, des tests non paramétriques ont été utilisés. Une *p* value inférieure à 0.05 était considérée comme significative.

Les ROIs droite et gauche ont été regroupées pour chaque région anatomique pour la présentation des résultats (Fig. 15).

CBF (mL/100g/min)	NGC Albert	NGC manuelle	*p*
DOL 3 (n = 17)	52.8 [42.6 – 93.6]	53.7 [40.7 – 92.7]	0.579
DOL 10 (n = 20)	30.2 [24.1 – 48.8]	30.5 [23.5 – 45.8]	0.348

Tableau 4 : Comparaison des valeurs médianes de CBF (mL/100g/min) obtenues dans les ROI automatiques Albert et les ROI manuelles des noyaux gris centraux [95% Intervalle de confiance]. Test non paramétrique (test de Wilcoxon) pour échantillons appariés.

CBF (mL/100g/min)	Droite DOL3	Gauche DOL3	*p*	Droite DOL10	Gauche DOL10	*p*
Cortical GM	27.8 [21.7 – 44.4]	30.3 [20.0 – 45.6]	0.854	26.9 [17.2 – 31.4]	22.6 [19.0 – 31.8]	0.621
NGC Albert	50.1 [41.6 – 93.4]	55.5 [43.7 – 93.8]	0.003	29.1 [25.7 – 48.0]	33.5 [22.1 – 49.5]	0.956
NGC manuelle	51.0 [40.8 – 92.0]	55.8 [42.9 – 95.0]	0.057	28.9 [26.0 – 44.5]	32.3 [21.2 – 48.1]	0.648
Lobe frontal	26.2 [20.5 – 38.8]	23.5 [20.7 – 38.1]	0.818	25.3 [17.2 – 35.5]	24.0 [18.4 – 33.0]	0.348
Lobe pariétal	24.0 [23.5 – 46.0]	30.5 [19.8 – 47.7]	0.352	24.9 [16.2 – 34.4]	24.0 [17.6 – 30.8]	0.927
Lobe temporal	31.5 [23.5 – 43.1]	29.9 [28.9 – 41.3]	0.579	25.3 [22.7 – 35.1]	23.0 [19.1 – 26.7]	0.312
Lobe occipital	37.5 [19.5 – 49.3]	35.2 [18.4 – 49.6]	0.611	26.1 [14.5 – 30.7]	20.1 [13.7 – 30.2]	0.869

Tableau 5 : Comparaison des valeurs médianes de CBF (mL/100g/min) obtenues dans les ROI à droite et à gauche [95% Intervalle de confiance]. Un test non paramétrique (test de Wilcoxon) pour échantillons appariés a été utilisé.

Figure 15 : ROIs frontales, pariétales, temporales et occipitales, et noyaux gris centraux appliquées sur la cartographie de perfusion (sujet 220 IRM précoce de J3)

Applications cliniques

La mise au point de la chaine de traitement précédemment décrite a été réalisée sur des IRM cérébrales de nouveau-nés souffrant d'asphyxie périnatale, dans le cadre d'une étude prospective réalisée au CHU de Rennes à l'Hôpital Sud. Cette étude a obtenue l'accord du comité d'éthique et le recueil de l'accord des parents a été obtenu pour chaque enfant.

L'objectif principal de cette étude était d'évaluer l'évolution de la perfusion cérébrale en ASL entre le 3^{iéme} et le 10^{iéme} jour de vie (J3 et J10) chez les enfants traités par hypothermie pour asphyxie périnatale. L'objectif secondaire était de comparer les valeurs de CBF entre les nouveau-nés présentant des lésions ischémiques en IRM et ceux ayant une IRM normale.

Il s'agit de la première étude dans la littérature étudiant le CBF en ASL chez un même sujet à deux reprises dans les 15 premiers jours de vie. Les 4 études de la littérature existantes sur ASL et HIE rapportent des données sur des IRM acquises une fois, à des délais variables entre le premier jour de vie et la deuxième semaine.

Nous avons inclus tous les nouveau-nés hospitalisés dans l'unité de réanimation néonatale du CHU de Rennes et éligibles à un traitement par hypothermie, entre avril 2015 et décembre 2017. Chaque nouveau-né bénéficiait d'une IRM précoce (vers J3) et tardive (vers J10). Au total 28 nouveau-nés ont été inclus (16 garçons et 12 filles). L'analyse statistique a été réalisée sur 37 examens, dont 17 IRM précoces et 20 IRM tardives. 8/17 nouveau-nés (47%) avaient une IRM précoce anormale et 7/20 nouveau-nés (35%) présentaient une IRM tardive anormale. Les valeurs de CBF dans les NGC étaient significativement plus faibles a J10 qu'a J3 ($p < 0,05$). Il n'y avait pas de différence significative entre J3 et J10 pour les autres ROI. A J3, le CBF moyen était significativement plus élevé dans la substance grise corticale, les noyaux gris centraux (NGC), les lobes frontaux et pariétaux chez les sujets ayant une IRM anormale par rapport à ceux ayant une IRM normale ($p < 0,05$).

Les résultats de cette étude démontrent que l'étude de la perfusion cérébrale chez les nouveau-nés avec asphyxie périnatale semble plus pertinente assez tôt, dans les premiers jours de la vie. La corrélation des valeurs de perfusion cérébrale à J3 avec le devenir neuro développemental reste à évaluer (recul nécessaire d'au minimum 2 ans). (Fig. 17 et 18)

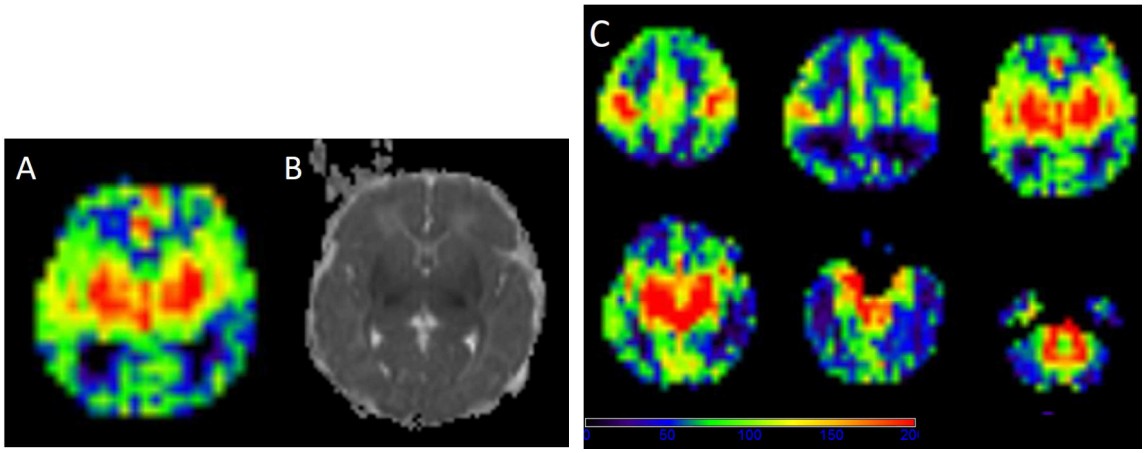

Figure 17 : Image axiale de cartographie de perfusion ASL (A et C) et cartographie ADC (B) chez le sujet 210 sur l'IRM précoce. Il existe une hyperperfusion des noyaux gris centraux et du cortex cérébral, avec une atteinte uniquement des noyaux gris centraux en diffusion.

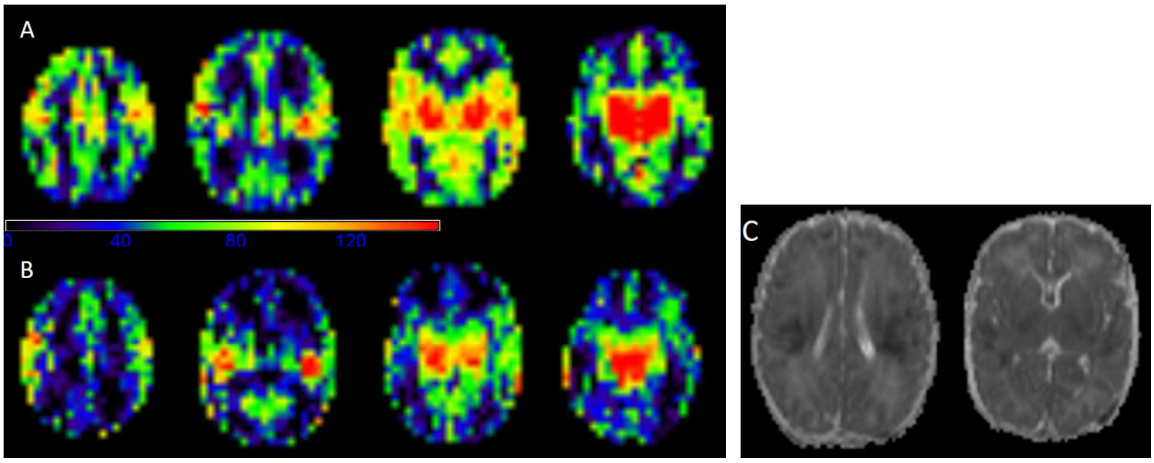

Figure 18 : Cartographie de perfusion ASL chez le sujet 220 sur l'IRM précoce (A) et tardive (B) et cartographie ADC (C). Il existe une hyperperfusion des NGC sans atteinte visible en diffusion. En revanche il existe une atteinte diffuse cortico-sous corticale, fronto-temporo-pariétale bilatérale, en diffusion.

“Changes in brain perfusion in successive arterial spin labelling MRI scans in neonates with hypoxic-ischaemic encephalopathy”. Neuroimage: Clinical 2018. *Article soumis*

Changes in brain perfusion in successive arterial spin labeling MRI scans in neonates with hypoxic-ischemic encephalopathy

Maïa Proisy [1.2], Isabelle Corouge [1], Antoine Leghouy [1], Amélie Nicolas [2], Valérie Charon [2], Nadia Mazille [3], Stéphanie Leroux [3], Bertrand Bruneau [2], Christian Barillot [1], Jean-Christophe Ferré [1.2]

Corresponding author: Maïa Proisy, maia.proisy@chu-rennes.fr

(1) Univ Rennes, Inria, CNRS, INSERM, IRISA, Empenn ERL U-1228, F-35000 Rennes, France

(2) CHU Rennes, Radiology Department, F-35033 Rennes, France

(3) CHU Rennes, Neonatology Department, F-35033 Rennes, France

Abstract

The primary objective of this study was to evaluate changes in cerebral blood flow (CBF) using arterial spin labeling MRI between day 4 of life (DOL4) and day 11 of life (DOL11) in neonates with hypoxic-ischemic encephalopathy (HIE) treated with hypothermia. The secondary objectives were to compare CBF values between the different regions of interest (ROIs) and between infants with ischemic lesions on MRI and infants with normal MRI findings.

We prospectively included all consecutive neonates with HIE admitted to the neonatal intensive care unit of our institution who were eligible for therapeutic hypothermia. Each neonate systematically underwent two MRI examinations as close as possible to day 4 (early MRI) and day 11 (late MRI) of life. A custom processing pipeline of morphological and perfusion imaging data adapted to neonates was developed to perform automated ROI analysis.

Twenty-eight neonates were included in the study between April 2015 and December 2017. There were 16 boys and 12 girls. Statistical analysis was finally performed on 37 MRIs, 17 early MRIs and 20 late MRIs. Eleven neonates had both early and late MRIs of good quality available. Eight out of 17 neonates (47%) had an abnormal early MRI and 7/20 neonates (35%) had an abnormal late MRI. CBF values in the basal ganglia and thalami (BGT) and temporal lobes were significantly higher on DOL4 than on DOL11. There were no significant differences between DOL4 and DOL11 for the other ROIs. CBF values were significantly higher in the BGT vs. the cortical GM, on both DOL4 and DOL11. On DOL4, the CBF was significantly higher in the cortical GM, the BGT, and the frontal and parietal lobes in subjects with an abnormal MRI compared to those with a normal MRI. On DOL11, CBF values in each ROI were not significantly different between the normal MRI group and the abnormal MRI group, except for the temporal lobes.

This article proposes an innovative processing pipeline for morphological and ASL data suited to neonates that enable automated segmentation to obtain CBF values over ROIs. We evaluate CBF on two successive scans within the first 15 days of life in the same subjects. ASL imaging in asphyxiated neonates seems more relevant when used relatively early, in the first days of life. The correlation of intra-subject changes in cerebral perfusion between early and late MRI with neurodevelopmental outcome warrants investigation in a larger cohort, to determine whether the CBF pattern change can provide prognostic information beyond that provided by visible structural abnormalities on conventional MRI.

Keywords: Neonates; Asphyxia; Cerebral perfusion; MRI; ASL

Abbreviations

HIE = Hypoxic-Ischemic Encephalopathy; ASL = Arterial Spin Labeling; CBF = Cerebral Blood Flow; DOL = Day Of Life; ROI = Region Of Interest; BGT = Basal Ganglia and Thalami; PW = Perfusion-Weighted; T1w = T1-weighted image; T2w = T2-weighted image

Highlights

- A processing pipeline suited to neonates was developed for automated ROI analysis
- Basal ganglia and thalamic CBF values were significantly higher on DOL4 vs. DOL11
- Neonates with abnormal morphological MRI had hyperperfusion in grey matter on DOL4
- No perfusion differences were found on DOL11 between normal and abnormal MRIs

1. Introduction

Hypoxic-ischemic encephalopathy (HIE) is the leading cause of neonatal encephalopathy and occurs after perinatal asphyxia in full-term neonates. HIE is a major cause of perinatal mortality and morbidity (Volpe, 2012). MRI plays a key role in the diagnosis and prognosis of this pathology. The time to perform MRI varies by center and there is no consensus on optimal timing. An early MRI (performed during the first week of life) reliably detects severe injuries and there is good agreement between early MRI and late MRI (after 1 week) (Agut et al., 2014; Boudes et al., 2015; Chakkarapani et al., 2016; Charon et al., 2015; Skranes et al., 2015). In addition to MRI scoring, some quantitative biomarkers such as DWI with measurements of apparent diffusion coefficient (ADC) or proton MR spectroscopy could contribute to an early diagnosis and prognosis (Alderliesten et al., 2011; Cheong et al., 2006). The brain perfusion model and its relationship to other biomarkers could help guide the development of therapies in order to improve management of high-risk neonates.

Cerebral perfusion imaging is challenging in neonates due to physiological and technical issues (Proisy et al., 2016). The Arterial Spin Labeling (ASL) MRI perfusion sequence is one of the most suitable imaging modalities owing to its non-invasive and non-irradiating nature. Moreover, this perfusion imaging sequence can be easily incorporated into standard brain MRI in neonates with HIE, after acquisition of morphological images. However, the post-processing of ASL data requires specific adaptations to this age group, in particular with

respect to the automated segmentation of brain tissues and the parameters used for the quantification models of cerebral blood flow (CBF) (Varela et al., 2015).

There are a dozen articles in the literature concerning the study of cerebral perfusion in neonates using ASL, four of which are focused on neonates with HIE. Brain perfusion measurement may vary according to the timing of the MRI scan. Regarding the MRI time point for the studies (ranging from day 1 of life (DOL1) to the second week of life), some of the studies showed brain hyperperfusion in infants with HIE (De Vis et al., 2015; Pienaar et al., 2012), while others showed hypoperfusion (Massaro et al., 2013). In one study (Wintermark et al., 2011), two successive MR images were taken of each asphyxiated neonate during the first week of life. On DOL1, hypoperfusion was found in the brain areas subsequently exhibiting injury in the neonates treated with hypothermia and who developed MR imaging evidence of HIE brain injury. On DOL2, the CBF values were higher in the injured brain areas in these neonates. Moreover, De Vis et al. (De Vis et al., 2015) showed good performance for ASL in predicting outcome after HIE. ASL perfusion in the basal ganglia and thalami was higher in the adverse outcome group than in the favorable outcome group.

The primary objective of our study was to evaluate the changes in CBF between an early MRI (at day 4 of life) and a late MRI (at day 11 of life) in infants with HIE treated with hypothermia. The secondary objectives were to compare CBF values between the different regions of interest (ROIs) and between infants with ischemic MRI lesions and those with normal MRI.

2. Materials and Methods

2.1. Patients

This prospective study included all consecutive neonates with HIE admitted to the neonatal intensive care unit of our institution between April 2015 and December 2017. The criteria of national guidelines (Saliba and Debillon, 2010) were used to determine eligibility for therapeutic hypothermia. All included neonates were at least 36 weeks' gestation with birth weight ≥1800 g. They had signs of perinatal asphyxia with an acute perinatal event (such as severe foetal heart rate abnormalities, cord prolapse or placental abruption) and at least one of the following criteria: APGAR score ≤5 at 10 minutes; mechanical ventilation or intubation at 10 minutes after birth; metabolic acidosis, including cord, arterial, venous or capillary blood

pH <7 or base deficit ≥16 mmol/L or lactate ≥11 mmol/L within 60 minutes of birth. Neonates with stroke, congenital malformation or metabolic disorders were not included. Hypothermia was induced within 6 hours after birth and continued for 72 hours, with a target temperature of 33-34°C.

The institutional medical ethics review board approved the study and parental consent was obtained.

2.2. MR acquisition

Each included neonate systematically underwent two MRI scans as follows: an early MRI performed as close as possible to day 4 of life (DOL4) and a late MRI performed as close as possible to day 11 of life (DOL11). The early MRI was performed after rewarming, at the end of hypothermia treatment. The conventional MRI scans were acquired first then ASL images were acquired at the end.

All MRI scans were acquired using a Siemens 1.5T Magnetom Aera scanner (Siemens; Erlangen, Germany) with a 20-channel head/neck coil.

The neonates received no additional medication for the imaging study. Ventilated infants were sedated with morphine and midazolam. Spontaneously breathing infants were not sedated and were fed before the MRI scan and wrapped with a "vacuum immobiliser".

The brain MRI protocol included routine sequences as follows: 3D T1-weighted (T1w) images acquired in the sagittal plane (TR/TE = 2090/4.9ms; resolution = 1 x 1 x 1 mm^3); axial, sagittal and coronal T2-weighted (T2w) turbo spin-echo images; axial gradient-echo T2-weighted and axial DWI with b values of 0s/mm² and 1000s/mm². Apparent diffusion coefficient (ADC) maps were automatically generated.

The perfusion 2D pulsed ASL MRI sequence used was PICORE Q2TIPS (Luh et al., 1999). Imaging parameters were as follows: TR/TE/TI1/TI2 = 3500 / 12 / 700 / 2000 ms; in-plane resolution = 4x4 mm^2; slice thickness = 8 mm; gap = 2 mm; 9 slices; 30 label/control pairs; total scan time = 3 min 39 s. The first volume of the ASL series was used as the M0 reference image.

2.3. Processing of imaging data

We developed a specific processing pipeline, adapted to neonatal data, for both anatomical and perfusion images in order to estimate average CBF values over the grey matter of a set of regions of interest (ROIs). The anatomical processing of our neonate images included brain extraction, reorientation and brain tissue segmentation. Our ROIs were derived from a custom

anatomical atlas we built from ALBERTs data (Gousias et al., 2012). The processing of perfusion ASL images leads to a quantitative CBF map for each subject and at each time point. Combined with anatomical segmentations, this quantitative map yields CBF statistics in our ROIs. An overview of the processing pipeline is given in Figure 1.

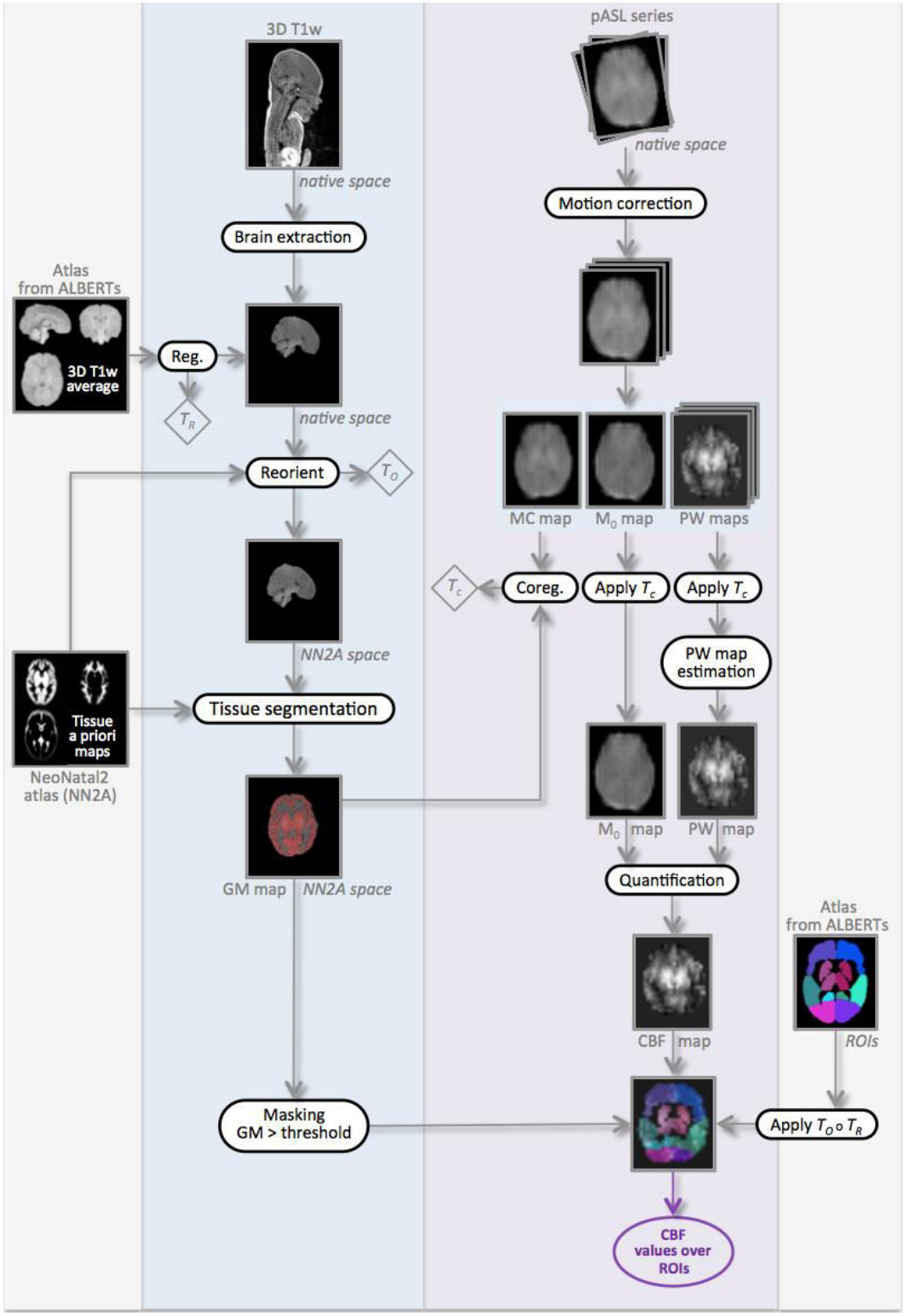

Figure 1: Overview of our processing pipeline illustrated in one subject, at day of life 4 (DOL4). The transformations T_R, T_O and T_C resulting from the different registration steps are indicated in diamonds. The circle symbol represents the composition of transformations.

2.3.1. Processing of anatomical data

Construction of custom atlas

As mentioned above, we first built a custom anatomical atlas from ALBERTs data (available at http://brain-development.org/brain-atlases/neonatal-brain-atlas-albert/). The ALBERTs data consist of 20 neonate brain T1w and T2w images with associated manual delineation of 50 regions. As shown in Figure 2, our customised atlas was based on an amended version of the method developed by Guimond et al. (Guimond et al., 2000). It takes into account both overall changes and local deformations to provide an unbiased atlas up to a rigid transformation (code available in Anima-Script[1]). The registration process used in atlas creation involves two steps: an affine registration step followed by a diffeomorphic one, both using block-matching algorithms (Commowick et al., 2012b, 2012a) available in Anima[2].

This method produces an average neonatal brain from the ALBERTs T1w images. To obtain the 50 associated segmentations, we applied the same transformation as between the individual T1w and the average T1w to the ROI map and fused the labels by majority voting. Last, for brain extraction purposes, we created a whole-brain mask by merging all the labels and applying special closing (dilation followed by hole filling and erosion).

In addition, we selected and merged subsets of ROIs from the 50 segmentation map in order to form the regions in which the CBF analysis would be performed. They are: the frontal, temporal, parietal and occipital lobes, and the basal ganglia and thalamus (BGT) for the left and right hemispheres. A "cortical GM" ROI was additionally defined as the union of the four lobes in order to obtain values for cortical GM without BGT.

[1] Open source processing scripts using Anima tools: https://github.com/Inria-Visages/Anima-Scripts-Public

[2] Open source software for medical image processing from the VISAGES team: https://github.com/Inria-Visages/Anima-Public

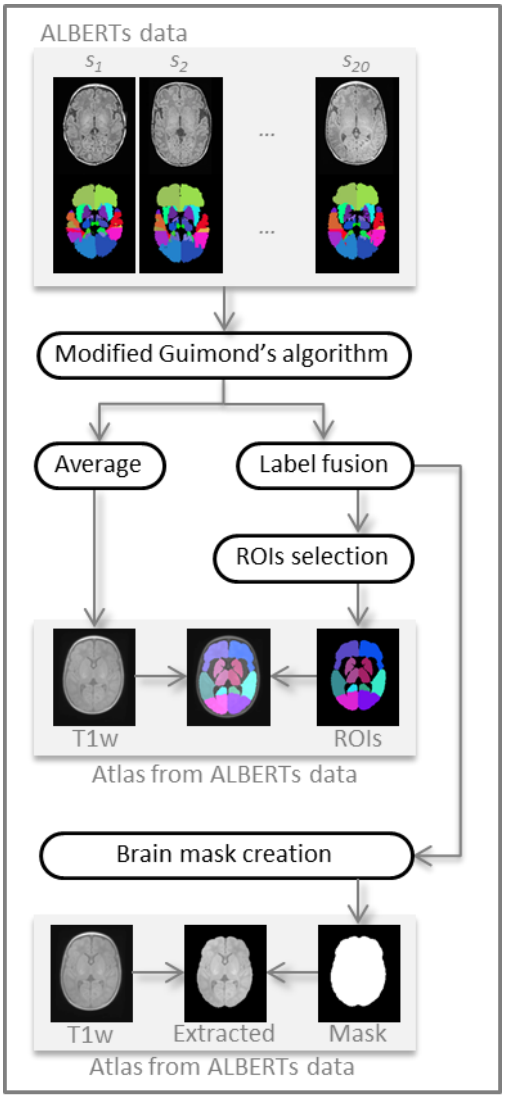

Figure 2: Steps of the construction of our custom atlas from ALBERTs data (20 neonate subjects along with 50 manually drawn ROIs). Our custom atlas results in an average T1w image with associated ROIs, as well as an extracted average brain and a binary brain mask.

Brain extraction

For each subject's DOL4, the first step of anatomical processing was brain extraction. This processing is illustrated in Figure 3. As ALBERTs and our own data show massive differences in the field of view (FOV), it was neither straightforward nor appropriate to perform brain extraction directly from the whole-brain mask computed above. We first had to crop our data to make them compatible with ALBERTs. For this purpose we used another in-house atlas built according to the previously depicted method, but from 18 subjects selected from our neonate 3D T1w image database — so with a similar FOV — along with their associated segmentations manually drawn by a junior radiologist (AN) at our institution. These segmentations, though not as fine as those of ALBERTs, still allowed us to extract

regions common to both atlases, the largest one being the cerebrum. By computing the rigid transformation between the two cerebrums, the in-house atlas could be cropped according to the ALBERTs FOV. We then propagated this desired FOV by computing another rigid transformation, T_s, this time between the in-house atlas and the subject, which enabled cropping of the subject image.

The custom atlas we built from ALBERTs data could then be registered onto our subject using an affine transformation T_A followed by a diffeomorphism transformation T_M to perform brain extraction using the whole-brain mask.

Henceforth, we will only consider the extracted brain of our subjects.

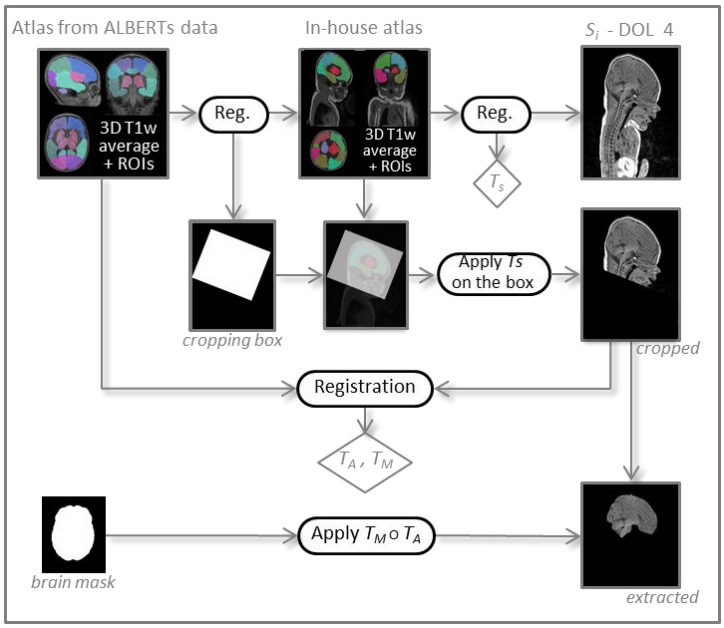

Figure 3: Processing steps for brain extraction. The transformations T_S, T_A and T_M resulting from the different registration steps are indicated in diamonds. The circle symbol represents the composition of transformations.

Reorientation and tissue segmentation

The extracted brain was segmented into grey matter (GM), white matter (WM) and cerebro-spinal fluid (CSF) probability maps using the SPM8 toolbox (Wellcome Department of Imaging Neuroscience, University College London, London, UK). Instead of using the default SPM8 template (MNI ICMB152) tissue probability maps as an a priori for brain tissue classification, we chose the "Neonatal2 atlas — 44 weeks old, postmenstrual" (NN2 atlas) available at http://brain-development.org/brain-atlases/consistent-high-definition-spatio-

temporal-neonatal-brain-atlas/, which is age-adapted to our population (Serag et al., 2012). Note that we defined the grey matter a priori probability map as the sum of the NN2 atlas cortex, deep grey matter, brainstem and cerebellum maps. The quality of the segmentation was visually checked.

Beforehand, as the data and the a priori maps needed to be roughly aligned to ensure correct segmentation with SPM8, the extracted brain was reoriented by a rigid transformation T_O onto the NN2 atlas using Anima software (Commowick et al., 2012a).

Processing of DOL11 anatomical data

Similarly to DOL4 data, the DOL11 3D T1w data first underwent brain extraction. Then, using Anima, the DOL11 image was coregistered to the DOL4 time point with an affine registration to recover the slight yet non-negligible changes due to brain growth over this period. Reorientation could then be done using the transformation computed for DOL4 before performing segmentation into brain tissues as described above.

2.3.2. Processing of perfusion data

The ASL images for all subjects and all time points were processed using a custom-built ASL pipeline based on SPM8 software and Matlab® (The MathWorks, Inc.).

The native ASL series was first visually inspected in order to detect too-large motion and perform manual suppression of control/label pairs where appropriate. It was then motion-corrected by a rigid body transformation minimising the sum of squared differences cost function. A two-pass procedure first realigned all the control and label volumes onto the first volume of the series, and then registered the series to the mean of the images aligned in the first pass.

Leaving aside the first volume of the series, M0, the ASL images were pairwise subtracted to produce a series of perfusion-weighted maps. Along with the M0 map, this series was coregistered to the 3D T1w image (once brain-extracted and reoriented) using a rigid transformation T_C. The latter was estimated by maximising normalised mutual information between the mean control image, i.e. the average of all the realigned control volumes and the 3D T1 GM map.

The perfusion-weighted (PW) map is usually obtained by averaging across the repetitions. However, as the conventional arithmetic mean is very sensitive to outliers, we instead used Huber's M-estimator to robustly estimate the PW map (Maumet et al., 2014).

This robust PW map was eventually converted into a quantitative ASL CBF map by applying the standard kinetic model (Buxton et al., 1998; Wong et al., 1998)

$$\mathrm{CBF}= 6000.\frac{\lambda\Delta M\times e^{\frac{TI_2+idx_{sl}\times TI_{sl}}{T_{1b}}}}{2\alpha TI_1 M_{0b}}\ [\mathrm{mL/100g/min}]$$

where the factor 6000 converts the unit from mL/g/s to mL/100g/min. The labeling efficiency α was assumed to be 98% and the blood/tissue water partition coefficient λ to be 0.9 mL/g (Alsop et al., 2015). ΔM is the PW map. TI_1 = 700 ms is the temporal width of the bolus. TI_2, inversion time, is the time from the initial pulse to image acquisition (2000 ms). TI_2 is adjusted for each slice to take into account the time interval TI_{sl} (47 ms) between slice acquisitions in our 2D multislice ASL sequences. idx_{sl} is the slice index (0 for the first slice). T_{1b} is the longitudinal relaxation time of blood that was assumed to be 1350 ms (Alsop et al., 2015). M_{0b} is the longitudinal magnetisation of blood at equilibrium and is approximated by the M0 map.

2.3.3. Calculation of CBF statistics over ROIs

ROI analysis was used to measure mean, standard deviation, min and max values of CBF. The ROI mask built from ALBERTs data was transformed to the CBF map of each subject by a composition of transformations, T_O and T_R, T_R itself being the composition of a diffeomorphism with an affine transform between our custom ALBERTs atlas and the subject brain, and T_O being the reorientation transformation toward the Neonatal2 atlas. The data were interpolated only once with a nearest-neighbour scheme. Thus, the ROI mask, the grey matter mask of the subject and the CBF map were in coregistration.

The CBF statistics were lastly computed over each ROI (the frontal, temporal, parietal and occipital lobes, the BGT and the cortical GM ROI) intersected with the voxels having a grey matter probability higher than 0.7. In addition, the CBF statistics over the whole brain (i.e. over the voxels whose tissue sum was higher than 0.85) were also computed as an overall value for perfusion.

2.4. Data analysis

2.4.1. Qualitative analysis

ASL CBF maps were rated as having good, moderate or poor image quality by MP (7 years' experience with ASL images). Images were considered as good quality when no or only

minor artefacts were present. Images were considered as moderate quality when moderate artefacts were present and did not prevent image interpretation. Images were considered poor quality when marked artefacts were present or images were considered unreadable.

Two experienced paediatric radiologists (VC and MP with, respectively, 7 and 9 years' experience) scored brain injury on MRI (T1, T2 and DWI). Early and late MRIs were assessed independently. The reviewers were blinded to the ASL sequence, clinical details and outcome of the neonates but knew the age at the time of the MRI. Assessment of brain injury was based on a previously described simplified classification (Charon et al., 2015) adapted from the Barkovich system (Barkovich et al., 1998). It distinguishes between normal/subnormal MR images — including normal MRI, punctate periventricular white matter injuries (PPWMI) and watershed pattern with a Watershed (W) score ≤2 on the scoring system described by Barkovich et al. (single infarction or abnormal signal in anterior or posterior watershed white matter) — and abnormal MR images including a watershed pattern with W score >2, central or diffuse patterns. The differences were resolved by consensus between the two reviewers.

2.4.2. Quality check

In addition to visual evaluation of the ASL data, we also performed an automated quality check. As the PW map may present with negative values due to the inherent low resolution and SNR of ASL, the percentage of negative values was calculated in the whole brain, GM and WM.

2.4.3. Quantitative analysis

Quantitative (continuous) data were expressed as median [95% confidence interval] across subjects. Normality of data distribution was checked by Shapiro-Wilk tests. As the distribution of the sample was not normal for the majority of data and because of the small sample size, non-parametric tests were used. The Wilcoxon test for paired samples was used to evaluate difference between DOL4 and DOL11 for each ROI, and differences between ROIs on DOL4 and DOL11. The Mann-Whitney test for independent samples was used to evaluate differences between normal and abnormal MRI for each ROI. A p value <0.05 (two-tailed probability) was considered significant. Statistical analysis was performed using MedCalc Statistical Software version 18.2.1 (MedCalc Software bvba; Ostend, Belgium; http://www.medcalc.org).

3. Results

3.1. Study population

Twenty-eight (28) neonates were included in the study between April 2015 and December 2017. There were 16 boys and 12 girls. All of them underwent the early MRI (DOL4). There was no late MRI (DOL11) for 5 neonates, due to non-availability of an ASL sequence (n=4) or death of the subject before DOL11 (n=1), giving 51 scans in total.

The median age of the early MRI was day of life 3.7 (range: 3-5) and that of the late MRI was day of life 10.6 (range: 9-12). The mean gestational age at birth was 39.7 weeks (range: 36.7-41.9). Blood hematocrit values were available in 25/28 subjects at DOL4 and 11/23 subjects at DOL11, and the respective means were 43% ± 6% (range: 27-58) and 38% ± 7% (range: 26-55).

3.2. MR imaging

3.2.1. Qualitative analysis and quality check

Fourteen (27%) MRIs were excluded because of poor CBF map image quality and more than 20% negative values in GM. A visual scoring of 3 and a threshold set at 20% of negative values in GM were in agreement for excluding subjects. Statistical analysis was performed on 37 MRIs, specifically 17 early MRIs and 20 late MRIs. Eleven neonates had both early and late MRIs of good quality available.

Regarding the manual suppression of pairs on preliminary visual inspection, a mean of 6 label/control pairs were deleted (range [2-14]) on DOL4 in 4 neonates, and 7.4 (range [2-15]) on DOL11, in 12 neonates. Conventional MRI scoring by two experienced pediatric radiologists concluded that 8 out of 17 neonates (47%) had an abnormal early MRI and that 7 out of 20 neonates (35%) had an abnormal late MRI. Among the 11 neonates with both early and late MRI available, 5 had normal MRI, 1 had watershed involvement with a W score ≤2, 1 had a watershed pattern with W score >2, 3 had a central pattern and 1 had a diffuse pattern. Among the 6 neonates who had only an early MRI available, 2 had normal MRI, 1 had PPWM involvement, and 3 had a diffuse pattern. Among the 9 neonates who had only a late MRI available, 7 had normal MRI, 1 had a watershed pattern with W score >2 and 1 had a central pattern.

For every patient, the scoring result was the same for the early and late MRI. No patients changed groups between the two time points.

3.2.2. Quantitative analysis

The results are provided in bilateral ROIs. ROIs are illustrated in Figure 4.

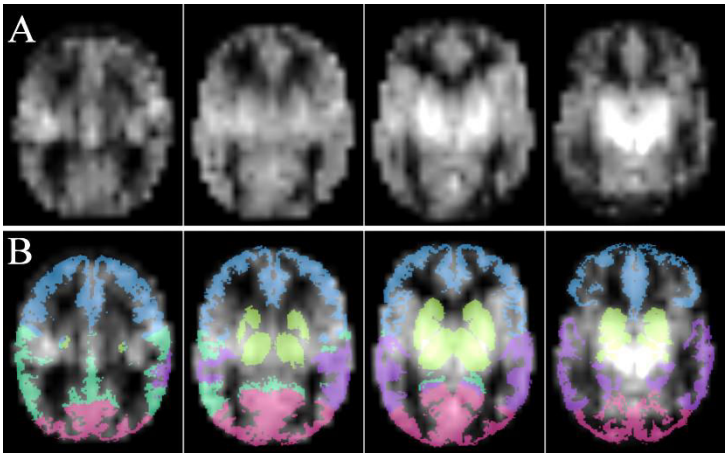

Figure 4: Axial images of an ASL perfusion map (A) and ROI as overlay (B) with frontal (blue), parietal (dark green), occipital (pink) and temporal (purple) lobes, and basal ganglia and thalami (light green).

3.2.2.1. Changes in CBF values between early and late MRI

The medians of CBF means in the BGT and temporal lobes were significantly different between the early and the late MRI ($p = 0.0049$ and 0.042 respectively) with higher CBF values observed at DOL4. There were no significant differences between early and late MRIs for the other ROIs. Figure 5 shows the CBF changes in the BGT for the 11 paired subjects between DOL4 and DOL11.

ROI	DOL4 [n=11]	DOL11 [n=11]
Brain	23.8 [14.6-48.3]	19.0 [15.5-28.3]
Cortical GM	24.8 [16.3-51.6]	22.3 [15.6-37.6]
BGT	55.4 [37.8-101.2]	28.3 [19.0-47.0] **
Lobes		
Frontal	25.6 [16.2-50.3]	22.9 [13.8-39.8]
Temporal	31.5 [20.8-47.3]	23.1 [20.6-34.1] **
Parietal	25.2 [14.1-61.6]	20.7 [15.3-43.6]
Occipital	29.3 [15.5-53.7]	19.1 [15.0-36.5]

Table 1: Cerebral blood flow values (mL/100g/min) in brain regions of interest, expressed as the median [95% CI]. CBF = Cerebral Blood Flow; DOL4 = day 4 of life; DOL11 = day 11 of life; ROI= Region Of Interest; BGT= Basal Ganglia and Thalami; Cortical GM = Grey matter in lobes. ** = *significant difference [p <0.05] with the previous column [Wilcoxon test for paired sample].*

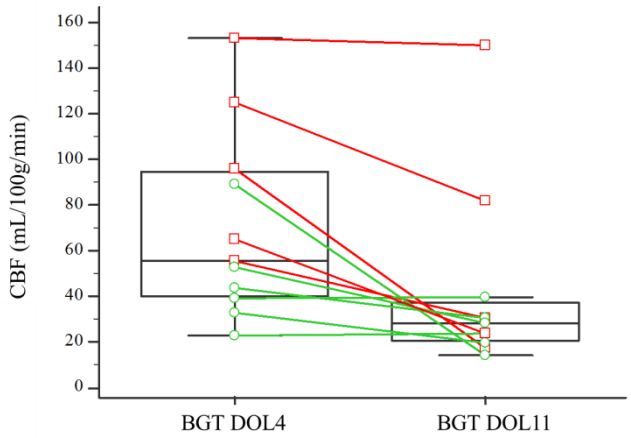

Figure 5: Changes in cerebral blood flow in the basal ganglia and thalami for each subject (paired sample, n=11) between day 4 and day 11 of life. The box-and-whisker plots show the lower and upper quartiles (box edges), medians (line in boxes) and minimum/maximum values (lines at ends of whiskers). The dot-and-line diagrams show infants with injury (n=5) (red squares and lines) and without injury (n=6) (green circles and lines) on MRI. Differences between DOL4 and DOL11 were significant (p=0.049).

BGT= Basal Ganglia and Thalami; CBF = Cerebral Blood Flow; DOL4 = day 4 of life, DOL11 = day 11 of life.

3.2.2.2. Comparison of CBF values between ROIs

The medians of CBF means in each ROI are summarized in Table 2 and Figure 6. The BGT yielded the highest median CBF values at both time points. CBF values were significantly different in the BGT vs. the cortical GM, on both the early MRI (p<0.0001) and the late MRI (p=0.0020). There were no significant differences between the lobes except between the temporal and frontal lobes on the early MRI (p=0.0395).

Note that no comparison vs. brain has been performed. Whole brain CBF values are shown for comparison purposes with studies in literature using ASL or other brain perfusion imaging techniques that provide overall CBF values.

ROI	DOL4 [n=17]	DOL11 [n=20]
Brain	30.5 [19.1-37.5]	21.1 [16.3-27.1]
Cortical GM	30.5 [20.8-45.0]	24.6 [18.4-32.1]
BGT	52.8 [42.6-93.6]	30.2 [24.1-48.8]
Lobes		
Frontal	25.2 [21.8-38.2]	25.1 [17.7-34.6]
Temporal	31.5 [25.4-42.1]	23.2 [21.1-30.1]
Parietal	25.8 [18.8-50.5]	23.5 [17.9-34.3]
Occipital	36.9 [19.0-51.1]	23.2 [15.9-32.6]

Table 2: Cerebral blood flow values (mL/100g/min) in brain regions of interest, expressed as the median [95% CI]. CBF = Cerebral Blood Flow; DOL4 = day 4 of life; DOL11 = day 11 of life; ROI= Region Of Interest; BGT= Basal Ganglia and Thalami; Cortical GM = Grey matter in lobes.

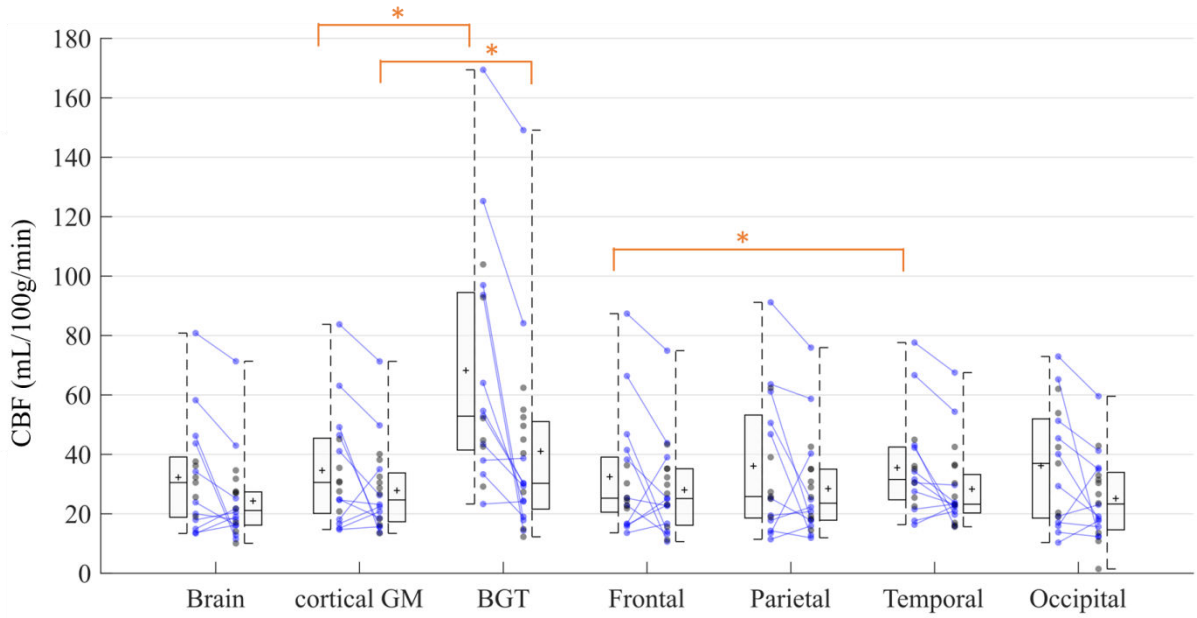

Figure 6: Cerebral blood flow in ROIs on day 4 of life (n=17) and day 11 of life (n=20). Box-and-whisker plots show the lower to upper quartiles (box edges), medians (line in boxes) and minimum/maximum values (lines at ends of whiskers). The mark represents the mean. The dot-and-line diagrams (in blue) show infants with both early and late MRI (n=11). The asterisk represents significant difference [p <0.05] [Wilcoxon test for paired samples].

BGT= Basal Ganglia and Thalami; CBF = Cerebral Blood Flow; DOL4 = day 4 of life; DOL11 = day 11 of life; Cortical GM = Grey matter in lobes; ROI= Region Of Interest.

3.2.2.3. CBF values in ROIs by normal vs. abnormal MRI morphology

The medians of CBF means in each ROI are summarized in Table 3 and Figure 7. On DOL4, the median CBF was significantly different in cortical GM (p=0.0433), BGT (p=0.0269), frontal (p=0.0209) and parietal lobes (p=0.0161) in subjects with an abnormal MRI compared to those with a normal MRI. There were no significant differences between the two groups for the whole brain and the temporal and occipital lobes. On DOL11, the median CBF in each ROI was not significantly different between the normal MRI group and the abnormal MRI group, except for the temporal lobes (p=0.0357). In addition, if we compare the difference between the medians of the normal and abnormal MRI groups on DOL4 and on DOL11, the gap between the normal and abnormal groups is reduced on day 11 compared to day 4 (p=0.0364).

ROI	DOL4		DOL11	
	Normal [n= 9]	Abnormal [n=8]	Normal [n=13]	Abnormal [n=7]
Brain	19.9 [15.3-35.6]	35.8 [23.3-62.5]	18.0 [15.1-24.3]	26.8 [15.9-57.2]
Cortical GM	24.6 [16.8-30.8]	43.0 [25.2-66.9]*	22.3 [15.9-29.5]	32.5 [18.1-60.2]
BGT	43.4 [29.7-87.3]	80.5 [44.3-133.6]*	29.3 [17.0-42.5]	49.5 [21.0-116.9]
Lobes				
Frontal	22.7 [15.9-25.1]	37.2 [23.6-70.3] *	23.1 [14.8-30.9]	35.2 [16.7-59.4]
Temporal	30.4 [18.3-41.9]	35.1 [24.7-68.7]	22.7 [16.5-27.6]	36.2 [21.4-61.0] *
Parietal	19.4 [14.7-25.7]	55.8 [24.3-68.8] *	20.7 [16.2-32.7]	25.6 [16.9-67.4]
Occipital	20.3 [16.0-51.5]	43.9 [17.4-64.1]	19.1 [12.3-28.3]	32.9 [17.9-50.5]

Table 3: Cerebral blood flow values (mL/100g/min) in brain regions of interest by normal vs. abnormal MRI scoring. Values in ROIs are expressed as medians [95% CI].
CBF = Cerebral Blood Flow; DOL4 = day 4 of life; DOL11 = day 11 of life; ROI= Region Of Interest; BGT= Basal Ganglia and Thalami; Cortical GM = grey matter in lobes. * = *significant difference [p <0.05] with the previous column [Mann-Whitney test for independent samples].*

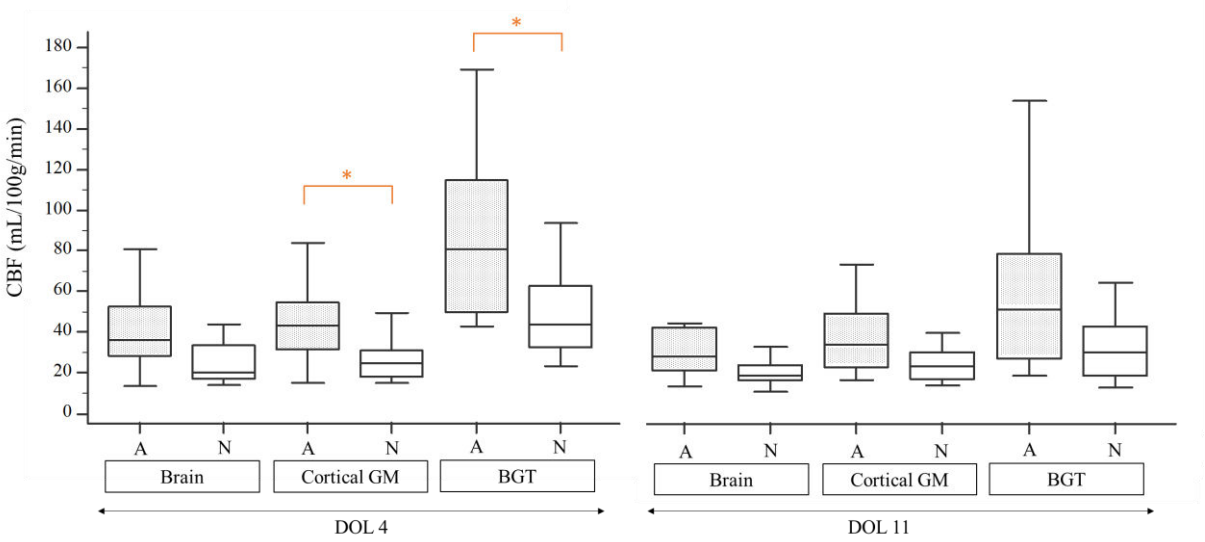

Figure 7: **Cerebral blood flow in brain, grey matter in lobes, and basal ganglia and thalami on day 4 of life for subjects with normal MRI (n=9) vs. abnormal MRI (n=8) and on day 11 of life for subjects with normal MRI (n=13) vs. abnormal MRI (n=7)..** Box-and-whisker plots show the lower and upper quartiles (box edges), medians (line in boxes) and minimum/maximum values (lines at ends of whiskers). Differences between infants with vs. without injury on MRI were significant (asterisk) on DOL 4 in the BGT (p=0.0269) and in the cortical GM (p=0.0433) [Mann-Whitney test for independent samples].

A = Abnormal MRI; BGT= Basal Ganglia and Thalami; CBF = Cerebral Blood Flow; DOL4 = day 4 of life; DOL11 = day 11 of life; Cortical GM = Grey matter in lobes; N = Normal MRI; ROI= Region Of Interest.

4. Discussion

The ASL MRI sequence is highly suitable for studying cerebral perfusion in neonates and is easier to implement than other techniques. However, because of less specific pipelines than in adults the post-processing of images in infants is not yet automated. Usual brain extraction and segmentation methods are not well suited for neonate subjects. This may be explained by differences in shape compared to older children but the main reason is that axons are not yet fully myelinated and so the contrast is not optimal. This study provided us with the opportunity to develop a processing pipeline of morphological and ASL data suited to neonates. We were able to automatically segment our ROIs whereas in all except one study (Tortora et al., 2017) ROIs were placed manually. Automated segmentation has the advantage

of being more reproducible and allowing faster processing of large amounts of data. However, visual checking of the images and segmentations obtained currently remains necessary.

In our study, CBF values in the BGT were higher at DOL4, probably due to hyperperfusion of the BGT in subjects with an abnormal MRI. Our results are consistent with the literature. Indeed an association between ischemia and perfusion has been demonstrated (Pienaar et al., 2012). In this study, the regions with decreased diffusivity showed an increase in CBF on MRIs performed between DOL0 and DOL4 in 9 children with ischemic lesions. Wintermark et al. have shown that cooled neonates with HIE have a lower CBF on DOL1 and a higher CBF on DOL2 in injured brain areas. Conversely, in neonates who were not treated with hypothermia but who developed HI brain injury, hyperperfusion was already seen on DOL1 and appeared to peak at around DOL2-3 (Wintermark et al., 2011). Another study on ASL in a cohort of 19 term asphyxiated neonates and 4 healthy controls that were scanned at least once during the first month of life (on DOL1, DOL2-3, DOL10 or DOL30) showed similar results (Boudes et al., 2014). They reported that brain perfusion and variations in cerebral blood flow values between the newborns were the highest on days 2–3 of life and in the asphyxiated newborns developing brain HI injury. However, no statistics reported comparison of CBF between each DOL. During the second week of life Massaro et al. found that 8 children with MRI lesions had lower CBF values in the thalamus than the children with HIE with no lesions on MRI. In contrast, children with normal MRI or watershed involvement were more likely to have hyperperfusion than controls (Massaro et al., 2013). Using dynamic susceptibility contrast (DSC) MRI, persistent cortical grey matter hyperperfusion on late scans on DOL11, instead of normalization of CBF in basal ganglia and white matter, has been reported in two term neonates with severe HI cerebral lesions (Wintermark et al., 2008).

Our study did not reveal any statistically significant differences in children with normal vs. abnormal MRI on late MRI. One explanation for this finding may be that changes in cerebral perfusion related to the ischemic perinatal insult have normalized during the second week of life. However we can observe in Table 3 and Figure 7 that the median CBF is still higher on DOL11 in neonates with injury compared to those without. This could mean that the differences have not been found significant due to the small size of our cohort and to wide standard-deviations, as discussed below. Yet, we also observe that the gap between the normal and abnormal MRI groups – even if persisting on DOL11 - is reduced compared to DOL4. We may hypothesize that the gap will continue to diminish in the next weeks of life.

We also found hyperperfusion in the cerebral cortex (cortical GM) on early MRI in subjects with abnormal MRI. Cortical hyperperfusion is less described in the literature and most of the

studies have reported results in the BGT probably because the ROIs were manually placed, as discussed previously. The pattern of injury in asphyxiated infants is related to the type and severity of the insult. The most common pattern of injury involves the basal ganglia, but cortical involvement may be seen in infants with a chronic or repetitive insult. One neonate presented with extended cortical involvement on MRI, with relative sparing of the central grey matter seen on conventional MRI including DWI, despite having high CBF values in the BGT (125.2 mL/100g/min on DOL4 and 84.1 on DOL11). Similarly, De Vis et al. reported that one infant in their cohort had a watershed injury pattern and an adverse outcome and hyperperfusion in the BGT, indicating that hyperperfusion can occur in areas without injury on conventional MRI. Furthermore, we remark that for this subject hyperperfusion persisted on DOL11 in the BGT as well as in the cortical grey matter.

In the literature, the hyperperfusion observed on early MRI is known as the "reperfusion phenomenon" which occurs after the hypoxic ischemic event (Lassen, 1966; Pryds et al., 1990). The reperfusion phase is divided into two periods: a latent phase and an energy failure phase. The energy failure phase can occur 6 to 15 hours after reperfusion and last a few days, leading to delayed cell death (Saliba and Debillon, 2010). The severity of this second phase is related to poor outcome (Batista et al., 2007; Rosenbaum et al., 1997). It still remains unclear whether hyperperfusion contributes to the injury or, on the other hand, represents a compensatory mechanism (Greisen, 2014). Wintermark et al. raised the question of the timing of the transition between the hypoperfusion phase and the hyperperfusion phase during the first days of life (Wintermark et al., 2011). Our study raises the question of the length of the hyperperfusion phase and the pattern of CBF normalisation with regard to insult severity. As suggested in a previous report using DSC perfusion weighted-MRI, late hyperperfusion might represent the most severely infarcted areas taking more time to recuperate autoregulation of CBF (Wintermark et al., 2008). As an example, one neonate with a central pattern brain injury had a CBF value of 169.4 mL/100g/min in the BGT on DOL4, which persisted on DOL11 with a value of 149.1 mL/100g/min. This neonate had an adverse outcome and died a few days later.

We found significantly higher CBF values in the BGT vs. cortical grey matter at both time points, findings that are consistent with literature data even in healthy neonates. In premature infants at term-equivalent age (TEA), De Vis et al. (De Vis et al., 2013) found CBF values of 12±3 and 29±9 mL/100g/min in the whole brain and the BGT, respectively. The values reported by Miranda et al. (Miranda et al., 2006) in 6 full-term children were 16.6±5.9 mL/100g/min in the whole brain and 30.2±5.5 mL/100g/min in the BGT. There were no

significant differences between the different lobes, except between the frontal and temporal lobes on DOL4. We have difficulty explaining these results and they must be interpreted with caution because of the small sample size. Moreover artefacts may be more frequent in temporal lobes because of magnetic susceptibility effects due to the air/tissue interface in mastoids. The EPI readout of the PASL sequence is known to be very sensitive to magnetic susceptibility artefacts and this could lead to perfusion measurement errors. This may also explain the isolated temporal lobe hyperperfusion in subjects with an abnormal MRI on DOL11 compared to subjects with a normal MRI. The differences in perfusion reported in literature in neonates rather concern the frontal and occipital lobes in premature infants (Ouyang et al., 2017a), as seen in term-equivalent-age or healthy infants (Kim et al., 2018).

Our study has limitations. First, the low number of subjects. In common with many articles in the literature on the same topic, the frequency of the pathology and recruitment by centre each year precludes large cohorts. Nevertheless, we have a similar number of subjects to the few cohorts reported in the literature. Despite our cohort of 28 neonates, only 11 had both early and late MRIs available and of good quality. The other MRI scans were not excluded and we were still able to perform unpaired analysis. For ethical reasons, our study did not have a control group — it is difficult to scan healthy subjects within the first two weeks of their life. Second, there was insufficient follow-up in the current study to evaluate the neurodevelopmental prognosis at 2 years. It would be interesting to correlate neurological outcomes with CBF changes during the first 2 weeks of life in a future study, as performed by De Vis et al. on early MRI (De Vis et al., 2015). These authors observed hyperperfusion in the basal ganglia and thalami in 8 children with HIE with a poor neurodevelopmental outcome versus 20 children with HIE who had a good outcome, on MRI performed in the first week of life. These data are promising because the CBF values would thus make it possible to determine a neurodevelopmental prognosis at an early stage, independently of the conventional imaging. The reported cut-off value for CBF was 51 mL/100g/min in the BGT. When using this cut-off value, our results were concordant, as median CBF values in the BGT in neonates with abnormal MRI on early MRI were 80.5 [44.3-133.6] mL/100g/min vs. 43.4 [29.7-87.3] in neonates with normal conventional MRI. However, it could be problematic to use a threshold value given the high inter-subject variability in CBF values as shown in our study and in the literature in healthy children (Avants et al., 2015; Carsin-Vu et al., 2018; Taki et al., 2011) or in neonates (Boudes et al., 2014). As an example, one neonate that presented with a diffuse pattern of injury and died had a CBF value of 44.7 mL/100g/min in

the BGT on early MRI. Conversely, one neonate with no injury on conventional MRI had a CBF value of 93.7 mL/100g/min in the BGT on early MRI and 14.4 mL/100g/min on late MRI. In the same way, it would be interesting to determine a cut-off value on late MRI as performed by De Vis et al. on early MRI. Moreover, a cut-off value could also be determined in the cortical grey matter, given that BGT values may not be used as basal perfusion values are not the same, as demonstrated in our results.

The number of excluded patients is relatively high in our study (27%). The proportion of excluded patients is quite similar in the literature (around 25%) (Boudes et al., 2014; Tortora et al., 2017). The quality criteria used are variable and not detailed in the majority of the papers. Boudes et al. (Boudes et al., 2014) used a quality score developed for their study, consisting of visual analysis based on GM/WM identification and artefacts. De Vis et al. (De Vis et al., 2015) rated ASL images as having good, moderate or poor image quality by using quality criteria that included artefacts and negative voxels. We did much the same by combining visual inspection and automated measurement of voxel negatives in grey matter.
It is interesting that all the infants who were excluded did not have any motion artefacts. Understanding why the quality of the maps was poor is crucial. One hypothesis could be that labeling failed due to very low blood flow velocities and CBF. Acquiring ASL sequences in neonates is not as easy to achieve as in older children or adults. Indeed, in addition to the intrinsically lower SNR and resolution of the ASL sequence, the SNR is much lower in neonates because of the small size of the head and the (physiologically) low cerebral perfusion. An improvement could be expected with a pseudocontinuous ASL (pCASL) labeling scheme that was not available when we started the study on our machine. However, as shown in a study comparing PASL and pCASL (Boudes et al., 2014) to assess brain perfusion in healthy and asphyxiated newborns, the two sequences had a similar success rate. In literature studies reporting ASL data in neonates, 8 used a PASL (Boudes et al., 2014; De Vis et al., 2015; De Vis et al., 2013; Miranda et al., 2006; Tortora et al., 2017; Varela et al., 2015; Wintermark et al., 2014, 2011) and 5 used a pCASL labeling scheme (Boudes et al., 2014; Massaro et al., 2013; Ouyang et al., 2017b; Pienaar et al., 2012; Watson et al., 2016). Using a stronger magnetic field would improve the SNR but not change this proportion as all but one study (Pienaar et al., 2012) in the literature was performed using 3T MRI scanners.
Finally, we used an estimated T1b for quantification and this may affect CBF values particularly in neonates who have variable hematocrit values (Varela et al., 2015). De Vis et al. 2014 demonstrated that the average change in CBF was 11% between perfusion values

using an assumed T1b and a corrected T1b. The formula that exists for calculating T1b from each patient's hematocrit (Varela et al., 2011), which is now used in ASL studies in neonates, has been implemented for 3T magnetic fields. Hematocrit values were available in our population, but we did not find a valid formula at 1.5T in the literature. We have therefore used an assumed T1b as in most of the other studies. This can distort CBF values.

In conclusion, we developed a processing pipeline for morphological and ASL data suitable for neonates based on automated segmentation to obtain mean CBF values in ROIs, including the BGT and cortical grey matter. This is a novel approach as the majority of previous studies using ASL in neonates in the literature used manual drawn ROIs. Our study is one of the first to look at changes over time during the first and second week of life on two successive scans. Given that the perfusion differences observed on early MRI between subjects with vs. without injury on MRI were no longer significant on the late scan in our study, ASL sequences in this pathology seem to be more relevant when acquired relatively early, in the first days of life, in line with previous studies and reflecting the reperfusion phenomenon. However, persistent hyperperfusion on late MRI scans in some of our subjects, as also seen in the literature, indicates that this phase may be of inconstant length. The correlation of intra-subject changes in perfusion between early and late MRI with neurodevelopmental outcome warrants investigation in a larger cohort, to determine whether the CBF change pattern can provide additional prognostic information.

Acknowledgements

We thank our radiologist and radiographer colleagues who helped during the research study; the neonatologist from our institution for patient inclusion in the study; Elise Bannier for improvements to the ASL sequence and management of images before processing; and Tracey Westcott for English language editing.

Funding sources

This work was supported by the *Société Française de Radiologie*, Paris, France [2017 Research Grant] and the *Agence Nationale de la Recherche*, France [Project: ANR-15-CE23-009, MAIA, Programme: Appel à projets génériques 2015].

References

Agut, T., León, M., Rebollo, M., Muchart, J., Arca, G., Garcia-Alix, A., 2014. Early identification of brain injury in infants with hypoxic ischemic encephalopathy at high risk for severe impairments: accuracy of MRI performed in the first days of life. BMC Pediatr. 14, 177. https://doi.org/10.1186/1471-2431-14-177

Alderliesten, T., de Vries, L.S., Benders, M.J.N.L., Koopman, C., Groenendaal, F., 2011. MR imaging and outcome of term neonates with perinatal asphyxia: value of diffusion-weighted MR imaging and ^{1}H MR spectroscopy. Radiology 261, 235–42. https://doi.org/10.1148/radiol.11110213

Alsop, D.C., Detre, J.A., Golay, X., Günther, M., Hendrikse, J., Hernandez-Garcia, L., Lu, H., MacIntosh, B.J., Parkes, L.M., Smits, M., van Osch, M.J.P., Wang, D.J.J., Wong, E.C., Zaharchuk, G., 2015. Recommended implementation of arterial spin-labeled perfusion MRI for clinical applications: A consensus of the ISMRM perfusion study group and the European consortium for ASL in dementia. Magn. Reson. Med. 73, 102–16. https://doi.org/10.1002/mrm.25197

Avants, B.B., Duda, J.T., Kilroy, E., Krasileva, K., Jann, K., Kandel, B.T., Tustison, N.J., Yan, L., Jog, M., Smith, R., Wang, Y., Dapretto, M., Wang, D.J.J., 2015. The pediatric template of brain perfusion. Sci. Data 2, 150003. https://doi.org/10.1038/sdata.2015.3

Barkovich, A.J., Hajnal, B.L., Vigneron, D., Sola, A., Partridge, J.C., Allen, F., Ferriero, D.M., 1998. Prediction of neuromotor outcome in perinatal asphyxia: evaluation of MR scoring systems. AJNR. Am. J. Neuroradiol. 19, 143–9.

Batista, C.E.A., Chugani, H.T., Juhász, C., Behen, M.E., Shankaran, S., 2007. Transient hypermetabolism of the basal ganglia following perinatal hypoxia. Pediatr. Neurol. 36, 330–3. https://doi.org/10.1016/j.pediatrneurol.2007.01.004

Boudes, E., Gilbert, G., Leppert, I.R., Tan, X., Pike, G.B., Saint-Martin, C., Wintermark, P., 2014. Measurement of brain perfusion in newborns: pulsed arterial spin labeling (PASL) versus pseudo-continuous arterial spin labeling (pCASL). NeuroImage. Clin. 6, 126–33. https://doi.org/10.1016/j.nicl.2014.08.010

Boudes, E., Tan, X., Saint-Martin, C., Shevell, M., Wintermark, P., 2015. MRI obtained during versus after hypothermia in asphyxiated newborns. Arch. Dis. Child. - Fetal Neonatal Ed. 100, F238–F242. https://doi.org/10.1136/archdischild-2014-306550

Buxton, R.B., Frank, L.R., Wong, E.C., Siewert, B., Warach, S., Edelman, R.R., 1998. A general kinetic model for quantitative perfusion imaging with arterial spin labeling. Magn. Reson. Med. 40, 383–96.

Carsin-Vu, A., Corouge, I., Commowick, O., Bouzillé, G., Barillot, C., Ferré, J.-C., Proisy, M., 2018. Measurement of pediatric regional cerebral blood flow from 6 months to 15 years of age in a clinical population. Eur. J. Radiol. 101, 38–44. https://doi.org/10.1016/j.ejrad.2018.02.003

Chakkarapani, E., Poskitt, K.J., Miller, S.P., Zwicker, J.G., Xu, Q., Wong, D.S.T., Roland, E.H., Hill, A., Chau, V., 2016. Reliability of Early Magnetic Resonance Imaging (MRI) and Necessity of Repeating MRI in Noncooled and Cooled Infants With Neonatal Encephalopathy. J. Child Neurol. 31, 553–559. https://doi.org/10.1177/0883073815600865

Charon, V., Proisy, M., Ferré, J.-C., Bruneau, B., Tréguier, C., Beuchée, A., Chauvel, J., Rozel, C., 2015. Comparison of early and late MRI in neonatal hypoxic–ischemic encephalopathy using three assessment methods. Pediatr. Radiol. 45. https://doi.org/10.1007/s00247-015-3419-4

Cheong, J.L.Y., Cady, E.B., Penrice, J., Wyatt, J.S., Cox, I.J., Robertson, N.J., 2006. Proton MR spectroscopy in neonates with perinatal cerebral hypoxic-ischemic injury: metabolite peak-area ratios, relaxation times, and absolute concentrations. AJNR. Am. J. Neuroradiol. 27, 1546–54.

Commowick, O., Wiest-Daessle, N., Prima, S., 2012a. Block-matching strategies for rigid registration of multimodal medical images, in: Proceedings - International Symposium on Biomedical Imaging. pp. 700–703. https://doi.org/10.1109/ISBI.2012.6235644

Commowick, O., Wiest-Daesslé, N., Prima, S., 2012b. Automated diffeomorphic registration of anatomical structures with rigid parts: application to dynamic cervical MRI. Med. Image Comput. Comput. Assist. Interv. 15, 163–70.

De Vis, J.B., Hendrikse, J., Petersen, E.T., de Vries, L.S., van Bel, F., Alderliesten, T., Negro, S., Groenendaal, F., Benders, M.J.N.L., 2015. Arterial spin-labeling perfusion MRI and outcome in neonates with hypoxic-ischemic encephalopathy. Eur. Radiol. 25, 113–21. https://doi.org/10.1007/s00330-014-3352-1

De Vis, J.B., Petersen, E.T., de Vries, L.S., Groenendaal, F., Kersbergen, K.J., Alderliesten, T., Hendrikse, J., Benders, M.J.N.L., 2013. Regional changes in brain perfusion during brain maturation measured non-invasively with Arterial Spin Labeling MRI in neonates. Eur. J. Radiol. 82, 538–543. https://doi.org/10.1016/j.ejrad.2012.10.013

De Vis, J.B., Petersen, E.T., Kersbergen, K.J., Alderliesten, T., de Vries, L.S., van Bel, F., Groenendaal, F., Lemmers, P.M.A., Hendrikse, J., Benders, M.J.N.L., 2013. Evaluation of perinatal arterial ischemic stroke using noninvasive arterial spin labeling perfusion

MRI. Pediatr. Res. 74, 307–13. https://doi.org/10.1038/pr.2013.111

Gousias, I.S., Edwards, A.D., Rutherford, M.A., Counsell, S.J., Hajnal, J. V, Rueckert, D., Hammers, A., 2012. Magnetic resonance imaging of the newborn brain: manual segmentation of labelled atlases in term-born and preterm infants. Neuroimage 62, 1499–509. https://doi.org/10.1016/j.neuroimage.2012.05.083

Greisen, G., 2014. Cerebral blood flow and oxygenation in infants after birth asphyxia. Clinically useful information? Early Hum. Dev. 90, 703–705. https://doi.org/10.1016/j.earlhumdev.2014.06.007

Guimond, A., Meunier, J., Thirion, J.-P., 2000. Average Brain Models: A Convergence Study. Comput. Vis. Image Underst. 77, 192–210. https://doi.org/10.1006/CVIU.1999.0815

Kim, H.G., Lee, J.H., Choi, J.W., Han, M., Gho, S.-M., Moon, Y., 2018. Multidelay Arterial Spin-Labeling MRI in Neonates and Infants: Cerebral Perfusion Changes during Brain Maturation. AJNR. Am. J. Neuroradiol. https://doi.org/10.3174/ajnr.A5774

Lassen, N.A., 1966. The luxury-perfusion syndrome and its possible relation to acute metabolic acidosis localised within the brain. Lancet (London, England) 2, 1113–5.

Luh, W.M., Wong, E.C., Bandettini, P.A., Hyde, J.S., 1999. QUIPSS II with thin-slice TI1 periodic saturation: a method for improving accuracy of quantitative perfusion imaging using pulsed arterial spin labeling. Magn. Reson. Med. 41, 1246–54.

Massaro, A.N., Bouyssi-Kobar, M., Chang, T., Vezina, L.G., du Plessis, A.J., Limperopoulos, C., 2013. Brain Perfusion in Encephalopathic Newborns after Therapeutic Hypothermia. Am. J. Neuroradiol. 34, 1649–1655. https://doi.org/10.3174/ajnr.A3422

Maumet, C., Maurel, P., Ferré, J.-C., Barillot, C., 2014. Robust estimation of the cerebral blood flow in arterial spin labeling. Magn. Reson. Imaging 32, 497–504. https://doi.org/10.1016/j.mri.2014.01.016

Miranda, M.J., Olofsson, K., Sidaros, K., 2006. Noninvasive Measurements of Regional Cerebral Perfusion in Preterm and Term Neonates by Magnetic Resonance Arterial Spin Labeling. Pediatr. Res. 60, 359–363. https://doi.org/10.1203/01.pdr.0000232785.00965.b3

Ouyang, M., Liu, P., Jeon, T., Chalak, L., Heyne, R., Rollins, N.K., Licht, D.J., Detre, J.A., Roberts, T.P.L., Lu, H., Huang, H., 2017a. Heterogeneous increases of regional cerebral blood flow during preterm brain development: Preliminary assessment with pseudo-continuous arterial spin labeled perfusion MRI. Neuroimage 147, 233–242. https://doi.org/10.1016/j.neuroimage.2016.12.034

Pienaar, R., Paldino, M.J., Madan, N., Krishnamoorthy, K.S., Alsop, D.C., Dehaes, M., Grant,

P.E., 2012. A quantitative method for correlating observations of decreased apparent diffusion coefficient with elevated cerebral blood perfusion in newborns presenting cerebral ischemic insults. Neuroimage 63, 1510–1518. https://doi.org/10.1016/j.neuroimage.2012.07.062

Proisy, M., Mitra, S., Uria-Avellana, C., Sokolska, M., Robertson, N.J., Le Jeune, F., Ferré, J.-C., 2016. Brain Perfusion Imaging in Neonates: An Overview. AJNR. Am. J. Neuroradiol. https://doi.org/10.3174/ajnr.A4778

Pryds, O., Greisen, G., Lou, H., Friis-Hansen, B., 1990. Vasoparalysis associated with brain damage in asphyxiated term infants. J. Pediatr. 117, 119–25.

Rosenbaum, J.L., Almli, C.R., Yundt, K.D., Altman, D.I., Powers, W.J., 1997. Higher neonatal cerebral blood flow correlates with worse childhood neurologic outcome. Neurology 49, 1035–41.

Saliba, E., Debillon, T., 2010. [Hypothermia for hypoxic-ischemic encephalopathy in fullterm newborns]. Arch. Pediatr. 17 Suppl 3, S67-77. https://doi.org/10.1016/S0929-693X(10)70904-0

Serag, A., Aljabar, P., Ball, G., Counsell, S.J., Boardman, J.P., Rutherford, M.A., Edwards, A.D., Hajnal, J. V, Rueckert, D., 2012. Construction of a consistent high-definition spatio-temporal atlas of the developing brain using adaptive kernel regression. Neuroimage 59, 2255–65. https://doi.org/10.1016/j.neuroimage.2011.09.062

Skranes, J.H., Cowan, F.M., Stiris, T., Fugelseth, D., Thoresen, M., Server, A., 2015. Brain imaging in cooled encephalopathic neonates does not differ between four and 11 days after birth. Acta Paediatr. 104, 752–758. https://doi.org/10.1111/apa.13016

Taki, Y., Hashizume, H., Sassa, Y., Takeuchi, H., Wu, K., Asano, M., Asano, K., Fukuda, H., Kawashima, R., 2011. Correlation between gray matter density-adjusted brain perfusion and age using brain MR images of 202 healthy children. Hum. Brain Mapp. 32, 1973–1985. https://doi.org/10.1002/hbm.21163

Tortora, D., Mattei, P.A., Navarra, R., Panara, V., Salomone, R., Rossi, A., Detre, J.A., Caulo, M., 2017. Prematurity and brain perfusion: Arterial spin labeling MRI. NeuroImage Clin. 15, 401–407. https://doi.org/10.1016/j.nicl.2017.05.023

Varela, M., Hajnal, J. V, Petersen, E.T., Golay, X., Merchant, N., Larkman, D.J., 2011. A method for rapid in vivo measurement of blood T1. NMR Biomed. 24, 80–8. https://doi.org/10.1002/nbm.1559

Varela, M., Petersen, E.T., Golay, X., Hajnal, J. V, 2015. Cerebral blood flow measurements in infants using look-locker arterial spin labeling. J. Magn. Reson. Imaging 41, 1591–

600. https://doi.org/10.1002/jmri.24716

Volpe, J.J., 2012. Neonatal encephalopathy: an inadequate term for hypoxic-ischemic encephalopathy. Ann. Neurol. 72, 156–66. https://doi.org/10.1002/ana.23647

Watson, C.G., Dehaes, M., Gagoski, B.A., Grant, P.E., Rivkin, M.J., 2016. Arterial Spin Labeling Perfusion Magnetic Resonance Imaging Performed in Acute Perinatal Stroke Reveals Hyperperfusion Associated With Ischemic Injury. Stroke 47, 1514–9. https://doi.org/10.1161/STROKEAHA.115.011936

Wintermark, P., Hansen, A., Gregas, M.C., Soul, J., Labrecque, M., Robertson, R.L., Warfield, S.K., 2011. Brain Perfusion in Asphyxiated Newborns Treated with Therapeutic Hypothermia. Am. J. Neuroradiol. 32, 2023–2029. https://doi.org/10.3174/ajnr.A2708

Wintermark, P., Hansen, A., Warfield, S.K., Dukhovny, D., Soul, J.S., 2014. Near-infrared spectroscopy versus magnetic resonance imaging to study brain perfusion in newborns with hypoxic-ischemic encephalopathy treated with hypothermia. Neuroimage 85 Pt 1, 287–93. https://doi.org/10.1016/j.neuroimage.2013.04.072

Wintermark, P., Moessinger, A.C., Gudinchet, F., Meuli, R., 2008. Temporal evolution of MR perfusion in neonatal hypoxic-ischemic encephalopathy. J. Magn. Reson. Imaging 27, 1229–34. https://doi.org/10.1002/jmri.21379

Wong, E.C., Buxton, R.B., Frank, L.R., 1998. Quantitative imaging of perfusion using a single subtraction (QUIPSS and QUIPSS II). Magn. Reson. Med. 39, 702–8.

[NeuroImage: Clinical] New Manuscript: Submission Confirmation

Neuroimage Clinical <eesserver@eesmail.elsevier.com>

jeu. 25/10/2018 14:56

À :PROISY Maia <Maia.PROISY@chu-rennes.fr>;

*** Automated email sent by the system ***

Title: Changes in brain perfusion in successive arterial spin labelling MRI scans in neonates with hypoxic-ischaemic encephalopathy
Corresponding Author: Dr. Maïa PROISY
Authors: Isabelle Corouge; Antoine Legouhy; Amélie Nicolas; Valérie Charon; Nadia Mazille; Stéphanie Leroux; Bertrand Bruneau; Christian Barillot; Jean-Christophe Ferré
Article Type: Regular Article

Dear Dr. PROISY,

This is to confirm that the above-mentioned manuscript has been received for consideration in NeuroImage: Clinical.

You will be able to check on the progress of your manuscript by logging on to the Elsevier Editorial System for NeuroImage: Clinical as an Author:

https://ees.elsevier.com/ynicl/

If you need to retrieve password details, please go to: http://ees.elsevier.com/ynicl/automail_query.asp.

Your paper will be given a manuscript number shortly and you will soon receive an e-mail with this number for your reference.

Please be aware that NeuroImage: Clinical offers the 3D visualization viewer for the neuroimaging data embedded in published online articles. Hence, we would like to encourage you to upload the neuroimaging data (in NIfTI format) as supplementary material with your manuscript to our online submission system during the article revision stage. More information can be found at: http://www.elsevier.com/3DNeuroimaging

Thank you for submitting your manuscript to NeuroImage: Clinical. Should you have any questions, please feel free to contact our office.

Kind regards,
Elsevier Editorial System
NeuroImage: Clinical

Chapitre 5 – Conclusion et perspectives

L'imagerie de perfusion ASL en IRM est particulièrement adaptée à l'imagerie pédiatrique. De par sa facilité de mise en œuvre, de nouvelles indications à l'étude de la perfusion cérébrale émergent comme en témoignent les récentes publications de la littérature, de plus en plus nombreuses.

Ce travail de thèse a permis de mettre au point l'acquisition de la séquence sur l'IRM pédiatrique du CHU de Rennes et de mettre au point deux chaines de traitement automatisées, adaptées aux nouveau-nés et aux enfants. Effectivement, il existe plusieurs particularités physiologiques cérébrales perfusionnelles et anatomiques, chez les nouveau-nés et les enfants, différentes selon les tranches d'âge (évolution de la perfusion cérébrales de la naissance à l'adolescence, évolution de la myélinisation et des volumes de substance grise et substance blanche…). Nous avons pu adapter la chaîne de traitement automatisée des données ASL aux tranches d'âges pédiatriques, et qui pourront être utilisées pour des travaux ultérieurs.

Plusieurs projets de recherche restent en cours et à achever, en particulier en collaboration avec le service de neurochirurgie (Pr Riffaud - CHU Rennes), pour étude de la perfusion cérébrale pré- et post-opératoire chez les enfants ayant un kyste arachnoïdien ou une craniosténose (patients inclus, problèmes de segmentation sur un cerveau avec forme modifiée). Concernant les nouveau-nés, des inclusions sont en cours depuis 1 an chez les prématurés, dans le cadre des projets de recherche Digi-NewB (Pr Patrick Pladys – CHU Rennes) et ANR MAIA (Pr François Rousseau – Télécom Bretagne, Brest). Un encadrement de master 2 SIBM est en cours sur ces données (Mme Marine Dubois, interne en radiologie). Un projet de recherche est également en cours à 3T chez les nouveau-nés au CHU Sainte-Justine à Montréal, dans le cadre d'une mobilité. Enfin, l'analyse des données acquises au cours de l'étude PERINE (Dr Fabienne Pelé – CHU Rennes) permettra d'étudier la variabilité inter-sujets de la perfusion cérébrale sur une tranche d'âge plus serrée avec une cohorte plus importante (100 enfants entre 10 et 11 ans).

Références

Alsop, D.C., Detre, J.A., Golay, X., Günther, M., Hendrikse, J., Hernandez-Garcia, L., Lu, H., MacIntosh, B.J., Parkes, L.M., Smits, M., van Osch, M.J.P., Wang, D.J.J., Wong, E.C., Zaharchuk, G., 2015. Recommended implementation of arterial spin-labeled perfusion MRI for clinical applications: A consensus of the ISMRM perfusion study group and the European consortium for ASL in dementia. Magn. Reson. Med. 73, 102–16. https://doi.org/10.1002/mrm.25197

Aslan, S., Xu, F., Wang, P.L., Uh, J., Yezhuvath, U.S., van Osch, M., Lu, H., 2010. Estimation of labeling efficiency in pseudocontinuous arterial spin labeling. Magn. Reson. Med. 63, 765–71. https://doi.org/10.1002/mrm.22245

Biagi, L., Abbruzzese, A., Bianchi, M.C., Alsop, D.C., Del Guerra, A., Tosetti, M., 2007. Age dependence of cerebral perfusion assessed by magnetic resonance continuous arterial spin labeling. J. Magn. Reson. Imaging 25, 696–702. https://doi.org/10.1002/jmri.20839

Boudes, E., Gilbert, G., Leppert, I.R., Tan, X., Pike, G.B., Saint-Martin, C., Wintermark, P., 2014. Measurement of brain perfusion in newborns: pulsed arterial spin labeling (PASL) versus pseudo-continuous arterial spin labeling (pCASL). NeuroImage. Clin. 6, 126–33. https://doi.org/10.1016/j.nicl.2014.08.010

Boulouis, G., Dangouloff-Ros, V., Boccara, O., Garabedian, N., Soupre, V., Picard, A., Couloigner, V., Boddaert, N., Naggara, O., Brunelle, F., 2017. Arterial Spin-Labeling to Discriminate Pediatric Cervicofacial Soft-Tissue Vascular Anomalies. Am. J. Neuroradiol. 38, 633–638. https://doi.org/10.3174/ajnr.A5065

Buxton, R.B., Frank, L.R., Wong, E.C., Siewert, B., Warach, S., Edelman, R.R., 1998. A general kinetic model for quantitative perfusion imaging with arterial spin labeling. Magn. Reson. Med. 40, 383–96.

Cadiot, D., Longuet, R., Bruneau, B., Treguier, C., Carsin-Vu, A., Corouge, I., Gomes, C., Proisy, M., 2018. Magnetic resonance imaging in children presenting migraine with aura: Association of hypoperfusion detected by arterial spin labelling and vasospasm on MR angiography findings. Cephalalgia 38, 949–958. https://doi.org/10.1177/0333102417723570

Carsin-Vu, A., Corouge, I., Commowick, O., Bouzillé, G., Barillot, C., Ferré, J.-C., Proisy, M., 2018. Measurement of pediatric regional cerebral blood flow from 6 months to 15 years of age in a clinical population. Eur. J. Radiol. 101, 38–44. https://doi.org/10.1016/j.ejrad.2018.02.003

Chiron, C., Raynaud, C., Mazière, B., Zilbovicius, M., Laflamme, L., Masure, M.C., Dulac, O., Bourguignon, M., Syrota, A., 1992. Changes in regional cerebral blood flow during brain maturation in children and adolescents. J. Nucl. Med. 33, 696–703.

Chugani, H.T., Phelps, M.E., Mazziotta, J.C., 1987. Positron emission tomography study of human brain functional development. Ann. Neurol. 22, 487–497. https://doi.org/10.1002/ana.410220408

Commowick, O., Wiest-Daesslé, N., Prima, S., 2012. Automated diffeomorphic registration of anatomical structures with rigid parts: application to dynamic cervical MRI. Med. Image Comput. Comput. Assist. Interv. 15, 163–70.

Dai, W., Robson, P.M., Shankaranarayanan, A., Alsop, D.C., 2012. Reduced resolution transit

delay prescan for quantitative continuous arterial spin labeling perfusion imaging. Magn. Reson. Med. 67, 1252–65. https://doi.org/10.1002/mrm.23103

De Vis, J.B., Hendrikse, J., Groenendaal, F., de Vries, L.S., Kersbergen, K.J., Benders, M.J.N.L., Petersen, E.T., 2014. Impact of neonate haematocrit variability on the longitudinal relaxation time of blood: Implications for arterial spin labelling MRI. NeuroImage. Clin. 4, 517–25. https://doi.org/10.1016/j.nicl.2014.03.006

De Vis, J.B., Hendrikse, J., Petersen, E.T., de Vries, L.S., van Bel, F., Alderliesten, T., Negro, S., Groenendaal, F., Benders, M.J.N.L., 2015. Arterial spin-labelling perfusion MRI and outcome in neonates with hypoxic-ischemic encephalopathy. Eur. Radiol. 25, 113–21. https://doi.org/10.1007/s00330-014-3352-1

Deibler, A.R., Pollock, J.M., Kraft, R.A., Tan, H., Burdette, J.H., Maldjian, J.A., 2008a. Arterial spin-labeling in routine clinical practice, part 3: hyperperfusion patterns. AJNR. Am. J. Neuroradiol. 29, 1428–35. https://doi.org/10.3174/ajnr.A1034

Deibler, A.R., Pollock, J.M., Kraft, R.A., Tan, H., Burdette, J.H., Maldjian, J.A., 2008b. Arterial spin-labeling in routine clinical practice, part 2: hypoperfusion patterns. AJNR. Am. J. Neuroradiol. 29, 1235–41. https://doi.org/10.3174/ajnr.A1033

Detre, J.A., Leigh, J.S., Williams, D.S., Koretsky, A.P., 1992. Perfusion imaging. Magn. Reson. Med. 23, 37–45.

Evans, A.C., Brain Development Cooperative Group, 2006. The NIH MRI study of normal brain development. Neuroimage 30, 184–202. https://doi.org/10.1016/j.neuroimage.2005.09.068

Ferré, J.-C., Petr, J., Bannier, E., Barillot, C., Gauvrit, J.-Y., 2012. Improving quality of arterial spin labeling MR imaging at 3 Tesla with a 32-channel coil and parallel imaging. J. Magn. Reson. Imaging 35, 1233–9. https://doi.org/10.1002/jmri.23586

Fonov, V., Evans, A.C., Botteron, K., Almli, C.R., McKinstry, R.C., Collins, D.L., Brain Development Cooperative Group, 2011. Unbiased average age-appropriate atlases for pediatric studies. Neuroimage 54, 313–327. https://doi.org/10.1016/j.neuroimage.2010.07.033

Gevers, S., Nederveen, A.J., Fijnvandraat, K., van den Berg, S.M., van Ooij, P., Heijtel, D.F., Heijboer, H., Nederkoorn, P.J., Engelen, M., van Osch, M.J., Majoie, C.B., 2012. Arterial spin labeling measurement of cerebral perfusion in children with sickle cell disease. J. Magn. Reson. Imaging 35, 779–87. https://doi.org/10.1002/jmri.23505

Giedd, J.N., Blumenthal, J., Jeffries, N.O., Castellanos, F.X., Liu, H., Zijdenbos, A., Paus, T., Evans, A.C., Rapoport, J.L., 1999. Brain development during childhood and adolescence: a longitudinal MRI study. Nat. Neurosci. 2, 861–863. https://doi.org/10.1038/13158

Gousias, I.S., Edwards, A.D., Rutherford, M.A., Counsell, S.J., Hajnal, J. V, Rueckert, D., Hammers, A., 2012. Magnetic resonance imaging of the newborn brain: manual segmentation of labelled atlases in term-born and preterm infants. Neuroimage 62, 1499–509. https://doi.org/10.1016/j.neuroimage.2012.05.083

Hales, P.W., Kawadler, J.M., Aylett, S.E., Kirkham, F.J., Clark, C.A., 2014. Arterial Spin Labeling Characterization of Cerebral Perfusion during Normal Maturation from Late Childhood into Adulthood: Normal 'Reference Range' Values and Their Use in Clinical Studies. J. Cereb. Blood Flow Metab. 34, 776–784. https://doi.org/10.1038/jcbfm.2014.17

Lange, N., Giedd, J.N., Castellanos, F.X., Vaituzis, A.C., Rapoport, J.L., 1997. Variability of human brain structure size: ages 4-20 years. Psychiatry Res. 74, 1–12.

Li, R., Xiao, H., Lyu, J., J.J. Wang, D., Ma, L., Lou, X., 2017. Differential diagnosis of mitochondrial encephalopathy with lactic acidosis and stroke-like episodes (MELAS) and ischemic stroke using 3D pseudocontinuous arterial spin labeling. J. Magn. Reson. Imaging 45, 199–206. https://doi.org/10.1002/jmri.25354

Liu, P., Chalak, L.F., Krishnamurthy, L.C., Mir, I., Peng, S., Huang, H., Lu, H., 2016. T1 and T2 values of human neonatal blood at 3 Tesla: Dependence on hematocrit, oxygenation, and temperature. Magn. Reson. Med. 75, 1730–1735. https://doi.org/10.1002/mrm.25775

Massaro, A.N., Bouyssi-Kobar, M., Chang, T., Vezina, L.G., du Plessis, A.J., Limperopoulos, C., 2013. Brain Perfusion in Encephalopathic Newborns after Therapeutic Hypothermia. Am. J. Neuroradiol. 34, 1649–1655. https://doi.org/10.3174/ajnr.A3422

Maumet, C., Maurel, P., Ferré, J.-C., Barillot, C., 2014. Robust estimation of the cerebral blood flow in arterial spin labelling. Magn. Reson. Imaging 32, 497–504. https://doi.org/10.1016/j.mri.2014.01.016

Miranda, M.J., Olofsson, K., Sidaros, K., 2006. Noninvasive Measurements of Regional Cerebral Perfusion in Preterm and Term Neonates by Magnetic Resonance Arterial Spin Labeling. Pediatr. Res. 60, 359–363. https://doi.org/10.1203/01.pdr.0000232785.00965.b3

Ouyang, M., Liu, P., Jeon, T., Chalak, L., Heyne, R., Rollins, N.K., Licht, D.J., Detre, J.A., Roberts, T.P.L., Lu, H., Huang, H., 2017. Heterogeneous increases of regional cerebral blood flow during preterm brain development: Preliminary assessment with pseudo-continuous arterial spin labeled perfusion MRI. Neuroimage 147, 233–242. https://doi.org/10.1016/j.neuroimage.2016.12.034

Pienaar, R., Paldino, M.J., Madan, N., Krishnamoorthy, K.S., Alsop, D.C., Dehaes, M., Grant, P.E., 2012. A quantitative method for correlating observations of decreased apparent diffusion coefficient with elevated cerebral blood perfusion in newborns presenting cerebral ischemic insults. Neuroimage 63, 1510–1518. https://doi.org/10.1016/j.neuroimage.2012.07.062

Proisy, M., Bruneau, B., Rozel, C., Tréguier, C., Chouklati, K., Riffaud, L., Darnault, P., Ferré, J.-C., 2016a. Arterial spin labeling in clinical pediatric imaging. Diagn. Interv. Imaging 97, 151–8. https://doi.org/10.1016/j.diii.2015.09.001

Proisy, M., Mitra, S., Uria-Avellana, C., Sokolska, M., Robertson, N.J., Le Jeune, F., Ferré, J.-C., 2016b. Brain Perfusion Imaging in Neonates: An Overview. AJNR. Am. J. Neuroradiol. https://doi.org/10.3174/ajnr.A4778

Raoult, H., Ferré, J.-C., Petr, J., Bannier, E., Stamm, A., Barillot, C., Gauvrit, J.-Y., 2012. Functional arterial spin labeling: Optimal sequence duration for motor activation mapping in clinical practice. J. Magn. Reson. Imaging 36, 1435–44. https://doi.org/10.1002/jmri.23782

Richards, J.E., Sanchez, C., Phillips-Meek, M., Xie, W., 2016. A database of age-appropriate average MRI templates. Neuroimage 124, 1254–1259. https://doi.org/10.1016/j.neuroimage.2015.04.055

Richards, J.E., Xie, W., 2015. Brains for All the Ages, in: Advances in Child Development and Behavior. pp. 1–52. https://doi.org/10.1016/bs.acdb.2014.11.001

Sanchez, C.E., Richards, J.E., Almli, C.R., 2012a. Neurodevelopmental MRI brain templates

for children from 2 weeks to 4 years of age. Dev. Psychobiol. 54, 77–91. https://doi.org/10.1002/dev.20579

Sanchez, C.E., Richards, J.E., Almli, C.R., 2012b. Age-specific MRI templates for pediatric neuroimaging. Dev. Neuropsychol. 37, 379–99. https://doi.org/10.1080/87565641.2012.688900

Serag, A., Aljabar, P., Ball, G., Counsell, S.J., Boardman, J.P., Rutherford, M.A., Edwards, A.D., Hajnal, J. V, Rueckert, D., 2012. Construction of a consistent high-definition spatio-temporal atlas of the developing brain using adaptive kernel regression. Neuroimage 59, 2255–65. https://doi.org/10.1016/j.neuroimage.2011.09.062

Smith, S.M., 2002. Fast robust automated brain extraction. Hum. Brain Mapp. 17, 143–55. https://doi.org/10.1002/hbm.10062

Sowell, E.R., Thompson, P.M., Holmes, C.J., Batth, R., Jernigan, T.L., Toga, A.W., 1999. Localizing age-related changes in brain structure between childhood and adolescence using statistical parametric mapping. Neuroimage 9, 587–97. https://doi.org/10.1006/nimg.1999.0436

Taki, Y., Hashizume, H., Sassa, Y., Takeuchi, H., Wu, K., Asano, M., Asano, K., Fukuda, H., Kawashima, R., 2011. Correlation between gray matter density-adjusted brain perfusion and age using brain MR images of 202 healthy children. Hum. Brain Mapp. 32, 1973–1985. https://doi.org/10.1002/hbm.21163

Tortora, D., Mattei, P.A., Navarra, R., Panara, V., Salomone, R., Rossi, A., Detre, J.A., Caulo, M., 2017. Prematurity and brain perfusion: Arterial spin labeling MRI. NeuroImage Clin. 15, 401–407. https://doi.org/10.1016/j.nicl.2017.05.023

Tzourio-Mazoyer, N., Landeau, B., Papathanassiou, D., Crivello, F., Etard, O., Delcroix, N., Mazoyer, B., Joliot, M., 2002. Automated Anatomical Labeling of Activations in SPM Using a Macroscopic Anatomical Parcellation of the MNI MRI Single-Subject Brain. Neuroimage 15, 273–289. https://doi.org/10.1006/nimg.2001.0978

Varela, M., Hajnal, J. V, Petersen, E.T., Golay, X., Merchant, N., Larkman, D.J., 2011. A method for rapid in vivo measurement of blood T1. NMR Biomed. 24, 80–8. https://doi.org/10.1002/nbm.1559

Varela, M., Petersen, E.T., Golay, X., Hajnal, J. V, 2015. Cerebral blood flow measurements in infants using look-locker arterial spin labeling. J. Magn. Reson. Imaging 41, 1591–600. https://doi.org/10.1002/jmri.24716

Wang, J., Licht, D.J., 2006. Pediatric Perfusion MR Imaging Using Arterial Spin Labeling. Neuroimaging Clin. N. Am. 16, 149–167. https://doi.org/10.1016/j.nic.2005.10.002

Watson, C.G., Dehaes, M., Gagoski, B.A., Grant, P.E., Rivkin, M.J., 2016. Arterial Spin Labeling Perfusion Magnetic Resonance Imaging Performed in Acute Perinatal Stroke Reveals Hyperperfusion Associated With Ischemic Injury. Stroke 47, 1514–9. https://doi.org/10.1161/STROKEAHA.115.011936

Wilke, M., Holland, S.K., Altaye, M., Gaser, C., 2008. Template-O-Matic: A toolbox for creating customized pediatric templates. Neuroimage 41, 903–913. https://doi.org/10.1016/j.neuroimage.2008.02.056

Williams, D.S., Detre, J.A., Leigh, J.S., Koretsky, A.P., 1992. Magnetic resonance imaging of perfusion using spin inversion of arterial water. Proc. Natl. Acad. Sci. U. S. A. 89, 212–6.

Wintermark, M., Lepori, D., Cotting, J., Roulet, E., van Melle, G., Meuli, R., Maeder, P., Regli, L., Verdun, F.R., Deonna, T., Schnyder, P., Gudinchet, F., 2004. Brain perfusion in children: evolution with age assessed by quantitative perfusion computed tomography. Pediatrics 113, 1642–52.

Wintermark, P., Hansen, A., Gregas, M.C., Soul, J., Labrecque, M., Robertson, R.L., Warfield, S.K., 2011. Brain Perfusion in Asphyxiated Newborns Treated with Therapeutic Hypothermia. Am. J. Neuroradiol. 32, 2023–2029. https://doi.org/10.3174/ajnr.A2708

Wintermark, P., Hansen, A., Warfield, S.K., Dukhovny, D., Soul, J.S., 2014. Near-infrared spectroscopy versus magnetic resonance imaging to study brain perfusion in newborns with hypoxic-ischemic encephalopathy treated with hypothermia. Neuroimage 85 Pt 1, 287–93. https://doi.org/10.1016/j.neuroimage.2013.04.072

Wong, A.M.-C., Yeh, C.-H., Liu, H.-L., Wu, T.-W., Lin, K.-L., Wang, H.-S., Toh, C.-H., 2017. Arterial spin-labeling perfusion imaging of children with subdural hemorrhage: Perfusion abnormalities in abusive head trauma. J. Neuroradiol. 44, 281–287. https://doi.org/10.1016/j.neurad.2017.02.003

Wong, E.C., Buxton, R.B., Frank, L.R., 1998. Quantitative imaging of perfusion using a single subtraction (QUIPSS and QUIPSS II). Magn. Reson. Med. 39, 702–8.

Yushkevich, P.A., Piven, J., Hazlett, H.C., Smith, R.G., Ho, S., Gee, J.C., Gerig, G., 2006. User-guided 3D active contour segmentation of anatomical structures: significantly improved efficiency and reliability. Neuroimage 31, 1116–28. https://doi.org/10.1016/j.neuroimage.2006.01.015

Bourses et Prix

- **Bourse de recherche SFR/CERF 2017** pour une aide à la mobilité « Comparaison de l'Arterial Spin Labelling (ASL) en IRM à 1.5T et 3T pour étude de la perfusion cérébrale chez les nouveau-nés avec encéphalopathie hypoxo-ischémique»
- **Bourse de recherche SFR/CERF 2012** pour le travail de master 2 « Mise au point d'une séquence d'ASL à 3T pour étude de la perfusion cérébrale chez le nouveau-né »
- **Prix d'article SFR/CERF 2017** au Dr Domitille Cadiot pour son travail « Magnetic resonance imaging in children presenting migraine with aura: Association of hypoperfusion detected by arterial spin labelling and vasospasm on MR angiography findings » publié dans Cephalalgia
- **Prix de communication orale SFIPP 2017** au Dr Domitille Cadiot pour sa communication orale « Imagerie par résonnance magnétique cérébrale chez les enfants présentant une migraine avec aura » au congrès annuel de la SFIPP ; Liège- Belgique.

Communications en lien avec la thèse

Cours comme orateur invité

- Proisy M et al. Pediatric brain perfusion MRI using arterial spin labeling: techniques and clinical use. 71st Korean Congress of Radiology – Seoul – Corée du Sud - Septembre 2015
- Proisy M et al. The role of whole body MRI in infectious and inflammatory pediatric disorders. 71st Korean Congress of Radiology – Seoul – Corée du Sud - Septembre 2015
- Proisy M et al. ASL chez l'enfant - Réunion annuelle de la Société Française de Neurochirurgie Pédiatrique - Saint – Malo, 4-5-6 Septembre 2015 – Le Nouveau Monde
- Proisy M, Bruneau B, Ferré J-C. Imagerie de perfusion cérébrale par ASL chez l'enfant et le nouveau-né. 37ème journées de Radiologie Pédiatrique. Hôpital d'Enfants Armand-Trousseau - Paris Janvier 2015.

- **Proisy M,** Ferré JC, Gauvrit JY, Brain Perfusion Imaging Techniques in Neonates – International Session: ASNR Introduces its First Bilingual Session: Society of French Neuroradiology (SFNR) - ASNR 52nd Annual Meeting in Montreal (May 2014)

Communications scientifiques orales

- **Proisy M**, Corouge I, Legouhy A, Nicolas A, Charon V, Mazille N, Leroux S, Bruneau B, Barillot C, Ferré J.-C. Changes in brain perfusion in successive arterial spin labelling MRI scans in neonates with hypoxic-ischaemic encephalopathy. *SPR Annual Meeting & Postgraduate Course, San Francisco, California, April 2019. Abstract Soumis*
- Cadiot D, Longuet R, Bruneau B, Tréguier C, Gomes C, Carsin-Vu A, Corouge I, **Proisy M.** Imagerie par résonnance magnétique cérébrale chez les enfants présentant une migraine avec aura. SFIPP 2017 – Liège
- A. Carsin-Vu, **M. Proisy**, O. Commowick, I. Corouge, C. Barillot, J.-C. Ferre. Evolution de la perfusion cérébrale en IRM Arterial Spin Labeling (ASL) chez l'enfant entre 6 mois et 15 ans. JFR 2016 – Paris
- **Proisy M**, Sokolska M, Uria-Avellanal C, Cady E, Robertson N-J, Golay X, Ferré J-C. Optimisation d'une technique d'Arterial Spin Labeling en IRM à 3T pour étude de la perfusion cérébrale chez le nouveau-né à risque d'encéphalopathie hypoxo-ischémique. JFR 2014 – Paris

Communications scientifiques affichées

- Sokolska M, **Proisy M**, uria-Avellanal C, Bainbridge A, Cady E, Thomas D, Robertson N, Golay X. Combined use of arterial spin labeling and MRS to determine the severity of injury in neonates with hypoxic-ischaemic encephalopathy. ISMRM – Milan, May 2014.
- **Proisy M**, Kendall G, Uria-Avellanal C, Bainbridge A; Melbourne A, Ourselin S, Huertas-Ceballos H, Golay X, Robertson NJ. Characterization of cerebral white matter damage in neonatal encephalopathy using 1H MR Spectroscopy, Diffusion weighted MR imaging and T2 relaxometry. ESPR 54th annual meeting 2013 – Porto

Publications en lien avec la thèse

Proisy, M., Bruneau, B., Rozel, C., Tréguier, C., Chouklati, K., Riffaud, L., Darnault, P., Ferré, J.-C., 2016a. Arterial spin labeling in clinical pediatric imaging. Diagn. Interv. Imaging 97, 151–8. https://doi.org/10.1016/j.diii.2015.09.001

Proisy, M., Mitra, S., Uria-Avellana, C., Sokolska, M., Robertson, N.J., Le Jeune, F., Ferré, J.-C., 2016b. Brain Perfusion Imaging in Neonates: An Overview. AJNR. Am. J. Neuroradiol. https://doi.org/10.3174/ajnr.A4778

Carsin-Vu, A., Corouge, I., Commowick, O., Bouzillé, G., Barillot, C., Ferré, J.-C., **Proisy, M.,** 2018. Measurement of pediatric regional cerebral blood flow from 6 months to 15 years of age in a clinical population. Eur. J. Radiol. 101, 38–44. https://doi.org/10.1016/j.ejrad.2018.02.003

Cadiot, D., Longuet, R., Bruneau, B., Treguier, C., Carsin-Vu, A., Corouge, I., Gomes, C., **Proisy, M.,** 2018. Magnetic resonance imaging in children presenting migraine with aura: Association of hypoperfusion detected by arterial spin labelling and vasospasm on MR angiography findings. Cephalalgia 38, 949–958. https://doi.org/10.1177/0333102417723570

Proisy, M., Corouge, I., Legouhy, A., Nicolas, A., Charon, V., Mazille, N., Leroux, S., Bruneau, B., Barillot, C., Ferré, J.-C., 2018. Changes in brain perfusion in successive arterial spin labelling MRI scans in neonates with hypoxic-ischaemic encephalopathy. Neuroimage: Clinical. *Article Soumis*

Publications sans lien avec la thèse

Berteloot, L., Proisy, M., Jais, J-P., Levy, M., Boddaert, N., Bonnet, D., Raimondi, F., (2018). Idiopathic, Heritable and Veno-occlusive Pulmonary Arterial Hypertension in childhood: Computed Tomography Angiography features in the initial assessment of the disease. Ped Radiol. *Accepted with Minor Revison*

Depoers, C., Lebaccon, F. A., Nyangoh Timoh, K., Morcet, J., **Proisy, M.,** Henno, S., … Arnaud, A. P. (2018). A pre-operative scoring system for adnexal mass in children and adolescents to preserve their future fertility. Journal of Pediatric and Adolescent Gynecology. https://doi.org/10.1016/j.jpag.2018.08.009

Delplanque, S., Lous, M. Le, **Proisy, M.,** Joueidi, Y., Bauville, E., Rozel, C., … Timoh, K. N. (2018). Fertility, pregnancy and clinical outcomes after uterine arteriovenous malformation management. J Minim Invasive Gynecol. https://doi.org/10.1016/j.jmig.2018.05.001

Fabre, C., **Proisy, M.,** Chapuis, C., Jouneau, S., Lentz, P.-A., Meunier, C., … Lederlin, M. (2018). Radiology residents' skill level in chest x-ray reading. Diagnostic and Interventional Imaging. https://doi.org/10.1016/j.diii.2018.04.007

Le Bras, A., **Proisy, M.,** Kuchenbuch, M., Gomes, C., Tréguier, C., Napuri, S., … Bruneau, B. (2018). Reversible lesions of the corpus callosum with initially restricted diffusion in a series of Caucasian children. Pediatric Radiology. https://doi.org/10.1007/s00247-018-4124-x

Bussat, A., **Proisy, M.,** Bruneau, B., Bouzillé, G., Chappé, C., & Riffaud, L. (2018). Edema of the optic tract in patients with tumors of the sellar region: clinical and visual implications in the pediatric population. Journal of Neurosurgery: Pediatrics, 1–7. https://doi.org/10.3171/2017.11.PEDS17526

Dubois, M., Cousin, E., Chouklati, K., Bruneau, B., & **Proisy, M.** (2018). Scurvy in a 3-year-old autistic girl: Whole-body magnetic resonance imaging findings. Diagnostic and Interventional Imaging, 99(1), 49–50. https://doi.org/10.1016/j.diii.2017.06.001

Arberet, C., **Proisy, M.,** Fausser, J. L., Curt, M., Bétrémieux, P., Tréguier, C., … Pladys, P. (2017). Isolated neonatal MRI punctate white matter lesions in very preterm neonates and quality of life at school age. Journal of Neonatal-Perinatal Medicine, 10(3), 257–266. https://doi.org/10.3233/NPM-1691

Charon, V., **Proisy, M.,** Bretaudeau, G., Bruneau, B., Pladys, P., Beuchée, A., … Rozel, C. (2016). Early MRI in neonatal hypoxic-ischaemic encephalopathy treated with hypothermia: Prognostic role at 2-year follow-up. European Journal of Radiology, 85(8). https://doi.org/10.1016/j.ejrad.2016.05.005

Morel, B., Jaudeau-Collart, A. C., **Proisy, M.,** Leiber, L. M., Tissot, V., Quéré, M. P., … Sirinelli, D. (2017). Variability in Imaging Practices and Comparative Cumulative Effective Dose for Neuroblastoma and Nephroblastoma Patients at 6 Pediatric Oncology Centers. Journal of Pediatric Hematology/Oncology. https://doi.org/10.1097/MPH.0000000000000915

Proisy, M., Riffaud, L., Chouklati, K., Tréguier, C., & Bruneau, B. (2017). Ultrasonography for the diagnosis of craniosynostosis. European Journal of Radiology, 90. https://doi.org/10.1016/j.ejrad.2017.03.006

Merdrignac, A., **Proisy, M.,** Fremond, B., Habonimana, E., Nardi, N., & Arnaud, A. P. (2016). An Unusual Intussusception. Journal of Pediatrics, 175. https://doi.org/10.1016/j.jpeds.2016.04.034

Charon, V., **Proisy, M.,** Ferré, J.-C., Bruneau, B., Tréguier, C., Beuchée, A., … Rozel, C. (2015). Comparison of early and late MRI in neonatal hypoxic–ischemic encephalopathy using three assessment methods. Pediatric Radiology, 45(13). https://doi.org/10.1007/s00247-015-3419-4

Le Fournier, L., Hénaux, P.-L., Haegelen, C., **Proisy, M.,** & Riffaud, L. (2015). Intradiploic growing skull fracture: review of mechanisms and literature. Child's Nervous System, 31(11). https://doi.org/10.1007/s00381-015-2793-4

Proisy, M., Loget, P., Bouvet, R., Roussey, M., Pelé, F., Rozel, C., … Bruneau, B. (2015). Non-specific post-mortem modifications on whole-body post-mortem computed tomography in sudden unexpected death in infancy. Journal of Forensic Radiology and Imaging, 3(1). https://doi.org/10.1016/j.jofri.2015.02.001

Proisy, M., Rouil, A., Raoult, H., Rozel, C., Guggenbuhl, P., Jacob, D., & Guillin, R. (2014). Imaging of musculoskeletal disorders related to pregnancy. American Journal of Roentgenology, 202(4). https://doi.org/10.2214/AJR.13.10988

Chouklati, K., **Proisy, M.,** Legeas, O., Habonimana, E., & Taque, S. (2014). Bilateral renal nodules revealed in diffusion-weighted imaging. Revue d'Oncologie Hematologie Pediatrique, 2(2). https://doi.org/10.1016/j.oncohp.2014.04.001

Proisy, M., Marchand, A. J., Loget, P., Bouvet, R., Roussey, M., Pelé, F., … Bruneau, B. (2013). Whole-body post-mortem computed tomography compared with autopsy in the investigation of unexpected death in infants and children. European Radiology, 23(6). https://doi.org/10.1007/s00330-012-2738-1

Tréguier, C., Chapuis, M., Branger, B., Bruneau, B., Grellier, A., Chouklati, K., … Gandon, Y. (2013). Pubo-femoral distance: An easy sonographic screening test to avoid late diagnosis of developmental dysplasia of the hip. European Radiology, 23(3). https://doi.org/10.1007/s00330-012-2635-7

Marchand, A. J., **Proisy, M.,** Ropars, M., Cohen, M., Duvauferrier, R., & Guillin, R. (2012). Snapping knee: Imaging findings with an emphasis on dynamic sonography. American Journal of Roentgenology, 199(1). https://doi.org/10.2214/AJR.11.7817

Annexes

Annexe 1 : Manuel d’utilisation AutoASL

User manual :

autoasl: SPM-based analysis of Arterial Spin Labeling data

February 22, 2016

Author

Camille Maumet	PhD student – VisAGeS team, Rennes
Jan Petr	Post-doctoral fellow – VisAGeS team, Rennes
Isabelle Corouge	Research Engineer – Neurinfo, Rennes

Project members

Elise Bannier	Research Engineer Neurinfo, Rennes
Christian Barillot	Researcher VisAGeS team, Rennes
Jean-Christophe Ferré	Radiologist CHU Pontchaillou, VisAGeS team, Rennes
Jean-Yves Gauvrit	Radiologist and Research scientist CHU Pontchaillou, Rennes
Pierre Maurel	Researcher VisAGeS team, Rennes

Version 0.1

Contents

Chapter 1

Introduction

1.1 Description

autoasl is a automation tool based on SPM8 to perform statistical analysis of arterial spin labeling MRI sequences.

1.2 License

This program is available under TODO, for more details please refer to the LICENCE file available with this program. In each source file, a copyright including a range (for example 2008-2011) means that the copyright apply for every year in the range (2008-2011 stand for 2008, 2009, 2010 and 2011).

1.3 Authors

Jan Petr, Camille Maumet and Isabelle Corouge are the main contributor to this project, they developed the application and provided the documentation. Other members contributed on a theoretical level to define the purpose of the application, and its functionality.

Chapter 2

Installation

2.1 Requirements

This program is working on Windows, Linux, Mac. In order to use autoasl, you will need `Matlab`.

2.2 Install

2.2.1 autoasl

autoasl is available for download at http://urltodownload-autoasl.htm. Unzip the archive.

2.2.2 Dependencies

autoasl is dependent on SPM8 (Wellcome Trust Center for Neuroimaging), `resize_img.m` by T. Nichols and `get_totals.m` by G. Ridgway. In order to install SPM8, please follow the instructions on SPM's website.

Download `resize_img.m` from http://www0.cs.ucl.ac.uk/staff/g.ridgway/vbm/resize_img.m and `get_totals.m` from http://www.cs.ucl.ac.uk/staff/g.ridgway/vbm/get_totals.m and save them in a folder available in matlab path.

2.3 Update Matlab path

You then need to update the path in order to specify the various locations where it should look to find code. To this aim, run `Matlab` then, in the menu `File`, select `Set Path...`. Then, click on `Add Folder` button and navigate through you computer up to the folder which contain autoasl source code.

Apparently, since newer matlab version, there can be a conflict with the `nanmean` function defined in SPM8. In that case, in the `Set Path...` menu, select every SPM8 (sub)folders and click on the `Move to bottom` button.

Chapter 3

Before starting

3.1 Convert images to NIFTI

autoasl reads and writes Nifti images. If your data is not in this format, please use a conversion tool before going further.

3.2 File organisation

To be recognized by autoasl, your files must be organised according to several rules. Thanks to this organisation, the program will then manage your data and select automatically the files required for the process you want to run.

Follow this guidelines in order to create you own file tree:

1. Create a root folder with the name of your current study (ex: `myPerfusionProject`).
2. Inside the root folder, create a new directory called `data`.
3. For each group involved in your study (ex: patient, control...) create a directory inside `data`. The name of group folders must start with `gr_` (ex: `gr_control`).
4. For each subject involved in your study create a folder inside of the appropriate group directory. The name of the subject folders must start with `su_`, ex: `su_LASTNAME_FirstName`).
5. Inside each subject folder, create a directory called `structural` and copy the anatomical T1 3D MRI image of the subject. The name of the image must start with `T13D_`.
6. Inside each subject folder, create a directory called `perfusion`
7. For each ASL sequence, create a directory inside `perfusion` and copy the ASL image. The name of the sequence folders must start with `seq_`, the name of the ASL image with `asl_`.

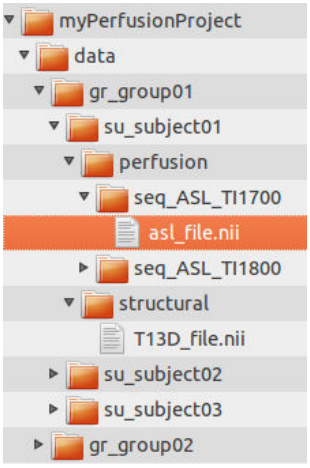

Example of file tree

3.3 Select Matlab working directory

To be able to reach your data, Matlab working directory must be located in the root folder of your experiment, to this aim:

- In Matlab click on ....
- Select your experiment root directory (in this example `myPerfusionProject`).

Chapter 4

Pre-processing

4.1 Introduction

4.2 Overview

Figure 4.1 describes the steps performed in order to prepare ASL perfusion data (pMRI) data to statistical analysis.

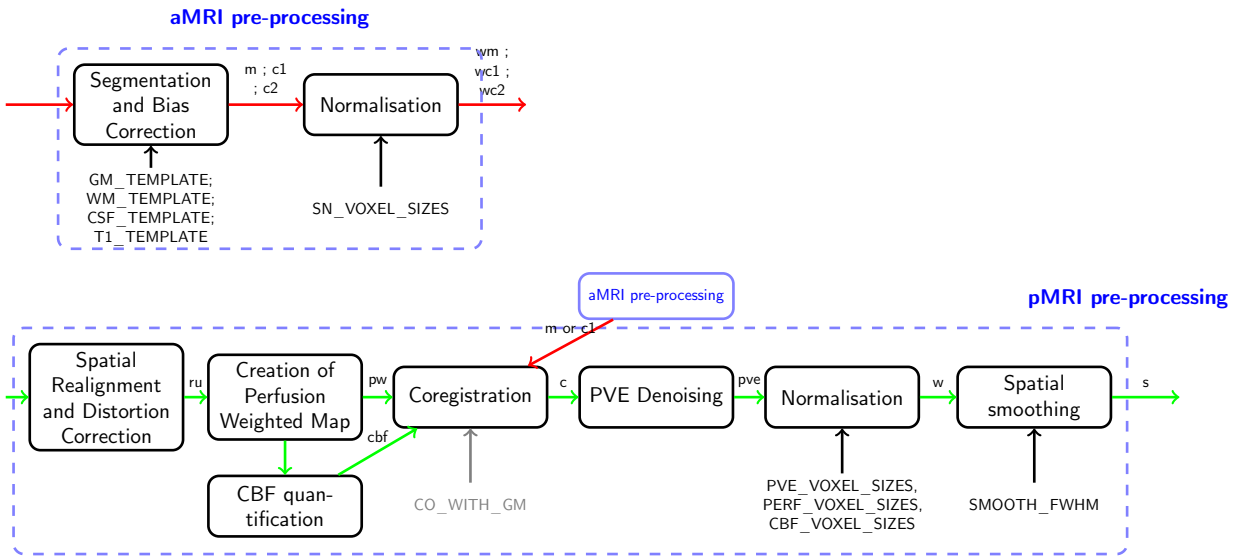

Figure 4.1: Pre-processing of anatomical and perfusion (ASL) MRI

4.3 Configuration

This section describes the pre-processing parameters that can be modified. All of them have a default value that might not be appropriate for your study. Please check all of them before starting an experiment. The minimal set of parameters that must be checked before starting an experiment is presented in part 4.3.1, the other parameters in part 4.3.2. Please keep in mind that both sets of parameters are important and can lead to significant changes in your analysis.

However a lack in checking the first set will potentially lead to wrong results while the influence of the latter on the meaningfulness of your results is less pregnant. If you would like to change the value of a parameter follow this steps:

1. Create a file called `user_defaults.m` in the root folder of your project (ex: `myPerfusionProject`).
2. Indicate which value should be used in Matlab syntax, the parameter name must be exactly the same, an example of syntax is available for each parameter.

4.3.1 Minimal set of parameters

Table 4.1 presents a recap of the parameters and their default values. Parameters that must be check for each experiment are in blue font.

Name	Definition	Default
Quantification		
LABEL_FIRST	True, if the first image of the series (after M0) is a label image.	`true`
ASL_TI2	Inversion time in seconds of your ASL sequence.	`1.7`
ASL_TI1	Bolus width in seconds of your ASL sequence.	`0.7`
ASL_TE	Echo time in seconds of your ASL sequence.	`0.0177`

Table 4.1: ASL Pre-processing: Minimal set of parameters

4.3.2 Additional parameters

. The following tables present the additional parameters. Green font indicates parameters which are part of the minimal set of parameters if another parameter (displayed in parenthesis in italics) has a given value.

Unwarping of EPI images using field maps		
Name	Definition	Default
UNWARP_EPI	True to use field map images to unwarp EPI data. If true following parameters must be checked	`false`
EPI_BASED	True if field maps are EPI-based (*UNWARP_EPI=true*).	`false`
TOTAL_EPI_READOUT_TIME	Total EPI Readout time is milliseconds, time required to cover k-space (*UNWARP_EPI=true*).	`40`
PHASE_ENCODING_DIR	Phase encoding direction of field map acquisition from `'AP'` for antero-posterior or `'PA'` postero-anterior (other directions not supported) (*UNWARP_EPI=true*).	`'AP'`
ECHO_TIMES	Short and long echo times of field map acquisition in milliseconds (*UNWARP_EPI=true*).	`[4.92 7.38]`

Intensity normalisation

Name	Definition	Default
INTENSITY_NORMALISATION	If true perform intensity normalisation of selected ASL maps (PW, CBF, PVE).	false
NORMALISE_DIVIDE	If true, estimate a multiplying factor as normalisation parameter, otherwise estimate an additional constant.	true
GM_MEAN_THRESH	For basic intensity normalisation, GM voxels filled with more than GM_MEAN_THRESH of grey matter are used to compute the normalisation parameter.	0.7
NO_ZEROS_ESTIMATE_MEAN	If true, ignore non positive values to estimate basic normalisation parameter.	false

Perfusion-weighted (PW) map creation

Name	Definition	Default
PERFUSION_FILES	True to compute PW files and include them in subsequent statistical analysis.	true
MEDIAN_PW	If true Compute pw map as median over the repeats.	false
ROBUST_LOCATION_PW	If true, compute pw map as Huber's M-estimator over the repeats.	false
ROBUST_LOCATION_PW_LOG	If true, compute pw map as Logistic M-estimator over the repeats.	false

Quantification of cerebral blood flow (CBF)

Name	Definition	Default
CBF_FILES	True to compute CBF quantification.	true
CBF_USE_M0	Type of control image, boolean. True to use M0 file (first acquired file in Siemens PASL Q2TIPS sequence) in quantification, false to use mean of control images.	true
CBF_TI2_INCREASE_WITH_SLICE	Changing TI2 with slice, boolean. True to have a specific acquisition time for each slice, false to use the same value for the volume.	true
ASL_SLICE_DELAY	Time required to acquire one ASL slice in s. (*CBF_TI2_INCREASE_WITH_SLICE=true*)	0.045
CBF_QUANTIFICATION_TYPE	Set of parameters from quantification, 2=Siemens / 4=Wang.	4
QUANTIF_NEG_TO_ZERO	Change negative values into zeros.	false

Partial Volume Effects (PVE) correction

Name	Definition	Default
PVE_FILES	True to compute PVE correction.	true
PVE_TYPE	Type of Partial Volume Effects (PVE) correction, 6=Petr's method with Total Variation filtering, 5=Aslanni's method.	6

Smoothing		
Name	Definition	Default
SMOOTH_FWHM	Full Width at Half Maximum of the 3D gaussian smoothing kernel in mm.	[8 8 8]

Outliers removal and denoising		
Name	Definition	Default
OUTLIER_PEIRCE	True to compute Peirce's method for outliers removal (Peirce 1852).	false
OUTLIER_ROSNER	True to compute Rosner's method for outliers removal (Rosner 1983).	false
OUTLIER_BISQUARE	True to compute outliers removal with Tukey's biweight (bisquare) M-estimator.	false
OUTLIER_TAN	True to compute outliers removal with Tan et al. 2009 outliers removal based on z-thresholding.	false
OUTLIER_METHOD3	If OUTLIER_PEIRCE or OUTLIER_ROSNER is true, remove volume presenting an outlying number of outliers based on original PW serie.	false
OUTLIER_METHOD2	If OUTLIER_PEIRCE or OUTLIER_ROSNER is true, remove volume presenting an outlying number of outliers based on voxelwise outlier removed pw serie.	false

Outliers simulation		
Name	Definition	Default
ADD_OUTLIERS	For simulation purpose, add outliers to perfusion-weighted series.	false
NUM_OUTLIERS_PER_SERIE	Percentage of outliers to add in the series (= percentage of outlying volumes).	40
OUTLIER_PERCENT_VOXEl_PER_VOLUME	Percentage of outlying voxel per outliers volume.	30
OUTLIER_EXTREME_VALUE	Absolute value of maximum and minimum outliers, outliers are drawn from a uniform distribution.	10
SIMU_ID	Simulation identifier (to be able to produce more than 1 simulated dataset).	[]

Coregistration on anatomical MRI		
Name	Definition	Default
CO_WITH_GM	If true coregister ASL data on grey matter data, otherwise coregister on bias corrected aMRI.	true
COREG_PW	If true coregister PW image on anatomical data, otherwise coregister mean of control images before subtraction.	false

Spatial normalisation		
Name	Definition	Default
PERF_VOXEL_SIZES	Voxel sizes in mm of PW image after normalisation.	[3 3 7.7]
CBF_VOXEL_SIZES	Voxel sizes in mm of CBF image after normalisation.	[3 3 7.7]
PVE_VOXEL_SIZES	Voxel sizes in mm of PVE-corrected CBF image after normalisation.	[1 1 1]

4.4 Execution

Once the parameters are set, use the following command to run the pre-processing:

```
autoasl('p', options)
```

The `options` parameter is optional.

The optional input `options` is a structure of strings used to select the group(s) and/or subject(s) of interest:

- `su_XX` to select (or do not select if preceded by a negative sign) subject `XX`
- `gr_XX` to select (or do not select if preceded by a negative sign) all subject from group `XX`
- other type of strings are ignored.

Examples

All subjects and sessions: Pre-processings are computed for all subjects and all sessions found in your file tree:

```
autoasl('p')
```

Select a subject: To run the pre-processing on the subject `su_mysubject` only use the following command:

```
autoasl('p', {'su_mysubject'})
```

Select a group: To run the pre-processing on all subjects from group `gr_control`:

```
autoasl('p', {'gr_control'})
```

Combining selections: Previous commands can be combined to select (or ignore) subject(s) and/or group(s). A few example below:

```
% Run the preprocessings for all subjects in group gr_control but su_control01
autoasl('p', {'gr_control', '-su_control01'})
```

4.5 Results

4.5.1 File tree update

When you start the pre-processings a directory called `pre-processing` is created inside the project root directory. In this folder, the structure is similar to the data directory: one folder per group containing one folder per subject.

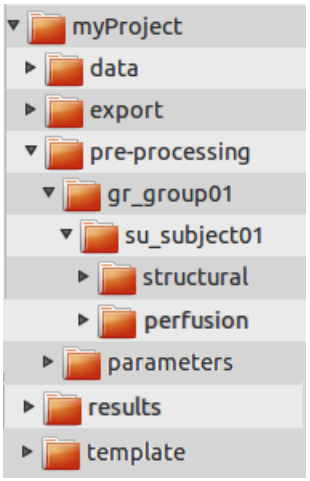

4.5.2 Pre-processed anatomical MRI

Files created during the pre-processings are stored in the folder `pre-processing`, inside the group and subject directories. For each subject, pre-processed aMRI are stored in the `structural` directories. You can find here a brief description of the produced files (with the default setting):

- `T13D_X` : original image
- `rT13D_X` : resized image (If resolution is higher than params.MAX_RESOLUTION then structural data will be first down-sampled to params.OUT_RESOLUTION (avoid memory fault))
- `mrT13D_X` : bias corrected image (obtained during the SPM segmentation)
- `c1rT13D_X` : segmented grey matter
- `c2rT13D_X` : segmented white matter
- `c3rT13D_X` : segmented CSF
- `mask0.5_c1rT13D_Xc1c2c3` : brain mask
- a lot of `rdc{1,2,3}cbfM04_45_pw_fcpwall_nr(t)asl_X_gm` : used during PVE correction

4.5.3 Pre-processed perfusion MRI

For each subject, pre-processed pMRI are stored in the `perfusion` directories. You can find here a brief description of the produced files (with the default setting):

- `asl_X` : original image
- `r(t)asl_X` : result of spatial realignment ('Realign: Estimate & Reslice'). With `"t"`: if `params.ALL_SESSIONS_TOGETHER==1`, all sessions are realigned together on the first volume of the first session
- `nr(t)asl_X` : same as the previous one without the first volume
- `m0_r(t)asl_X` : only the first volume (which is M0) of `r(t)asl_X`

- `mc_nr(t)asl_X` : mean of the control images in `nr(t)asl_X`
- `pwall_nr(t)asl_X` : perfusion weighted images obtained by pair-wise subtraction of `nr(t)asl_X`
- `cmc_nr(t)asl_X_gm` : result of coregistration of `mc_nr(t)asl_X_gm` on `c1rT13D_X`
- `cm0_r(t)asl_X_gm / cpwall_nr(t)asl_X_gm` : results of the application of the transformation obtained in previous step to `m0_r(t)asl_X / pwall_nr(t)asl_X`
- `fcpwall_nr(t)asl_X_gm` : conversion of `cpwall_nr(t)asl_X_gm` from `INT32` to `FLOAT`
- `pw_fcpwall_nr(t)asl_X_gm` : mean of all PW-volumes in `fcpwall_nr(t)asl_X_gm`
- `cbfM04_45_fcpwall_nr(t)asl_X_gm` : result of quantification on `fcpwall_nr(t)asl_X_gm` (using the first volume as `M0`, the quantification method number 4 (Wang 2011)) $\leftarrow N$ volumes
- `cbfM04_45_pw_fcpwall_nrtasl_X_gm` : result of quantification on `pw_fcpwall_nr(t)asl_X_gm` (using the first volume as `M0`, the quantification method number 4 (Wang 2011)) $\leftarrow 1$ volume
- `rmask0.5_c1rT13D_Xc1c2c3` : `mask0.5_c1rT13D_Xc1c2c3` resliced according to `cmc_nr(t)asl_X_gm` (which has been coregistered on `c1rT13D_X`)
- `pve6_cbfM04_45_pw_fcpwall_nr(t)asl_X_gm` : PVE correction of `cbfM04_45_pw_fcpwall_nrtasl_X_gm` (without CSF)
- `gmwmcsf6_cbfM04_45_pw_fcpwall_nr(t)asl_X_gm` : probabilistic mask obtained during PVE correction and used for calculation of `pve6_cbfM04_45_pw_fcpwall_nrtasl_X_gm`
- in the subdirectory `smootheda__b__c` : smoothed version of some files (using `params.SMOOTH_FWHM`)
- `rasl_X_realign_plot.ps` : estimated parameters during spatial realignment (if `params.ALL_SESSIONS_TOGETHER==1`, `rtasl_X_realign_plot.ps` is in the last session directory)
- `coreg_params.ps` : estimated parameters during coregistration
- `rp_(t)_asl_X.txt` : parameters of the spatial realignment (for each volume of the session)

The optional "`t`" in the names is related to the parameter `params.ALL_SESSIONS_TOGETHER`. If it is set to 1, all sessions are realigned together on the first volume of the first session and the letter "`t`" will be added in every name. Finally in the perfusion directory of a subject, one can find a file `meanrtasl_X` corresponding to the mean of all realigned volumes of all sessions.

Chapter 5

Statistical analysis

5.1 Introduction

TODO

5.2 Overview

TODO

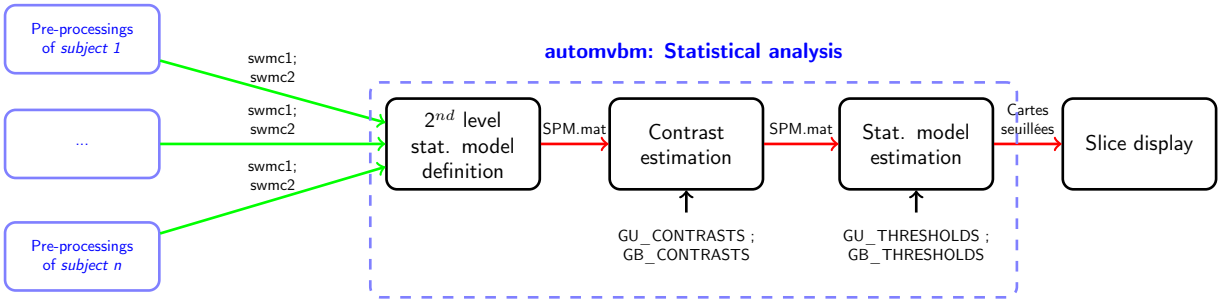

Figure 5.1: automorpho: statistical analysis

5.3 Configuration

This section describes the statistical analysis parameters that can be modified. All of them have a default value that might not be approriate for your study. Please check all of them before starting an experiment. The minimal set of parameters that must be checked before starting an experiment is presented in part 5.3.1, the other parameters in part 5.3.2. Please keep in mind that both sets of parameters are important and can lead to significant changes in your analysis. However a lack in checking the first set will potentially lead to wrong results while the influence of the latter on the meaningfulness of your results is less pregnant. If you would like to change the value of a parameter follow this steps:

1. Create a file called `user_defaults.m` in the root folder of your project (ex: `myPerfusionProject`).
2. Indicate which value should be used in Matlab syntax, the parameter name must be exactly the same, an example of syntax is available for each parameter.

5.3.1 Minimal set of parameters

5.3.2 Other parameters

TODO

5.3.3 Summary

TODO

5.4 Execution

Once the parameters are set, use the following command to run the statistical analysis:

```
autoasl('g', options)
```

The `options` parameter is optional.

The optional input `options` is a structure of strings used to select the group(s) and/or subject(s) of interest (cf. 4.4).

5.5 Results

5.5.1 File tree update

When you start a group statistical analysis a new directory is created inside `results` under `perfusion`. This directory contains one directory by subject. In order to identify the different analysis the name of the new folder starts with `mod_` followed by the date and hour when the analysis started.

TODO

Annexe 2 : Regroupement des 50 régions d'intérêts de l'atlas Albert (Gousias et al., 2012)

itkSegmentTable: 50

Temporal lobe right

1	255	0	0	1	1	Hippocampus right
3	255	255	0	1	1	Amygdala right
5	255	255	255	1	1	Anterior temporal lobe, medial part right
7	255	0	0	1	1	Anterior temporal lobe, lateral part right
9	7	255	7	1	1	Gyri parahippocampalis et ambiens anterior part right
11	7	7	255	1	1	Superior temporal gyrus, middle part right
13	7	255	255	1	1	Medial and inferior temporal gyri anterior part right
15	255	14	14	1	1	Lateral occipitotemporal gyrus, gyrus fusiformis anterior part right
25	21	21	255	1	1	Gyri parahippocampalis et ambiens posterior part right
27	21	255	255	1	1	Lateral occipitotemporal gyrus, gyrus fusiformis posterior part right
29	255	28	28	1	1	Medial and inferior temporal gyri posterior part right
31	255	255	28	1	1	Superior temporal gyrus, posterior part right

Temporal lobe left

2	0	255	0	1	1	Hippocampus left
4	0	0	255	1	1	Amygdala left
6	255	255	255	1	1	Anterior temporal lobe, medial part left
8	255	255	255	1	1	Anterior temporal lobe, lateral part left
10	255	255	7	1	1	Gyri parahippocampalis et ambiens anterior part left
12	255	7	255	1	1	Superior temporal gyrus, middle part left
14	248	248	248	1	1	Medial and inferior temporal gyri anterior part left
16	14	255	14	1	1	Lateral occipitotemporal gyrus, gyrus fusiformis anterior part left
24	255	255	21	1	1	Gyri parahippocampalis et ambiens posterior part left
26	255	21	255	1	1	Lateral occipitotemporal gyrus, gyrus fusiformis posterior part left
28	234	234	234	1	1	Medial and inferior temporal gyri posterior part left
30	28	255	28	1	1	Superior temporal gyrus, posterior part left

Posterior Fossa

17	255	255	14	1	1	Cerebellum right
18	14	14	255	1	1	Cerebellum left
19	255	14	255	1	1	Brainstem, spans the midline

Garder les ROI suivantes telle quelles

20	14	255	255	1	1	Insula left
21	241	241	241	1	1	Insula right
22	255	21	21	1	1	Occipital lobe left
23	21	255	21	1	1	Occipital lobe right

Frontal Lobe left

36	255	35	35	1	1	Frontal lobe left
32	28	28	255	1	1	Cingulate gyrus, anterior part left

Frontal Lobe right

37	35	255	35	1	1	Frontal lobe right
33	255	28	255	1	1	Cingulate gyrus, anterior part right

Parietal Lobe left

38	255	255	35	1	1	Parietal lobe left
34	28	255	255	1	1	Cingulate gyrus, posterior part left

Parietal Lobe right

39	35	35	255	1	1	Parietal lobe right
35	227	227	227	1	1	Cingulate gyrus, posterior part right

Basal ganglia left

40	255	35	255	1	1	Caudate nucleus left
42	220	220	220	1	1	Thalamus left
44	42	255	42	1	1	Subthalamic nucleus left
46	42	42	255	1	1	Lentiform Nucleus left

Basal ganglia right

41	35	255	255	1	1	Caudate nucleus right
43	255	42	42	1	1	Thalamus right
45	255	255	42	1	1	Subthalamic nucleus right
47	255	42	255	1	1	Lentiform Nucleus right

ROI non nécessaires

48	42	255	255	1	1	Corpus Callosum
49	213	213	213	1	1	Lateral Ventricle right
50	255	49	49	1	1	Lateral Ventricle left

UNIVERSITE BIOLOGIE BRETAGNE SANTE LOIRE

UNIVERSITÉ DE RENNES 1

Titre: Étude de la perfusion cérébrale par Arterial Spin Labeling en IRM à 1.5T chez le nouveau-né et l'enfant

Mots clés: Imagerie par résonance magnétique, Pédiatrie, Circulation cérébrale, Asphyxie périnatale

Résumé: L'imagerie IRM de perfusion par Arterial Spin Labeling (ASL) ou marquage des spin artériels a pour principal avantage d'être une méthode d'imagerie non invasive (non irradiante et sans injection de produit de contraste exogène), particulièrement adaptée à l'imagerie cérébrale pédiatrique. Sa facilité de mise en œuvre explique l'engouement pour cette séquence et de nombreuses applications cliniques émergentes. Cette technique initialement développée chez l'adulte nécessite une adaptation à la population pédiatrique, aussi bien des paramètres d'acquisition et de quantification que des algorithmes de traitement d'images. La perfusion cérébrale globale et régionale évolue physiologiquement, parallèlement à l'âge et au développement neurocognitif. Il existe plusieurs méthodes d'étude de la perfusion cérébrale pédiatrique. Dans ce contexte, deux revues de littérature ont été réalisées et publiées : l'une portant sur les différentes techniques d'imagerie de la perfusion cérébrale chez les nouveau-nés, l'autre se focalisant sur la technique d'ASL en pédiatrie et ses applications cliniques.
Puis la chaine de traitement des images morphologiques et de perfusion ASL, développée chez l'adulte au sein de notre unité, a été adaptée aux enfants puis aux nouveau-nés.
Ces deux populations ont effectivement des problématiques différentes, en particulier le rapport signal sur bruit de l'ASL est très bon chez les enfants, mais nettement moins bon chez les nouveau-
nés, et les images morphologiques ont un contraste différent en raison d'une myélinisation incomplète à la naissance. Grace à l'adaptation de la chaine de traitement, des travaux de recherche clinique ont pu être finalisés (2 publiés, 1 soumis) illustrant l'intérêt de l'étude de la perfusion cérébrale dans 3 situations : l'étude de l'évolution de la perfusion cérébrale normale chez l'enfant entre 6 mois et 15ans ; l'étude de la perfusion cérébrale chez les enfants souffrant d'une première crise de migraine avec aura ; et enfin l'étude de l'évolution de la perfusion cérébrale entre le 3ieme et le 10ieme jour de vie chez les enfants souffrant d'asphyxie périnatale et traités par hypothermie. Plusieurs projets restent en cours sur le sujet, avec d'autres challenges de traitement et d'analyse d'image (enfants de neurochirurgie avec modifications morphologiques du cerveau, ou enfants prématurés par exemple), dans la continuité ce qui a été fait au cours de cette thèse.

Title : Brain perfusion imaging using Arterial Spin labeling 1.5T MRI scan in neonates and children

Keywords : Magnetic resonance imaging, Pediatric, Brain perfusion, Neonatal asphyxia

Abstract: Physiological changes in overall and regional cerebral perfusion are related to age and neurocognitive development. Brain perfusion in the pediatric population can be assessed using a number of imaging techniques. Two literature reviews were undertaken and published on this topic: one based on brain perfusion imaging techniques in neonates, and the other based on the ASL technique in the pediatric population and its clinical applications.
The Arterial Spin Labeling (ASL) MRI perfusion sequence is one of the most suitable imaging techniques for children given that the procedure is non-irradiating and non-invasive (without exogenous contrast agent injection). There are many emerging cerebral perfusion imaging applications for children due to the highly convenient implementation of the ASL sequence, which can be easily incorporated into standard brain MRI protocols following acquisition of morphological images.
Certain technical adjustments to the imaging parameters are required to account for the fundamental differences between the pediatric and adult populations. Measuring cerebral blood flow (CBF) in neonates and children using ASL therefore requires a number of adaptations to acquisition and related parameters. The processing of ASL data also requires specific adaptations, in particular regarding the automated segmentation of brain tissues, and the parameters used for CBF quantification models.
The processing pipeline for both anatomical and perfusion images that had been previously developed by our team for adult data was adapted firstly for children and secondly for neonates. These two populations notably have specific age-related concerns; in particular the signal-to-noise ratio of ASL is very good in children, but much less so in neonates, and the morphological images have inverted contrast due to incomplete myelination at birth.
Following adaptation of the processing pipeline, several studies were completed (2 original articles published and 1 under review), showing the clinical benefits of studying cerebral perfusion in three situations: first physiological changes in cerebral perfusion in children between 6 months and 15 years; secondly changes in cerebral perfusion in children with a first attack of migraine with aura; and lastly changes in brain perfusion between day of life 3 and day of life 10 in asphyxiated neonates.
Several studies are still in progress, and these present new image processing challenges, involving, for example, children with neurosurgical conditions and morphological changes in the brain, or premature babies, in line with the work undertaken for this thesis.